Eindhoven University of Technology
Department of Structural Engineering and Design

Master Thesis

Design of a three-dimensional structure, made of a bio-based material and manufactured using Coreless Robotic Filament Winding (CRFW) technology

R.T. Damoiseaux

Final Version
Eindhoven, July 4, 2024

Title	Design of a three-dimensional structure, made of a bio-based material and manufactured using Coreless Robotic Filament Winding (CRFW) technology
Subtitle	Graduation Thesis for the final graduation project of the Master variant Structural Engineering and Design of the master 'Architecture, Building and Planning' at Eindhoven University of Technology
Date	July 4, 2024
Location	Eindhoven, The Netherlands
Author	R.T. (Rick) Damoiseaux
Student ID	1629476
E-Mail	r.t.damoiseaux@student.tue.nl
Department	Built Environment
Master	Architecture, Building and Planning
Master track	Structural Engineering and Design
Chair	Innovative Structural design - Resource Efficient Structural Engineering and Design (RESED)
Graduation Committee	Ir. A.P.H.W. Habraken Dr. Ir. S.P.G. Moonen Dr. Ing. M. Gil Pérez Ir. J. Versteege

Preface

In the Resource Efficient Structural Engineering and Design course led by A.P.H.W. Habraken, a great interest in sustainable construction methods emerged. In collaboration with A. Habraken, the concept of using Coreless filament winding to make a structure using flax fibres was created. This project, part of the Resource Efficient Structural Engineering and Design (RESED) workshop under the Innovative Structural Engineering and Design chair, focuses on using bio-based materials and new manufacturing techniques to reduce environmental impact and open new ways in structural design.

I would like to express my appreciation to my supervisors for their guidance and support throughout the project, especially to A.P.H.W. Habraken for his two-weekly assistance with my project and his valuable feedback. I also acknowledge the contribution of S.P.G. Moonen for sharing his expertise during the end phase of the project.

Special thanks to M. Gil Perez for her expertise in the executive part of the project. Her experience of winding with flax fibres and using the coreless filament winding technique enabled me to complete this project successfully.

I would like to acknowledge the help of the SED lab staff, especially H. Lamers, during the production and testing phases. T. van Alen, for his help with making the construction for the winding process and E. Wijen for his help with testing the elements. Finally, I appreciate the help of my fellow student, B. Schipper during the winding process.

Rick Damoiseaux
Eindhoven, July 4, 2024

Abstract

This master thesis examines the design and manufacturing of a three-dimensional structure using bio-based materials and Coreless Robotic Filament Winding (CRFW) technology. The primary material used in this study is flax, chosen for its sustainability and availability, and impregnated with partly bio-based epoxy resin. The research addresses two significant issues in the construction industry: environmental impact and labor shortages. By using CRFW technology, the study aims to optimize the design and manufacturing process of a structural element withstanding axial compressive forces.

The digital design process was executed using Rhinoceros and Grasshopper software, with optimization performed using the Karamba3D and Octopus plugins. Several design variants have been explored, focusing on achieving optimal structural performance while minimizing material usage. The optimization in Octopus resulted in three final design options, all based on consistent mass.

Before manufacturing, the existing filament winding setup was updated. The three design options were manufactured using the ABB IRB 1200-5/0.9 robot. This manufacturing process involved winding impregnated flax rovings into a 3D structure without the need for auxiliary structures with the CRFW technology. First, a trial run of winding the first option was done to verify and optimize the manufacturing setup. After this, the three design options were successfully manufactured without any issues. Post-manufacturing, the fiber composite structures were stored for a maximum of 24 hours at 20 degrees Celsius, followed by post-curing at 40 degrees Celsius for 8 hours.

After curing, the structure was calibrated using a numerical model created in Oasys GSA. This part of the research involved generating a staging analysis with the Oasys GSA software. The analysis simulated the step-by-step construction process to understand the structural behavior at different manufacturing stages. The GSA model was calibrated with the manufacturing process using photographs taken during manufacturing and measurements of the final structure. Also the material properties of the final design were calibrated with the final model. Afterwards, Karamba3D was used to simulate the compression tests of the structures. These test results were compared with the axial compression tests, performed in the SED laboratory.

The manufactured fibre composite structures were tested in axial compression, which resulted in a maximum compressive force of 28.5kN for option 1, 15.34 for option 2 and 16.69 for option 3.The numerical result for the buckling load factor was respectively 2.41, 7.45 and 12.96 times higher than the average force at which buckling started to occur. Since the filament-winded columns are not one single element but an interaction of multiple elements, local buckling occurs before the column buckles globally. The difference between the numerical model and the laboratory test can be addressed to the material properties and assumptions, fabrication errors leading to imperfections and test set-up and boundary conditions.

Based on this research, it is feasible to create an optimized design by robotic filament winding using bio-based flax fibers. The fabrication process was successfully optimized to use (flat) flax fibers in robotic manufacturing at TUe. The research shows that it is possible to simulate the fabrication process and verify test results using a numerical model in Oasys GSA and Karamba3D. Despite some imperfections, the structural performance of the winded structures is promising. However, there are important considerations and challenges in manufacturing these elements, including ensuring consistent quality, dealing with variability in material properties and achieving precise control over the winding process. In addition, analyzing the structural performance of these structures is complex because of the variability and potential for imperfections. Further research is needed to address these imperfections, improve the reliability of the fabrication process and determine whether robotic winding of filaments with flax and epoxy resin is suitable for large-scale structural applications.

Contents

List of Figures

List of Tables

1 Introduction

In modern construction industry, the aim to use sustainable materials and techniques has become essential, driven by the need to reduce environmental impact and greenhouse gas emissions, as buildings consume up to 40 percent of the world's energy and the construction industry is responsible for half of global greenhouse gas emissions [3]. Governments are looking at ways to accelerate investment in net-zero/low-carbon buildings, and the essential role of the building sector is well recognised as an element to achieve the Paris Agreement's goal of limiting global warming to below 2 degrees Celsius. [8] Traditional building materials often contribute significantly to these emissions. The preference for traditional materials is mainly due to expertise in their use and cost-effectiveness.

In the context of traditional building materials, a common problem relates to the limited use of structural components, as can be seen in various research papers about topology optimization of concrete structures [34], allowing for material savings and a shift to environmentally friendly alternatives. One such promising route lies in the innovation of coreless robotic filament winding, particularly using natural fibers, as a tool to revolutionize the construction industry and address the shortcomings of conventional materials. Bio-based materials, such as natural fibers, offer a potential solution to the problem of energy-related pollution in the construction industry. Materials derived from renewable resources, such as flax, jute and hemp, have properties that make them both environmentally sustainable and easily available. [13].

In addition, labour shortage in the construction industry is a growing problem worldwide. Increasing demand for construction projects and ageing staff have resulted in an insufficiently skilled workforce. This shortage affects project delays, increased costs and highlights the need for investment in training and recruitment to support the sector. There is a shortage of construction staff in the Netherlands. For instance 28 percent of vacancies in the construction sector are not filled, according to the UWV Netherlands [1]. Solving the labour shortage in the construction sector can be helped by introducing advanced manufacturing methods. By integrating automated processes, such as 3D printing, prefabrication and robotics. Robotic manufacturing methods for bio-based fibers are Filament winding with auxiliary structures and Coreless filament winding.

Previous studies on University of Technology in Eindhoven have demonstrated the feasibility of robotically winding structure with resin-impregnated sisal rope and auxiliary structures. The research of L.P.J. Krijnen [22] resulted in a three-dimensional column which was tested on axial compression. In Stuttgart, The research of Marta Gil Perez et al. [13] showed the possibility of natural fibers used in Coreless filament winding. Coreless robotic filament winding (CRFW) offers a manufacturing method without using auxiliary structures, providing an innovative solution for sustainable construction.

With the knowledge of the completed projects and in view of the aforementioned challenges, This research aims to design and manufacture a three-dimensional structure using bio-based materials and CRFW technology. By optimizing the design and manufacturing process, this study addresses the environmental impact and labor shortage issues in the construction industry. The primary material used is flax, chosen for its sustainability and availability, impregnated with partly bio-based epoxy resin. The research aims to develop a structural element capable of withstanding axial compressive forces, demonstrating the feasibility of using CRFW with bio-based materials for large-scale structural applications. It is important to conduct research of new materials since the building industry is doubtful to apply these materials in the built environment without thorough testing [2].

The research question of this graduation thesis is formulated as follows:

"How can a three-dimensional optimized parametric structural element, constructed with bio-based flax fibers, be manufactured using Coreless Robotic Filament Winding (CRFW) technology, and how do structural desk studies relate to lab testing?"

This thesis is organized into several chapters, each addressing different aspects of the research:

- Digital Design of the Structure - Digital design process using Rhinoceros and Grasshopper software, including the optimization of the structure using the Karamba3D and Octopus plugins.
- Manufacturing Method - The manufacturing process of the structure, including the setup of the filament winding and curing processes.
- Materialization - The materials used in the structure, particularly natural fibers and resin matrices, and their properties.
- Manufacturing of the Structure - The step-by-step manufacturing process, including the setup and testing of the new robotic filament winding method.
- Numerical Model - Presents the numerical model used to simulate the manufacturing process and the calibration of the model with the actual structure.
- Testing the Element - This chapter discusses the testing of the manufactured structure under axial compression and compares the results with the numerical model.
- Discussion - A discussion of the results, including the limitations and implications of the research.
- Conclusion - This chapter concludes the thesis by summarizing the findings and suggesting directions for future research.
- Recommendations - Recommendations for further research and potential applications of the findings.

By following this structure, the thesis provides a exploration of the design, manufacturing, and testing of a bio-based, robotically manufactured structural element. This graduation research aims to integrate new insights into constructing structures with bio-based materials with existing knowledge from previous studies. Specifically, this research is innovative for Eindhoven University of Technology by applying a new type of fiber with a flat cross section instead of a round one, requiring new applications in the manufacturing process. In addition, it uses a new manufacturing method to make structures without using internal formwork. Simultaneous impregnation of multiple fibers, allowing them to be bundled after impregnation, is also in development.

2 Digital design of the structure

This project focuses on designing a one-meter fiber composite 3D structure that is simply supported at both ends. The main objective is to optimize the structure to withstand axial compression. The structure will be manufactured with bio-based Flax fibers. Figure 1 illustrates the research focus, with the dashed line indicating the anticipated design for the filament-winded structure.

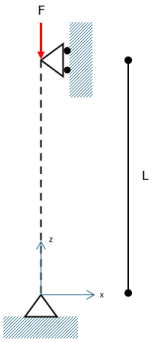

Figure 1: Schematization research question

2.1 Reference projects

In the construction industry, much research is done on new initiatives to optimize the use of materials. For example, research is done on the use of composites in construction. Figures 2-6 show reference projects for this research, where a structure or part of a structure is designed using digital design processes and robotics. Figures 2 - 5 show reference projects where research is conducted at the University of Stuttgart, especially the reference project showed in figure 5 is interesting since this pavilion is build with flax fibers.

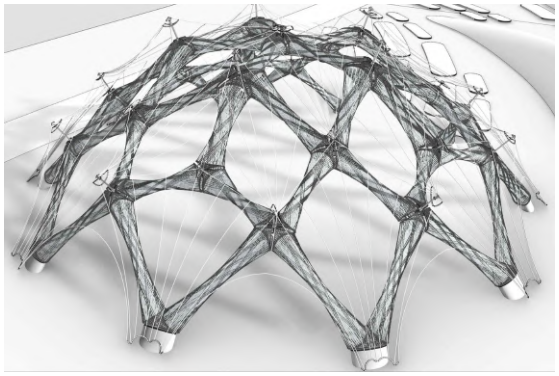

Figure 2: BUGA Fibre Pavilion [14]

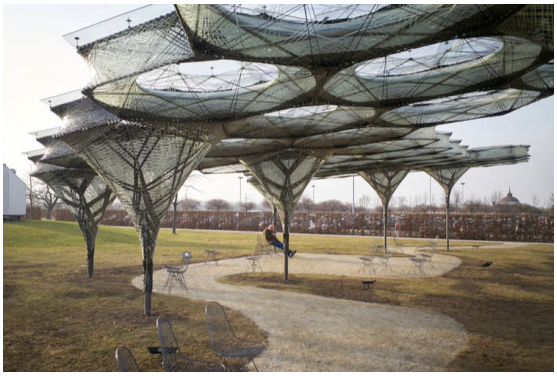

Figure 3: Elytra Filament Pavilion, 2016 [25]

Figure 4: ICD/ITKE Research Pavilion 2013-14 [9]

Figure 5: ICD/ITKE LivMats Pavilion [13]

Figure 6 and 7 show the previous research done at Eindhoven University of Technology. The research of L. Krijnen [22] resulted in a structurally optimized column which is manufactured with auxiliary structures and the research of T. Pannekeet [35], which resulted in an optimized roof beam created with the coreless filament winding technique.

Figure 6: Filament Winded Column [22]

Figure 7: Coreless Filament winded roof beam [35]

2.2 Reference Study

From these reference projects a lot of information is gained. The University of Stuttgart identifies crucial factors in the design process utilizing filament winding techniques for structures. Firstly, robotic filament winding is a tension-driven process with fibers spanning between anchor points or contact points with other fibers. Since fibers are stronger in tension and prone to buckling in compression, the fiber use in tension should be maximized at all times. Secondly, the fiber span should be reduced to increase the buckling strength, which can be done using fiber interlocking. Thirdly, adding surface curvature perpendicular to the stress direction increases the buckling strength. [7] [22]

Since the final form will be a compressive structural element, it is crucial to think about the possible failure modes. Slender structures under axial compression often fail due to buckling, as depicted in Figure 8, which illustrates the critical buckling shape and Euler's formula for predicting the critical load of a simply supported column. Given that the column's length is fixed at one meter, its critical length also remains at one meter. To accommodate manufacturing constraints of the robotic coreless filament winding technique, the optimal shape must be determined through a shape study, focusing on anticlastic shapes.

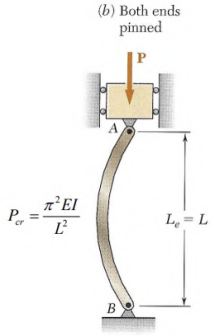

Figure 8: Euler formula for pinned column [28]

The research by Bodea S. et al. [5] applied the coreless multi-layered fiber system principle in their design logic, which is also utilized in the design of the Buga fiber pavilion, as illustrated in Figure 9. This principle uses a relatively structurally weak layer (glass fibers that are significantly weaker than the carbon fibers) as a lattice creating a surface, where the structurally stronger layer is winded where needed (flow of forces). The model of the this fiber lay-up system is set-up as follows: From the boundary frames and winding pins the global geometry is defined and the glass fibre lattice layup is simulated. Afterwards, the body produced by glass fibers is used to generate a surface. This surface is the base on which the carbon fibre layup is projected using the geodesic of the curve connecting winding pins. [14]

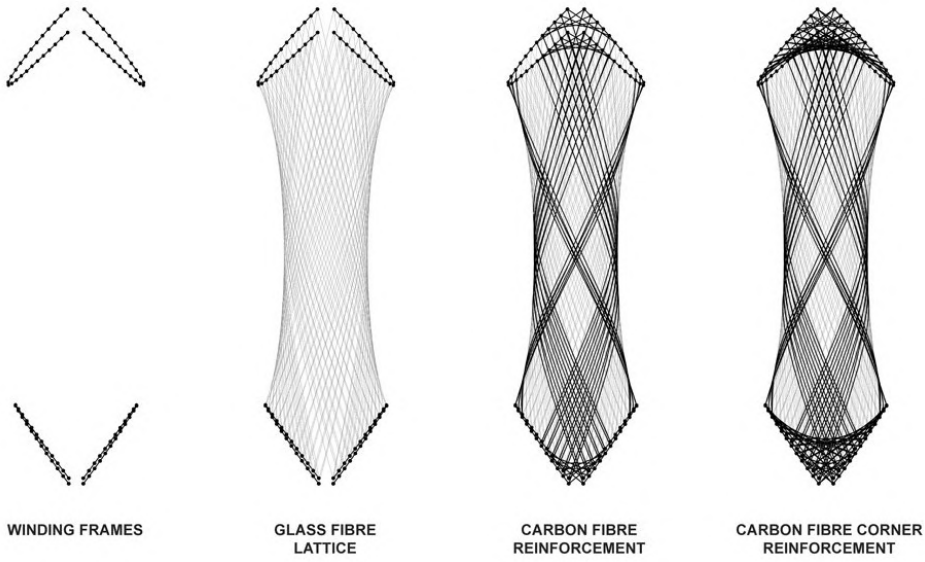

Figure 9: Coreless multi-layered fiber system principle [5]

2.3 Digital design

The digital design of the structure is performed in the parametric moddeling software Rhinoceros in cooperation with the plugin Grashopper (RG). The first part of the grasshopper script defines the geometrical part of the 3D structure. This geometrical part is composed in two stages. First, the shape is found which winding lines will serve as a supporting structure of the diagonals that are winded around this shape in the second stage. By defining the structure in RG several parameters are used to construct the element.

The shape is found to be a hyperboloid by using the skew line principle as demonstrated in the research paper of F.Maden et al [24]. This principle uses straight lines which are skewed at an angle and revolved about a vertical axis of the structure. Figure 10 shows the parameter set-up for generation of the design. The parameters which were needed to define this structure geometrically are: firstly two identical base curves with a radius of r (b) spaced at a distance h (a) are constructed on two horizontal planes. Secondly these base curves are segmented into n equal parts through points (c). The minimum number of points is limited to three, because the hyperboloid can be defined with at least three skewed lines. The segment angle is calculated by dividing 360 degrees (or 2π) by the number of segments. First, straight lines are made between these points before skewing (d). In mathematical terms the hyperboloid is created by rotating the points (c) a defined angle on the circumference of the base curves. Since these points are the winding pins, this angle is predefined by the segmentation. By rotating only the bottom points both clockwise and counterclockwise a hyperboloid shape emerges (e). However, a limit is defined to the angle that can be rotated, as the hyperboloid must remain a one sheet hyperboloid. When the points are rotated about the vertical axis, it will become a cone at 180 degrees and a two sheet hyperboloid at more than 180 degrees. The lines that form the hyperboloid represent the first winding sequence of the flax fibers. This winding sequence creates a formwork for the next layer. For simplicity, this layer is named the 'lattice layer'.

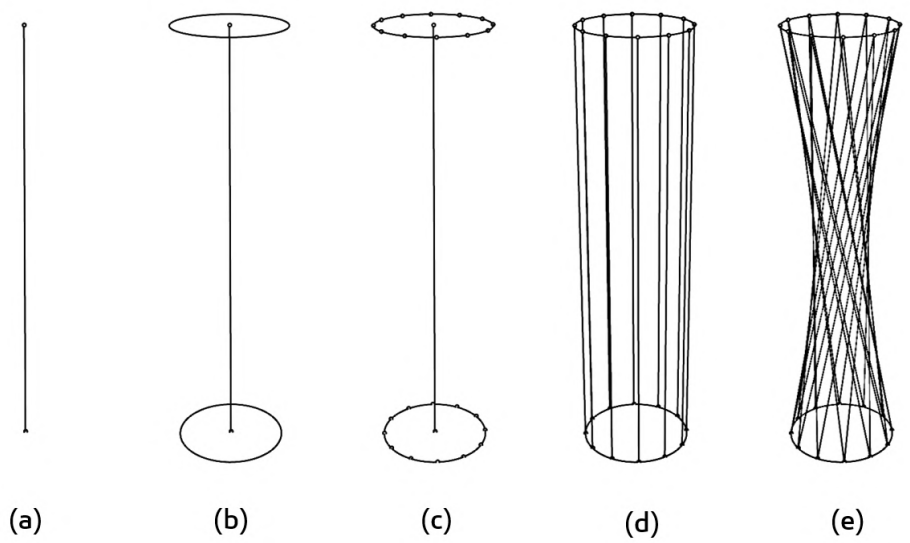

Figure 10: Parameter set-up

The hyperboloid body of lines of the lattice layer is transformed into a surface of revolution by using the intersections of the skew lines. This body serves as the base of the diagonal curves, which will form the next layer of winding lines. The next sequence of winding lines is called 'reinforcement layer' for simplicity. This layer is created by diagonal (spiral) lines. The generation of the diagonals follows the NURBS-based methodology, explained in the paper by A. Deetman et al. [15] This approach involves the implementation of small geodesic lines to achieve an optimal spiral pattern around the surface. Figure 11 shows the steps to create these curves. First, the surface of revolution is reparametrized, constraining both its vertical and horizontal domains within the 0 to 1 range. Subsequently, the surface is divided into sections along its length (a). For optimal results, it is advisable to divide the cross-section into numerous segments. Increasing the number of sections helps to minimize errors in the diagonals generation, leading to a more seamless spiral outcome. The starting point of the winding line is then defined at one of the two edges. From this starting point, the endpoint of the line is approximated using the Pythagorean theorem, taking into account the initial angle θ and the height of the first layer. Following this, a geodesic line is formed between the starting point and the estimated endpoint. This step is repeated up to the other side of the structure.

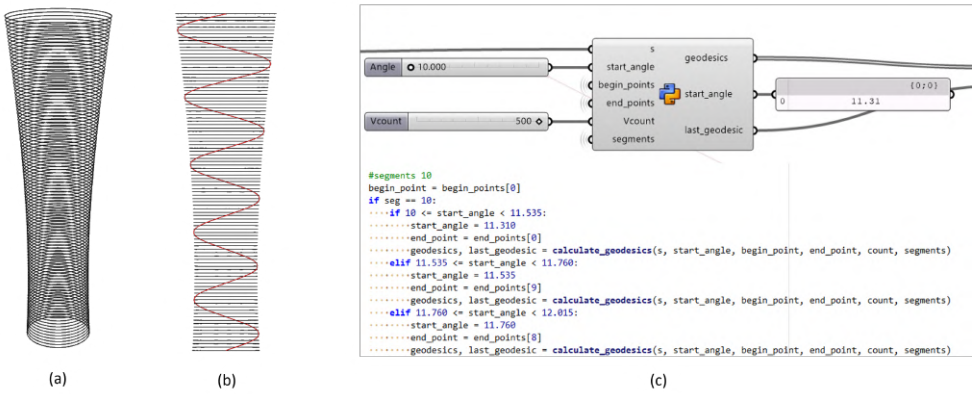

Figure 11: Generation of diagonals with Python component

When creating these diagonals, it is important to understand that they are referred to as 'locally geodesic.' Essentially, this means that within the segment where the diagonal is formed, it behaves like a geodesic line (shortest path between two points). However, when considering the entire surface, this line will not be globally geodesic. This is necessary to create a spiral. Because if it were a global geodesic line, this line would follow the shortest path from the begin to the end point across the surface. For example, consider a structure with 12 points forming a surface. A diagonal line is required from point 0 to point 12, where point 12 is equivalent to point 0, see figure 12. The geodesic connecting these points is parallel to the seam line of the structure and is not forming a spiral around the structure.

Figure 12: Geodesic line shortest path

When forming the structure, a shift is determined. The shift is the number of points that the upper point is shifted relatively to the bottom point. For example, when referring to a shift of 1, the top point is shifted either 1 point to the left or right to create the diagonals. With a higher value for the shift, the more slanted the diagonal will be across the surface.

The diagonals are generated using Python within the RG software. Initially, a code is written to calculate diagonals for all possible angles. A starting angle $\theta = 0°$gives a fiber path confined within the boundary, while the paths do not touch the other fibers for a starting angle of $\theta = 90°$. Extreme angles represent cases where fibre interaction cannot take place effectively, making them unsuitable for winding. Therefore, these angles are considered non-windable, the range for windable angles is set to a minimum of 10°and a maximum of 89°. To address the issue of generating diagonals between known start and end points (the winding pins), the Python script assigns an angle to each endpoint. This approach avoids relying on random endpoints and ensures precision in the design process.

The script collects data for a range of 11 to 16 points, as fewer points may lead to insufficient contact points, while more points may restrict the robot's movement along the winding pins. After gathering the data for all points and their corresponding angles, the script uses an if-loop to match each endpoint with its designated angle. This method improves the accuracy and efficiency of the design generation process (c). The Python script starts by generating a single diagonal. This diagonal is then duplicated, rotated, and mirrored to construct a network of diagonals.

The lattice layer, without any supporting structure, will act as a support for the reinforcement layer, which will be winded around it. However, it seems that the flax fibers in the lattice layer deform during the winding process. As a result, the model in RhinoGrasshopper is mainly used for the production of the structural elements, recognizing the deviation from reality. As mentioned previously, the structure constructed by the robots will be compared and calibrated with a numeric model. Using this geometrical model, various design variations can be generated. Figure 13 illustrates some examples that can be achieved with this model.

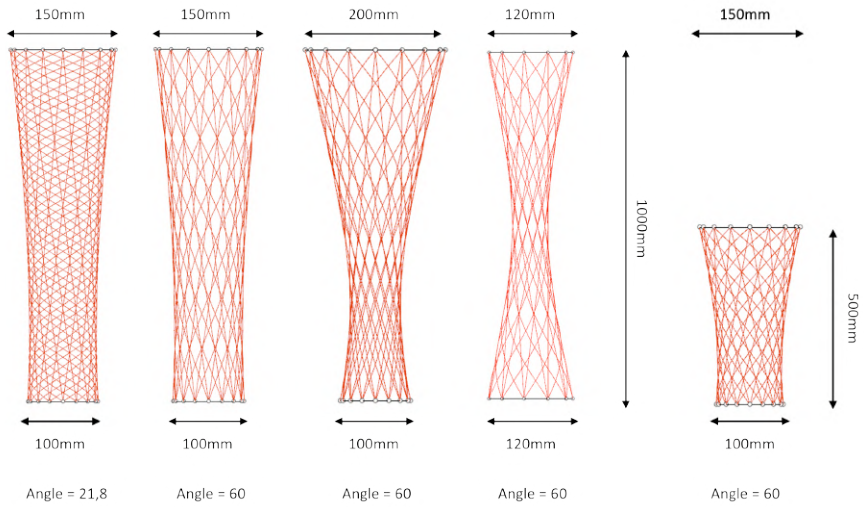

Figure 13: Possible design variants of geometrical model

2.4 Optimal form study

As described in section 2.2 slender structures loaded in compression are often prone to buckling. Research by L. Krijnen [22] shows that performing the construction synclastic is advantageous for stability, due to buckling because of the narrow construction. Since no core or auxiliary parts are going to be used in this project, it is impossible to filament wind a synclastic structure. Therefore, a shape study is considered for the optimal shape that will be used to wind the final element.

Three different shapes are used, see figure 14. The traditional circular column shape with no curvature (1), an anticlastic shape (2) and a combination of two anticlastic shapes generating a synclastic shape (3). First, these shapes are made as shell models. Keeping the surface of these shapes the same as a parameter (A). This comparison of shapes considers the buckling factors following from a Karamba3D calculation with a load of 1 kN. If it is considered as a shell structure to reduce the influence of the material arrangement of the winding lines, the combination of two anticlastic shapes appeared as the stiffer structure. The results of this calculation are displayed in Table 1. (The circular structure is only mentioned for comparison purposes, as the coreless filament winding technique cannot replicate this structure, because the flax fibers will deform by placing the reinforcement layer).

Table 1: Bfacs comparison

Nr.	Name	Bfacs (-)
1	Circular (no curvature)	119.42
2	Anticlastic structure	56.96
3	Combination (synclastic)	109.21

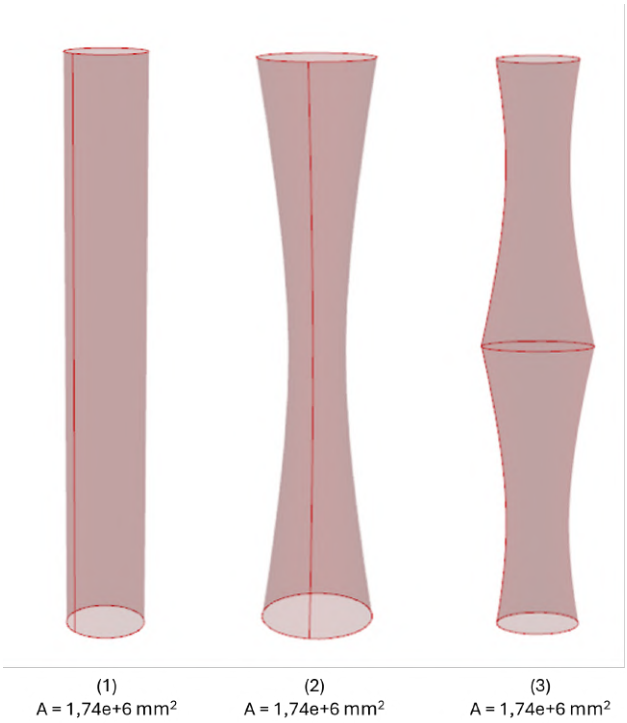

Figure 14: Three different shell models shape study

However, the analysis shows that the material and manufacturing technique used have a major impact on the performance of the structure. This is because more material tends to accumulate at the weaker points of the shape (e.g. more material in the centre of the anticlastic variant). As a result, when comparing different variants, the anticlastic variant is found to be the most effective in terms of material properties rather than relying only on shell structures for comparison. When comparing the two structures, both anticlastic and combination configurations are used to determine their respective performance. Different set-ups are tested while maintaining a consistent mass (equal to the length of the fibers to be used). Table 2 shows the results of the different configurations, these results show that when the same mass value and buckling factors (Bfacs) are used for comparison, the anticlastic variant shows better performance against buckling failure.

Table 2: Bfacs comparison anticlastic and combination variants

Option	BFacs (-)	Mass (kg)	Displ.(mm)	Length(m)
Anticlastic, 45°, 5mm	7.87	2.33	0.047	102.56*
Anticlastic, 45°, 8mm	46.89	6.22	0.016	102.56*
Anticlastic, 24.47°, 8mm	110.94	7.75	0.017	127.87*
Anticlastic, 11.31°, 8mm	196.58	12.49	0.018	203.48*
Combination, 45°, 5mm	7.42	2.33	0.080	102.79*
Combination, 45°, 8mm	39.93	6.22	0.023	102.79*
Combination, 24.47°, 8mm	68.60	7.63	0.021	125.26*
Combination, 11.31°, 8mm	113.90	11.81	0.021	193.79*

* If the required diameter cannot be achieved with just one winding sequence, the length will increase as additional sequences are needed to reach the desired diameter.

2.4.1 Structural behavior

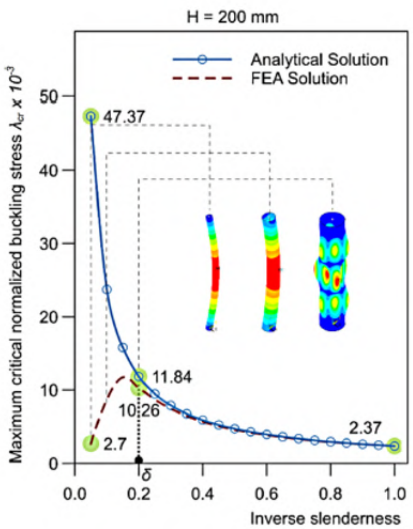

Figure 15: FEA and analytical solutions [17]

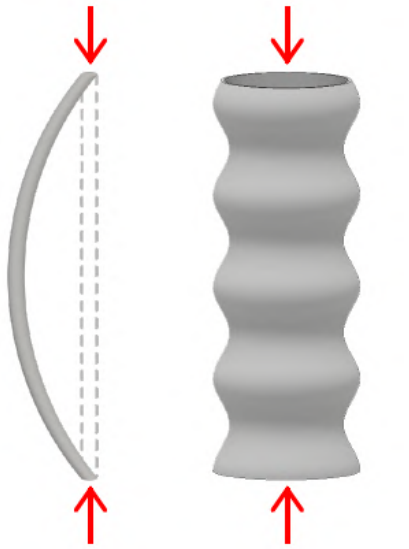

Figure 16: Local- versus Global buckling [4]

With these results, the behavior of the structure remains unidentified, especially whether it fails due to local buckling or global buckling. With local buckling, specific components within the structure fail, while with global buckling, the entire structure fails. Figure 16 shows the difference between local and global buckling. Analysis of the results shows that the structure is prone to local buckling under compressive loads. Regardless

of whether the structure is configured in an anticlastic or combination variant, the structure consistently fails due to local buckling. This is consistent with existing literature, which generally indicates that structures with winded filaments are prone to failure due to local buckling. Structural failure due to local buckling makes sense when considering the surface properties of the winded filaments. Local buckling often occurs in structures with complex laminates and an-isotropic materials such as fiber reinforced polymers, which have specific stiffness directions that vary across the surface of the structure. This variability in stiffness can lead to local stress concentrations that cause buckling in restricted areas, rather than across the entire structure. [29]

The study by Guo et al. [17] investigates the buckling behavior of cylindrical shells under axial compression. The shells are divided into groups with different heights and different inverse slenderness ratios (ratio of diameter to height). Both analytical solutions and Finite Element Analysis (FEA) are used to investigate and compare the buckling behavior. Figure 15 shows one of the studies performed in this paper of FEA and analytical solutions providing the maximum critical buckling stress for circular cylinders under a compression force of 1 Newton.

Important points of interest in this study are: 1) For higher inverse slenderness ratios (closer to 1.0), there is a closer agreement between FEA results and analytical solutions. This suggests that FEA results become more reliable the more the scale resembles a long and wide cylinder. 2) For very low inverse slenderness ratios, FEA results show significant deviations from analytical solutions. For example, at an inverse slenderness of 0.2, an asymmetric waveform is observed in the scale, while at even lower ratios global buckling of the entire cylinder occurs. 3) A threshold δ is identified on the inverse slenderness axis of the FEA curve separating the buckling behavior. Within the interval [δ, 1.0], the normalized buckling stress decreases with increasing inverse slenderness. Outside this interval, the FEA results deviate from the analytical solution and global buckling is more likely.

The study by Guo et al. illustrates that for designing structures under axial compression, it is crucial to carefully consider the ratio of diameter to height.

2.5 Optimized Final design options

As described in section 2.3, the lattice layer acts as a support for the reinforcement layer, which will be winded around it. However, The flax fibers in the lattice layer deform during the winding process. As a result, the model in Rhino Grasshopper is mainly used for the production of the structural elements. Therefore, an approach featuring three different designs, each representing a different configuration or angle, is adopted. In order to ensure design consistency across the three variants, attention is paid to determining the required fiber length and therefore maintaining the same mass for three different variants. It is necessary to ensure uniformity in fiber length among the variants, so an examination of multiplies within each configuration of the design is conducted. In particular, fiber length depends on three key design input parameters: 1) the radius of the top and bottom circles, 2) the number of points distributed along these end circles, and 3) the angular orientation of the reinforcement layer relative to the axis of the structure. Of note is the fixed nature of the lattice layer within each design, which maintains a consistent shift of 1 point. (Consequently, changes in the radius and number of points may affect the fiber length, but the fixed position of the lattice layer ensures uniformity in all three designs.)

Given the diversity of parameters affecting this length, performing a numerical analysis in a tool such as Excel would require unnecessary effort. Therefore, to determine the optimal design options, an optimization script was developed using the Octopus optimization plug-in. Octopus is a Grasshopper plug-in that applies evolutionary principles to parametric design and problem solving. It allows to search multiple goals simultaneously, producing a set of optimized compromise solutions between the extremes of each goal. [30]. The optimization procedure involves generating two different designs in which the radius and number of points remain consistent while the angle of the diagonal lines varies. This process produces two designs characterized by different total fiber lengths. A script was written to maximize the length of one design and

minimize that of the other. Moreover, an additional function was incorporated to ensure that only solutions that satisfy a specified criterion are generated; namely, the lengths of the designs must be within a tolerance range of 0.5 units, by means of a true boolean condition. This condition specifies that the length of one design always closely matches twice the number of meters of the other design, so that there is a consistent relationship between the two designs and thus they are multiples of each other. The octopus set-up is shown in figure 17.

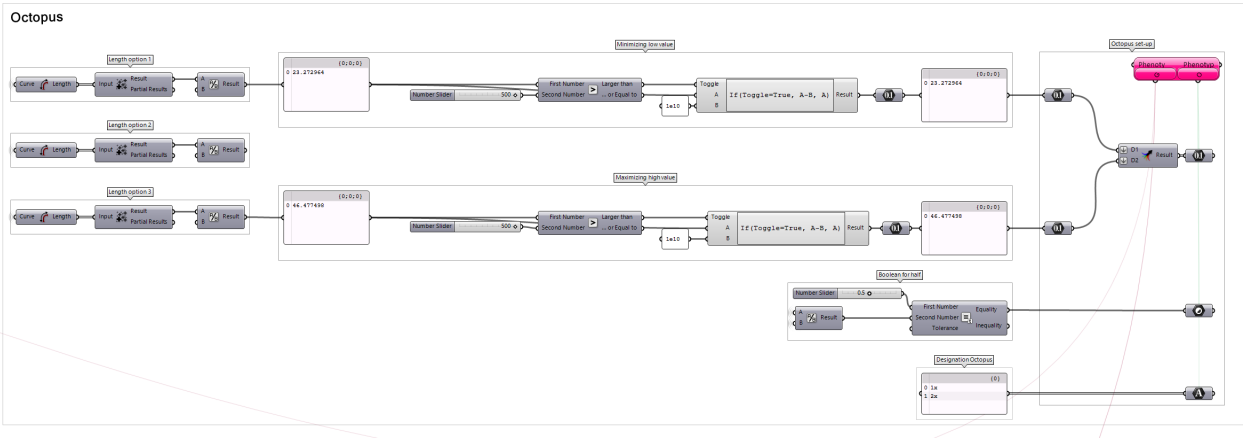

Figure 17: Octopus optimization set-up

Figure 19 shows the final result of the Octopus optimization, where the solutions closest to the origin represent the best design options. The design parameters associated with the solution are as follows:

Height of structure	1000 millimeter
Radius top and bottom	124 millimeter
Number of points	11 Points
Shift option 1	5 shifts (angle $\beta = 65.680°$)
Shift option 3	27 shifts (angle $\beta = 22.185°$)

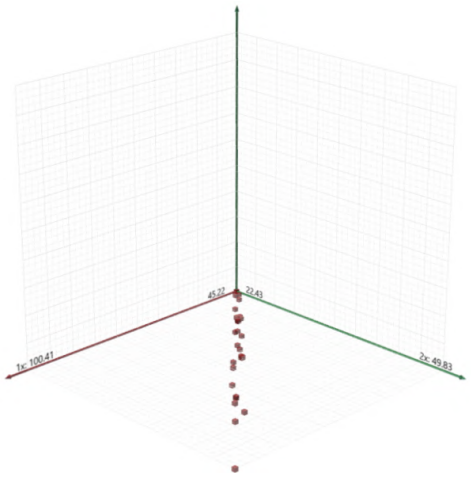

Figure 18: Octopus overview

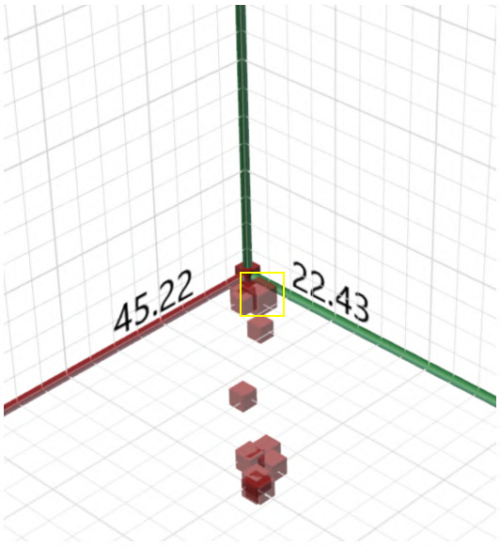

Figure 19: Octopus chosen option

Due to the complexity of identifying three feasible options within the existing Octopus script, Microsoft Excel was used to select the third option. All relevant data regarding the lengths of the optimized design were exported to an Excel spreadsheet. Through empirical analysis, an appropriate shift of 14 was determined that could be included as the second design option.

Table 3: Shift options

Shift	**Length (m)**	**No. of winding layers**
5	23,27	4x
14	30,58	3x
27	46,48	2x

Table 3 provides the meters required to generate each option, focusing only on the reinforcement layer since the lattice layer remains consistent across all options. To ensure the same fiber mass is used for each option, the option requiring the least amount of fiber will be winded more times than the other options, as indicated under the 'no. of winding layers' in Table 3. This process is visually represented in Figure 20.

Figure 20: Visual representation No. of windings

This results in the following total length of meters needed to theoretically manufacture the reinforcement layer of the structure shown in table 4. After manufacturing the final structures, the elements will be weighed to determine if the model generation matches reality.

Table 4: Total amount of meters

	Option 1	**Option 2**	**Option 3**
Meters Total**	93,10	91,73	92,96
Difference in m		1,37	0,14
Difference in %		1,46	0,15

** The total amount displayed in this table is only the amount of meters needed for the reinforcement layer of the structure.

2.5.1 Geometrical final design options

The final geometric design resulted in three options that will be manufactured by the ABB IRB 1200-5/0.9 robot. The three options require the same length of fiber for the lattice layer, this length is approximately 22.1 meters. Figure 21 shows the design options as these will be manufactured with corresponding angles of the lattice layer (α) and reinforcement layer diagonals (β). Where in the figure (α) is given a black colour and (β) a red colour.

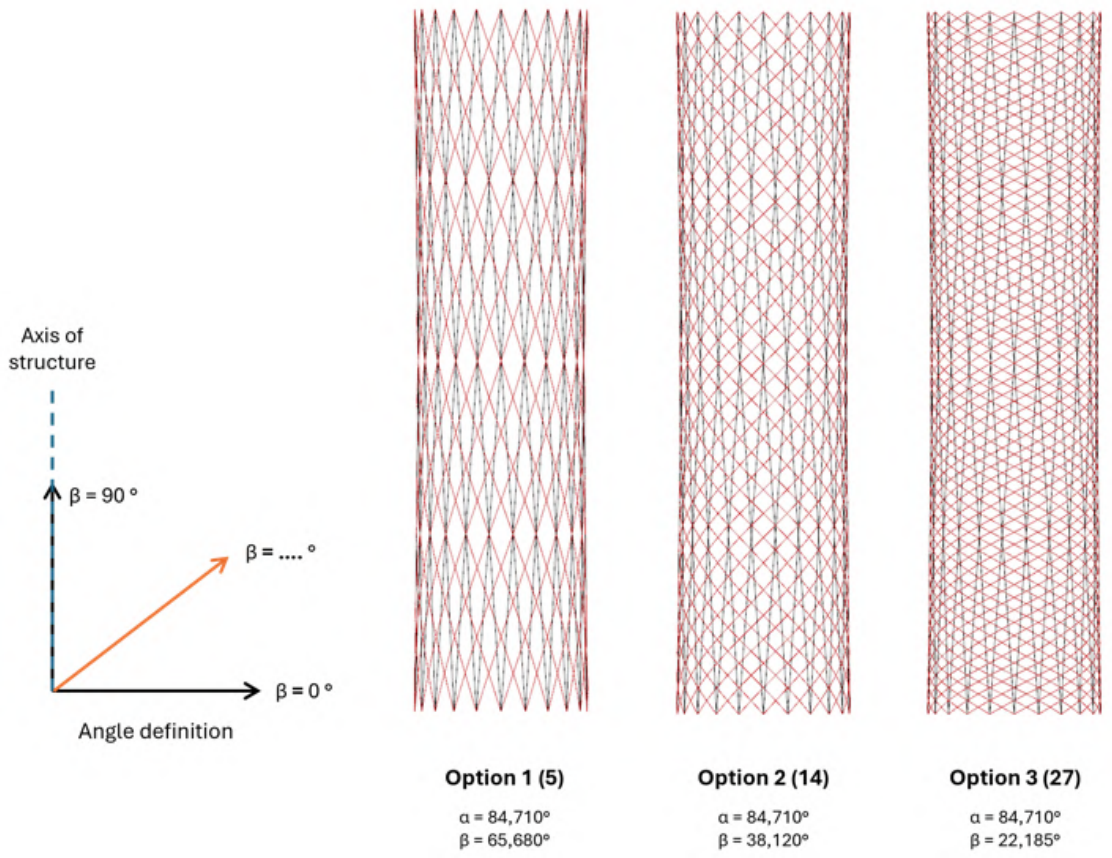

Figure 21: Final three design options

2.6 Assumptions

In creating the final design, several assumptions were used to design a structure that was feasible for manufacturing:

- Deformation of the flax fibers: M. Gil Pérez's previous research on manufacturing composite structures using flax fibers [13] revealed that the fibers are easily deformed and lack stiffness during winding in a wet state. This causes challenges in replicating structures exactly as modeled in Rhino Grasshopper. To address this issue, a new approach was considered. A manufacturing method based on the length of the fibers was devised, along with the corresponding manufacturing constraints (like amount of winding pins, height of the structure and radius of the top and bottom plate) . Consequently, a plan to translate the fabricated structures back into a numerical model is needed. This process aims to validate the model against the manufactured structure.

- Same length of fibers, same mass: Design choices are made based on the total length required for manufacturing, assuming equal fiber lengths and mass across options. However, the actual outcome may differ due to the deformability of fibers during winding. It is hypothesised that option 3 produces a more anticlastic structure compared to option 1 because of this effect. By evaluating the weight of each option after manufacturing, it can be verified that the structures indeed have the same mass and the hypothesis will be validated. This review will determine the validity of the mass-based comparability assumption.
- Parametricity of the model: The model is essentially parametric and can be easily adjusted as needed until later stages. However, it is worth noting the parametricity of the Python script. It allows for the creation of diagonals in models featuring 11 to 16 winding pins. This specific configuration was chosen due to time and manufacturing constraints. The design process faces limitations like the length of elements and the radius of end plates, which should not exceed certain values. The structure's design considers a minimum radius of 150 and a maximum of 250 millimeters, aligning with L. Krijnen's project [22]. It is crucial to ensure enough space for the robot to navigate between the winding pins. Therefore, a gap of at least 60 millimeters was maintained. With a minimum radius of 150 millimeters and 16 winding pins, this requirement is met. Hence, 16 winding pins were chosen as the maximum. For a robust design, 11 winding pins were set as the lower limit, resulting in six possible configurations. Although the script could be extended to accommodate more configurations and winding pins, it was considered as unnecessary for this project due to time constraints.

2.7 Output and translation to Robot

After the optimization of the structure, the final design options of the structures are known. To manufacture the structure by filament winding, an Euler path must be defined to wind the design options in one continuous session. An Euler path is a path that visits each edge of a graph exactly once. Similarly, an Euler circuit is an Euler path that starts and ends at the same node of a graph. [11] When designing the winding path, it is crucial to remember that the lattice layer must be winded before the diagonals, since the lattice layer acts as a formwork for the diagonals.

The Leafvein plug-in was used to define an Eulerian path. The Leafvein plug-in is a tool used to create a specific path for arranging layers in a particular order. In one part of the script, the winding path for the first layer was determined. For this, the 'Custom Graph' component was used, which uses a set of line segments of the relevant design as input. These segments were used to build a graph, with the start and end points of each segment forming the nodes of the graph. The output of this component feeds both the 'Node to Point' and 'Eulerian Cycle' components. The 'Eulerian Cycle' component produces a list of graph nodes that defines the desired path, while the output of the 'Node to Point' component allows this list to be translated into corresponding points. There is an additional option for determining the costum graph. Two nodes v and w, called endpoints, are attached to each edge. To create the winding pattern, an undirected graph was chosen. In an undirected graph, the edges are unordered pairs of nodes. In directed graphs, the edges are ordered pairs (v, w) of nodes, where v is the tail and w is the head of the edge [11].

This method was used to define an Eulerian path for the lattice layer and the reinforcement layer. The winding sequence is shown in figure 22 (e), where a polyline is drawn through the set of points to visualise the path. Logically, the second layer starts where the first layer ends. It is important to note that adjustments are made to the Euler path of the reinforcement layer. Specifically, the opposite diagonal lines are arranged to be winded consecutively. This arrangement prevents the formation of an asymmetric structure. If all diagonals were winded on one side first, the structure will deform irreversibly and lose its symmetry. Therefore, an extra feature is added to the path to ensure that these mirrored diagonals are always winded consecutively.

To complete the robot path, an Eulerian path was first generated that outlines the winding route (a), the eulerian path was created and translated into points that are in order of the winding path. At this stage, the path needs to be modified so that the robot can navigate smoothly around the winding pins. For this

purpose, semicircles were created around the winding attachment points (b). These semi-circles were integrated into the existing path, preserving the order of the points (c). The resulting path is then displayed as a polyline for visualisation (d). This process was repeated for the reinforcement layer, with the additional step of shifting the entire layer slightly outwards to avoid contact with the previously winded lattice layer. Finally, the lattice and reinforcement layers were combined into a single structure for the robot's trajectory (e).

The result is a list of points that defines a winding path with a single start and end point. This list of points serves as the input for the Robot Components script.

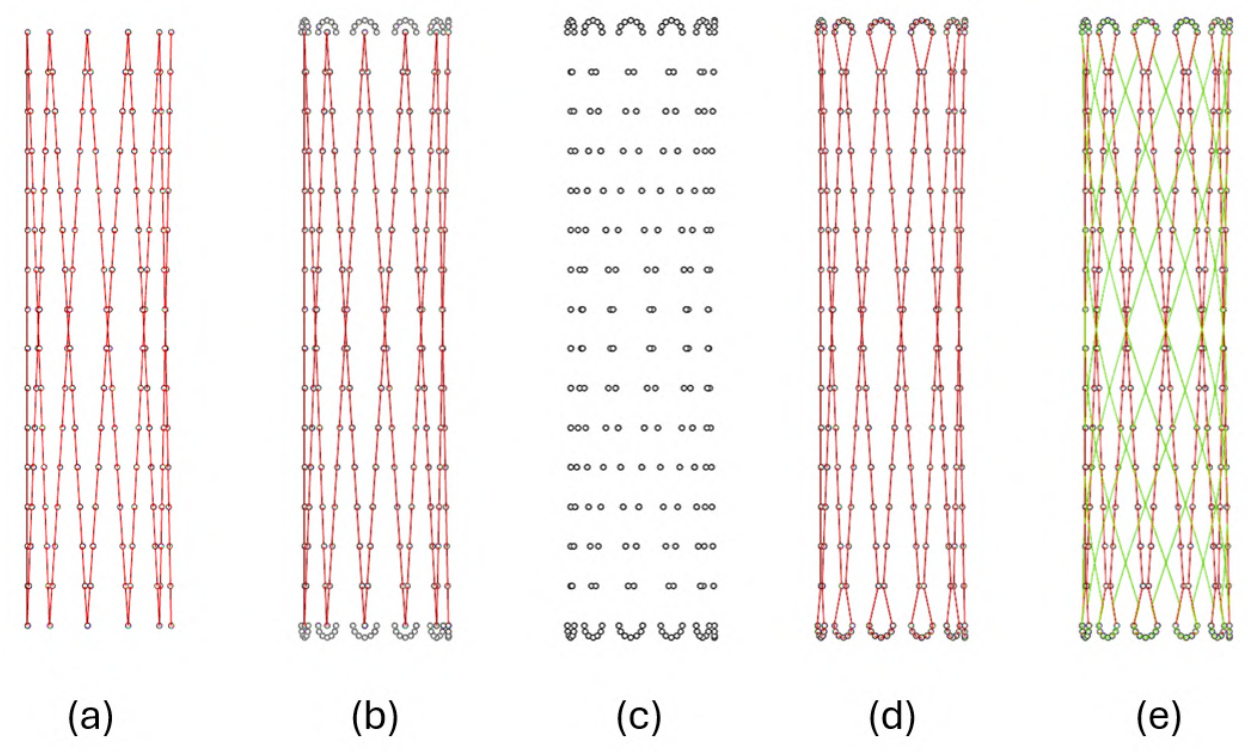

Figure 22: Generation of robot path

Several methods exist for hooking the fibers around the pins, as depicted in figure 23. A discussion started initially regarding the necessity of keeping the sleeves permanently in the structure after winding. However, it has been determined that this was unnecessary for compression testing, as the sleeves do not play a role in load induction. Therefore, options (b) and (c) have been neglected. Option (c) offers complete interlocking of the sleeves, which was unnecessary, while option (b) is only effective with a very sharp winding angle (angle configuration in Figure 21). Therefore, option (a) has been selected, where the fiber is looped around the winding pins in a semi-circle.

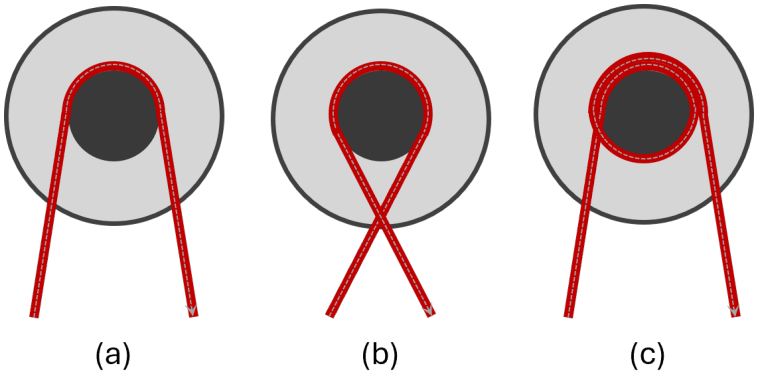

Figure 23: Hooking configurations: (a) v-configuration (b) y-configuration (c) o-configuration

2.7.1 Robot Components Script

The Rhino Grasshopper plugin Robot Components (RC) was used to generate the robot script. The output of the Grasshopper script, consisting of a list of points resulting from the path generation, serves as input for the RC script. All layers will be winded at once. Within RC, the robot nozzle and a rotating external axis, known as the 'turning table', are imported and calibrated.

A start and end point are implemented in the RC module for the robot script. The robot starts from a designated 'home' position and moves to the starting point in the sequence. The purpose of these start and end points is to avoid collisions between the robot and the end plates, the start point is located ten centimeters above the first point of the list. Once the robot reaches the start point, it can safely move downwards to continue along the list of points to produce the element.

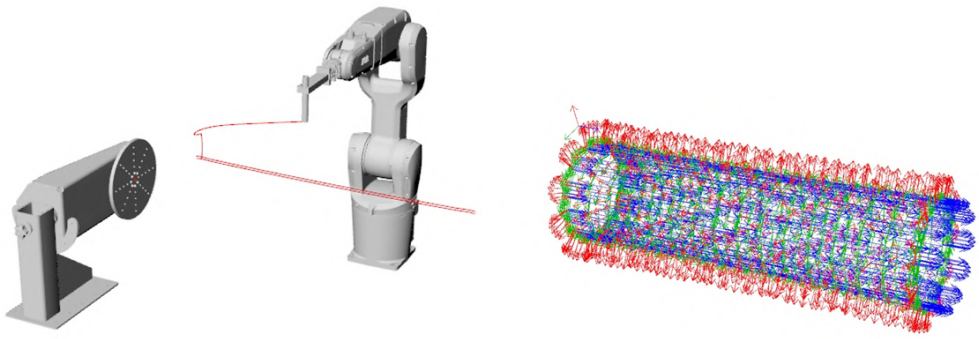

Figure 24: Robot set- up with generated path (a) Target plane orientation on movable work object (b)

To ensure accurate placement, all target points are aligned with the movable work object. This requires matching the planar orientation of the work object with that of the target points. Additionally, the external axis value and planar orientation of each point affect how the robot approaches them. To optimize movement efficiency, it is preferable for the robot to move laterally, from left to right, without unnecessary rotation. So, the target points should face outward, facilitating smooth movement along the structure. Once all orientations are set, the 'Robot Target' component combines the data to generate a list of robot targets, see figure 24 for the robot set-up and target planes.

This list, combined with the movable work object, dictates the robot's movements. A continuous speed of

100 mm/s is maintained for the winding process, with a joint movement to the first target and subsequent linear movements.

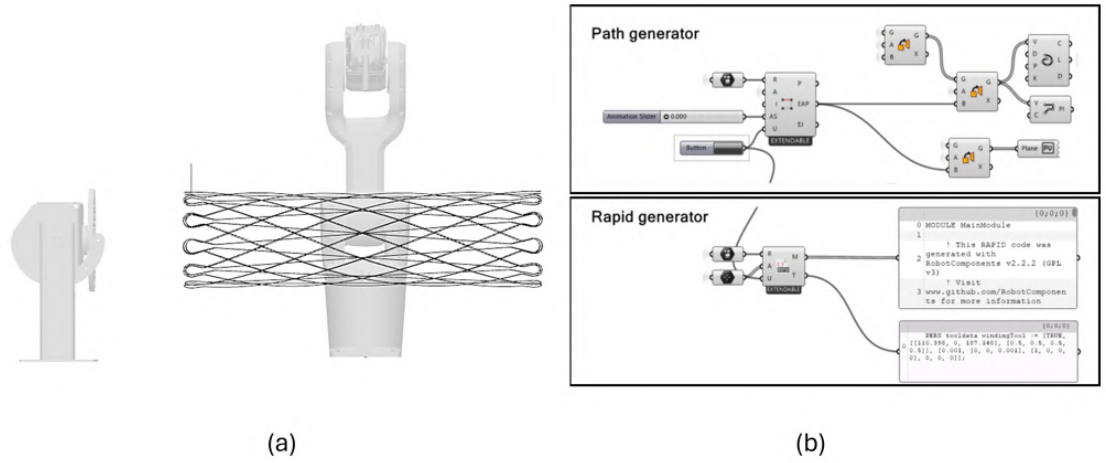

Figure 25: Robotic visualisation of winding path in robot studio (a) Path generator and Rapid code generator RobotComponents (b)

These actions are compiled into a list of actions for further processing by the 'Path Generator' and 'RAPID Generator' components. The former calculates the robot's path and simulates its execution, while the latter generates RAPID Program Module (PM) and System Module (SM) scripts. The PM script defines robot movements, while the SM script determines the robot head orientation based on the end effector. The resulting structure after winding path completion is depicted in figure 25. Also referring to Appendix D for an overview of the Grasshopper scripts and Appendix E for an overview of the RC script.

2.7.2 Robot Studio

While Robot Components path generator is fairly accurate, there is no provided guarantee that the simulated path does not differ when executed on a real robot. Therefore, the RAPID code is integrated into Robot Studio to simulate the winding process. Initially, errors appeared indicating that the robot axis was not in range, indicating that the robot arm was unable to complete the movement. This problem was solved by accurately defining the external axis values for each target point and ensuring alignment of all target planes, as described in section 2.7.1. After re-executing the scripts, the programm completed the full path without errors. With this validation, RAPID code scripts were ready for use in production.

3 Manufacturing method

This chapter describes the production method for manufacturing of the optimised structure using the robotic coreless filament winding technique. It includes explanations on the design of the robot end-effector, the winding procedure and the parameters that determine the curing cycle.

3.1 Robotic coreless filament winding

The manufacturing process of a design using the coreless filament winding (CFW) technique consists of three steps that produce the final design. First, the process begins with the impregnation of flax rovings in a resin bath. Through this immersion, the fibers undergo an impregnation process, which completely impregnates them with epoxy resin. The impregnated rovings are then passed through a robotic nozzle, where the design takes shape under precise guidance. Finally, the design is finished by curing.

The filament winding technique, a method used in composite manufacturing, has received attention in the building sector in recent years due to its potential to produce lightweight and high-strength composite structures. There are several methods to use robots in combination with the filament winding technique: Filament winding on a mandrel, coreless filament winding and spatial winding. See figure 26.

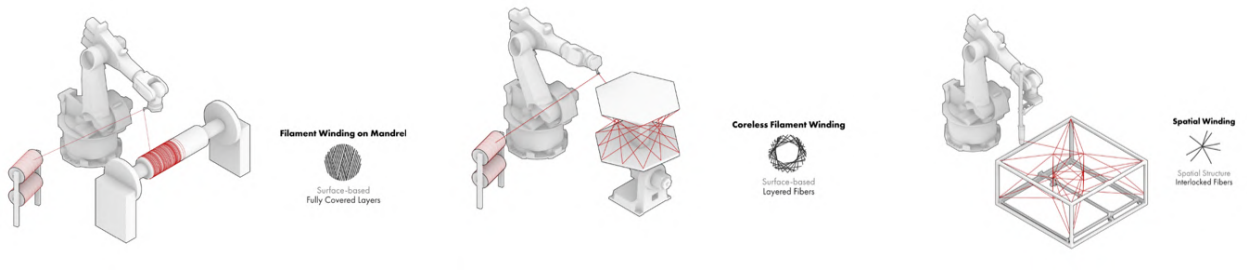

Figure 26: Various filament winding techniques [10]

This project uses the CFW technique where only the end plates are defined as supporting structure. This technique is based on layering fibers and is used to create surface-based geometries. The technique involves the deposition of continuous filaments by winding it around winding pins on both ends connected to an end plate. By eliminating the core, the aim is to reduce material waste and enhance the efficiency of the winding process. Other advantages of CFW are design flexibility: the absence of a core makes it easier to wind complex and asymmetric shapes. This offers design freedom and enables the production of components with advanced geometries. Using the CFW technique can have also several drawbacks. These include reduced stability during the winding process, longer production times due to the need to use alternative methods for making designs in the absence of a core, and challenges in matching actual results with simulations from the modelling software. Due to the absence of a core, the first layers are constantly subjected to deformation by subsequent winded layers, which complicates the comparison between the actual result and simulations.

3.2 Robot set-up

3.2.1 Robot

The ABB IRB 1200-5/0.9 robot, with a reach of 0.9 meters, is utilized for manufacturing purposes within the Structural Engineering and Design lab at TU/e. Appendix C: Product specifications ABB IRB 1200-5/0.9 provides technical information on the specific robot [22]. It is configured with a rotation table as the movable work object, allowing it to work horizontally on structural elements. Calibration of the robot and rotation table positions is crucial for accurate operation, feeding data into Robot Components and Robot Studio for control.

3.2.2 End effector

An end effector serves as an attachment at the end of a robotic arm, allowing the robot to interact with its surroundings. In this research, the function of the end effector is to guide resin impregnated fibers to predetermined target locations.

Previous versions of end-effectors used in similar projects were based on winding structures with sisal rope, which has a circular cross-section. However, given the shift towards using flax fibers in this project, the demand for a new end-effector arises. The proposed solution is to develop an ring-shaped end effector. This design allows the contact area with the fibers to be minimised, reducing friction during the winding process. This makes the winding process smoother and reduces the risk of fiber damage.

The new end-effector is modelled in 3D. Inspired by L. Krijnen's project, the same end-effector will be modified. By inserting threaded holes in the base of the end effector, an aluminium plate can easily be attached. This plate acts as a spacer between the end effector and the ring and prevents collisions between the end effector and the bolts of the end plates. A 3D view of the new end effector is illustrated in figure 27

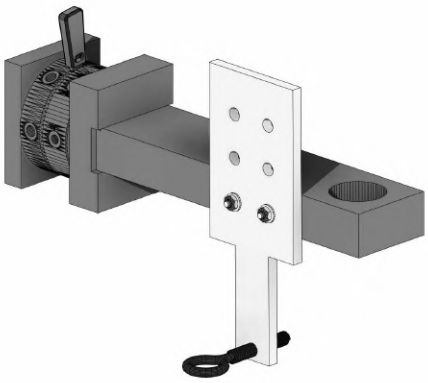

Figure 27: New end effector

3.3 Winding process

A previous study by L. Louer [23] and L. Krijnen [22] used an epoxy resin bath, designed by Louer, for a project involving sisal rope winding. However, this setup proved unsuitable for use with flax fibers. The configuration, shown in Figure 28 (a), was specifically designed for impregnating a single sisal rope with a circular cross-section. The impregnation length was limited to 20 centimetres. The rope was pre-tensioned via a rubber plate with a four-millimetre opening through which the rope passed.

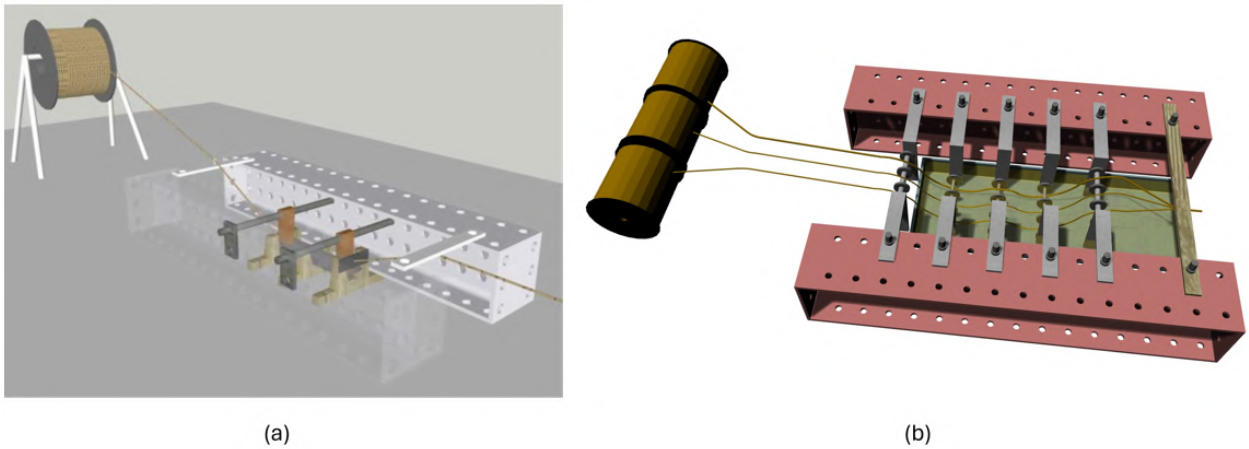

Figure 28: Existing resin bath set-up [23] (a) New resin bath set-up for multiple fibers (b)

For this project, a new setup that can be used for the CFW process with flax fibers was considered. Based on the already existing resin baths, a concept is devised to construct the same resin bath set-up with limited material. In this resin impregnation setup, three fibers can be impregnated simultaneously. Rollers and rings guide the fibers into the resin bath while maintaining separation. The bath itself will be made from a silicon container. Sufficient tension on the fibers ensures proper impregnation. Therefore, testing is necessary to ensure optimal impregnation, as detailed in section 5.4. The new set-up for the resin bath is illustrated in figure28 (b).

3.4 Curing

After manufacturing, the resin should be cured at elevated temperatures to harden. Appendix A Sicomin technical datasheet compared three different curing cycles for the SR InfuGreen 810 / SD 8824 system. The mechanical properties were optimized for a post-curing cycle of eight hours at 40 degrees Celsius. Before post-curing the structure should be stored at a minimum ambient temperature of 20 degrees Celsius. The Sicomin technical datasheet does not prescribe the relative humidity for optimal curing.

4 Materialization

4.1 Natural fibers

Flax fiber is considered a natural fiber. Natural fibers are characterised by its regrowth, fast growth, wide availability and bio-degradability. Natural fibers are abundant and more affordable compared with synthetic fibers, specifically higher density and energy requirements, renewability, no skin irritation and higher strength-to-weight ratio. These fibers with great potential are seen as substitutes for glass, carbon or other synthetic fibers. [5] Moreover, these advantages have led to the use of natural fibers for human needs and for industrial raw materials such as textiles, pulp and paper, accessories and bio-composites. [21]

4.2 Flax fibers

This research focuses on the application of bio-based natural flax fibers for structural applications, since it already showed high potential in previous research [13]. Flax is a plant (crop) that grows widely in the Netherlands, Belgium and France. Its cultivation can be divided into two categories:

- Fiber flax: for linen or fibers
- Oil flax: for linseed oil

Fiber flax is grown for its fiber. Figure 29 illustrates a cross-section of the stem of the flax plant consisting of the following parts: The skin of the stem, the bast containing the fiber bundles, the woody core and the lumen (cavity) of the stem. To obtain natural flax fibers, a process is needed to convert the raw plant into fibers, shown in figure 30. The first step is sowing seeds between March and April (1). To harvest flax the plants, the flax plant is pulled out of the ground root by root to preserve the longest possible fiber, and the flower heads are removed by rippling (2). Next the plants are spread over the ground for retting. During retting the pectin layer that binds the fibers to the bast and the flax stem is broken down (3). After the fibers are detached from the stem, the stem is broken on a so-called brake, by guiding it between ribbed rollers. The broken stems are then removed from the fiber bundles in the scutching turbine, which in effect scrapes the fibers, removing the broken ligneous fibers (4). The scutched fibers are called fiber bundles and are still relatively coarse and thick. The coarse fiber bundles are then combed in the hackling process, refining the ribbon-shaped fiber structure into fiber rovings which can be used in composites. [6]

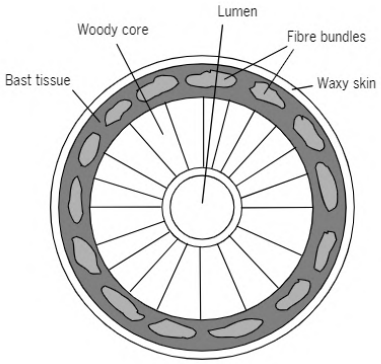

Figure 29: Cross-section flax stem [6]

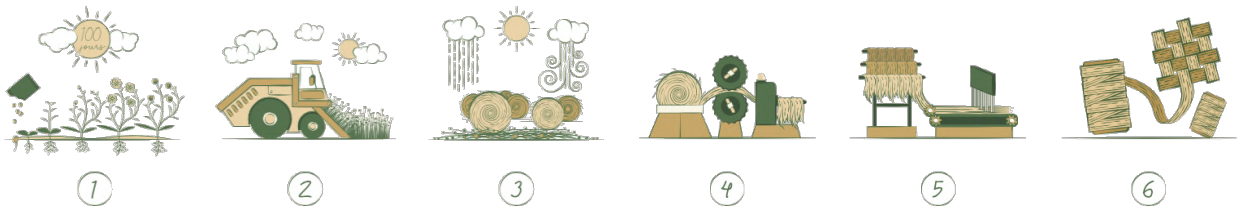

Figure 30: Flax roving production stages [16]

Because flax fibers are made from plants, the size and quality of fibers can be affected by environmental conditions such as growth, location, nutrients, temperatures and seasons. The harvesting stage, thickness and bonding between these fibers also affect their quality, while the shape, size, orientation and thickness of cell walls affect the properties of a single fiber. [6]. The presence of hydroxyl groups gives the fiber a strong hydrophilic character. The low moisture resistance results in weak fiber-matrix bonding, which compromises the mechanical properties of the composite and makes it very sensitive when exposed to the environment. A 60 % increase in relative humidity will reduce the modulus of elasticity of flax fibers by 35 %. It is essential to protect the fibers by means of coupling agents or suitable resin coating. [13].

Depestele flax fibers, specifically FR 2400 are used for this project. This choice was primarily guided by availability issues, as these were the only fibers available at this stage of the project. An important parameter when evaluating fibers is the tex value, which stands for textile linear density. Tex is a unit of measurement that represents the mass in grams per 1,000 meters of the fiber. This unit of measurement is important to understand the weight and thickness of the fiber, which in turn affect the mechanical properties and behavior during the winding process. FR 2400 represents a tex value of 2400. Where therefore 2400 is grams per 1000 meters of density. These Depestele fibers are bundled to a roving of about 11 mm ($\pm$ 2 mm) wide and minimum to maximum thickness of 0.3 to 0.5 mm respectively. Which characterizes the rovings as "flat" rovings. Flat rovings made from flax fibers are generally preferred over twisted rovings for composite structures because of several important advantages such as:

- Improved mechanical properties: because flat rovings offer better mechanical properties, such as higher tensile strength and stiffness. This is because the fibers are aligned in a parallel manner, allowing more effective load transfer and less stress concentration compared to twisted rovings, where twisting can create weak spots.
- Better resin impregnation: Flat rovings allow for more efficient resin impregnation. The even distribution of fibers facilitates better wetting and impregnation by the resin, resulting in a more homogeneous composite material with fewer weak spots.
- Less voids: The use of flat rovings reduces the voids in the composite structure. Twisted rovings can trap air and create voids during the manufacturing process, leading to potential defects and reduced structural integrity. [32]

For further information on this flax roving is referred to Appendix B: Datasheet FR2400 flax roving

4.3 Resin matrix

This study focuses on a one-meter three-dimensional structure constructed from flax fibers, which are impregnated with epoxy resin. The choice of resin influences the material's strength, and it is crucial to select one that aligns with the requirements of the manufacturing and curing process. Bio-based resins are still being developed and much of the existing literature on bio-composites refers to a mixture of natural fibers with oil-based matrices. There is a clear shift towards replacing oil-based polymers with bio-based alternatives. Today, oil-based epoxy resins are blended with bio-based components to preserve oil-based resins. The resulting products contain some bio-based materials and are increasingly used and evaluated alongside fiber materials. [13].

Numerous projects at the university of Eindhoven have used resin in fabricating structures. According to the research conducted by L. Krijnen, key factors in resin selection include gelling time, viscosity, exothermic peak temperature, and hardening temperature. L. Louer has previously investigated four resin matrices to determine the best performing one. Based on this prior work and the established knowledge on the Infugreen810 bio-based epoxy resin system, it is chosen for this research. Additionally, the SR InfuGreen 810 / SD 8824 system has been employed in previous studies at TU/e by L. Louer [23], L. Krijnen [22], and D. Janssen and L. Roex [31]. Therefore, the bio-based flax fibers will be impregnated with the two-component epoxy system SR InfuGreen 810 with SD 8824 hardener. The technical datasheet of the Sicomin epoxy system has been included in Appendix A: Sicomin technical datasheet.

4.3.1 Pot life of resin matrix

When working with SR Infugreen 810 and SD 8824 hardener, potlife is an important factor for proper application. Pot life refers to the time the mixture remains usable after the resin and hardener are combined. This affects both processability and the quality of the final product. [37]

Important factors influencing potlife include ambient temperature, manufacturer-specified mix ratio and mix volume, as larger volumes react faster. Exceeding the processing time of SR Infugreen 810 with SD 8824 hardener can lead to several negative results that affect material quality and processing. These include increased viscosity due to hardening during processing, uneven curing resulting in reduced mechanical properties, increased material waste and potential safety hazards such as the release of gasses during the exothermic reaction. [33]

The pot life of SR Infugreen 810 with SD 8824 hardener is about 50 minutes at a temperature of 20°C for a 500-gram mixture according to their datasheet.

4.4 Material properties composite material

To compare the experimental results with the model simulations, it is important to understand the material properties of the final composite. For a unidirectional composite, where all fibers are aligned in the direction of the applied load, the stiffness can be estimated by considering the structure as a simple beam. This assumption implies that the two components are perfectly bonded and deform together. The Voigt estimate or rule of mixtures (equation 1 [18]) can be applied to determine the longitudinal elastic modulus of the composite.

$$E_c = E_f * \mathrm{FVR} + E_m * (1 - \mathrm{FVR}) \tag{1}$$

This equation describes the longitudinal elastic modulus E_c which is computed with the elastic (young) moduli of the fiber and the matrix material, respectively E_f and E_m. The existing formula uses a volume fraction (V_f). However, in this study, the volume fraction will be determined from the weight of the fibers and the total weight of the composite. First the Fiber Mass Ratio (FMR) is calculated as follows:

$$w_i = \frac{m_i}{m_{tot}} * 100 \tag{2}$$

Equation 2 [36] describes the mass ratio w_i which is the mass of the fiber material m_i divided by the total mass of the final composite m_{tot}. By multiplying this value by 100 the FMR can be expressed as a percentage. To convert the FMR to the fiber volume ratio (FVR), the densities of both the fibers and the matrix need to be known. The following steps describe this conversion process in detail:

First, define the densities of the fibers (ρ_f) and the matrix (ρ_m). Next, the fiber mass ratio (FMR) is established by eq. 2. The mass of the matrix (M_m) can be calculated by the following formula using the mass of the fibers (M_f):

$$M_m = M_{tot} - M_f \tag{3}$$

Next, the volumes of the fibers (V_f) and the matrix (V_m) can be calculated. This is done by dividing the masses by their respective densities. Therefore, the volume of the fibers and the volume of the matrix are calculated as follows:

$$V_f = \frac{M_f}{\rho_f} \text{ and } V_m = \frac{M_m}{\rho_m} \tag{4}$$

Finally, the FVR is calculated by dividing the volume of the fibers by the sum of the volumes of the fibers and the matrix:

$$\text{FVR} = \frac{V_f}{V_f + V_m} \tag{5}$$

By combining eq. 1 to 5, equation 6 represents the calculation of the longitudinal elastic (young's) modulus of the composite:

$$E_{c-l} = E_f * \text{FVR} + E_m * (1 - \text{FVR}) \tag{6}$$

In examining the literature and previous projects involving natural fibers in composite structures, several key points emerge from the paper by Marta Gil Peréz et al [13], cited: The calculation is reduced to 70% of the original rule of mixtures based on previous CFW project experiences for three main reasons. Firstly, the rule of mixtures assumes proper bonding between fibers and resin, which is often not the case in CFW structures due to the presence of voids in the bundles. Secondly, the components are subjected to high compression loads, and the compression stiffness of a unidirectional composite is known to be lower than its tensile stiffness, leading to unpredictable structural behavior. Thirdly, the FVR must be estimated from small-scale specimens, which may differ from the final large-scale component, and deviations in the assumed FVR will reduce the resulting stiffness. Therefore equation 6 changes into equation 7, where this 70% reduction is implemented. This leads to the original formula as given in the Livmats pavilion research [13]:

$$E_{c-l} = 0.7 * (E_f * \text{FVR} + E_m * (1 - \text{FVR})) \tag{7}$$

Once the FVR of the structure is known by making small-scale specimens, the longitudinal elastic young's modulus can be calculated. The small scaled tests and resulting FVR is described in section 5.4.1

5 Manufacturing of the structure

The structure is manufactured through robotic coreless filament winding. This section elaborates on the full manufacturing process, addressing the end plate design, construction of resin bath, winding process and curing cycle.

5.1 Manufacturing process set-up

By assembling the final part, several components need to be fabricated to complete the manufacturing process. Based on the work of L. Krijnen [22], several elements of the previous winding project were replicated. Figure 31 illustrates the replication of the robot, the turntable and the support of the threaded rod, the support of the threaded rod has an integrated bearing nut, this enables attachment while maintaining rotational capability.

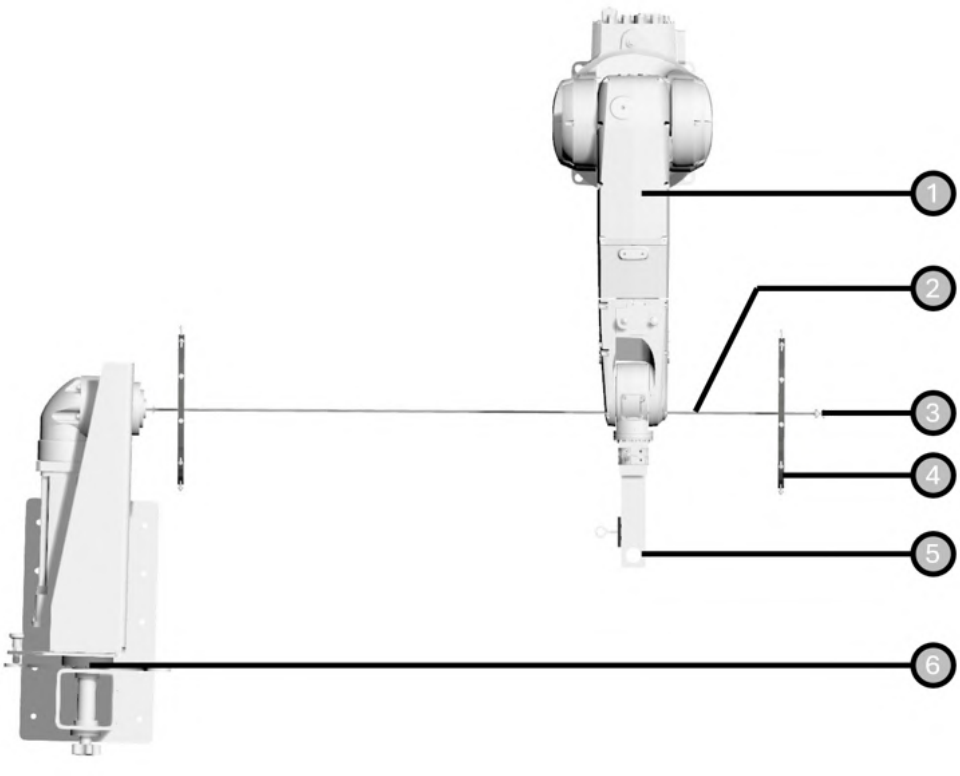

Figure 31: New manufacturing process set-up: (1) ABB IRB 1200-5/0.9 robot (2) Threaded rod (3) Support of threaded rod with bearing nut (4) New aluminium end plate with winding pins (5) New robot end-effector (6) Rotation external axis (turntable).

5.1.1 Aluminium end plates and connection with turntable

As mentioned previously, the current design was inspired by a the project of L. Krijnen [22]. Examination of this previous design reveals areas for improvement in this configuration. (b-c) The threaded rod had insufficient stiffness, which resulted in bending during fabrication and an imperfect final assembly.The solution to improve the strength of the threaded rod is to use a larger diameter and attach it to the current bearing nut using suitable fittings. Currently, the threaded rod used has a diameter of M16. (a) The plate connecting the threaded rod to the turntable proved to be less than optimal for attaching the structure to the turntable. Figure 32 shows the upgrades compared to L. Krijnen's set-up.

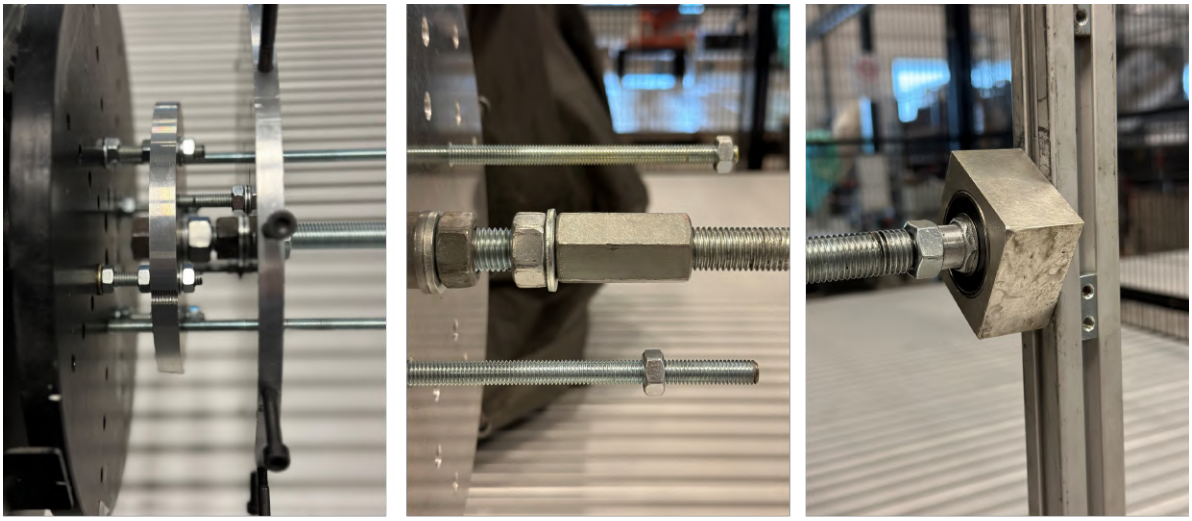

Figure 32: Upgrades set-up end plates: (a) Connection threaded rod - turntable (b) Coupling between threaded rods (c) Bearing nut adjusted to M16

From the design optimization performed in Octopus as described in section 2.5. The following design parameters associated with the solution of the optimization are:

Height of structure	1000 millimeter
Radius top and bottom	124 millimeter
Number of points	11 Points

These parameters outline the setup for the end-plate structure. The end plates, made from aluminium sheets, were divided into two circular pieces with a 248 millimeter diameter. They were positioned one meter apart using a threaded rod. Figure 33 shows the arrangement of the plate configuration as constructed in the lab. More holes have been drilled into the aluminium end plates. If more strength is required, threaded rods can be installed to reinforce the plates against the inward pulling force generated by the robot.

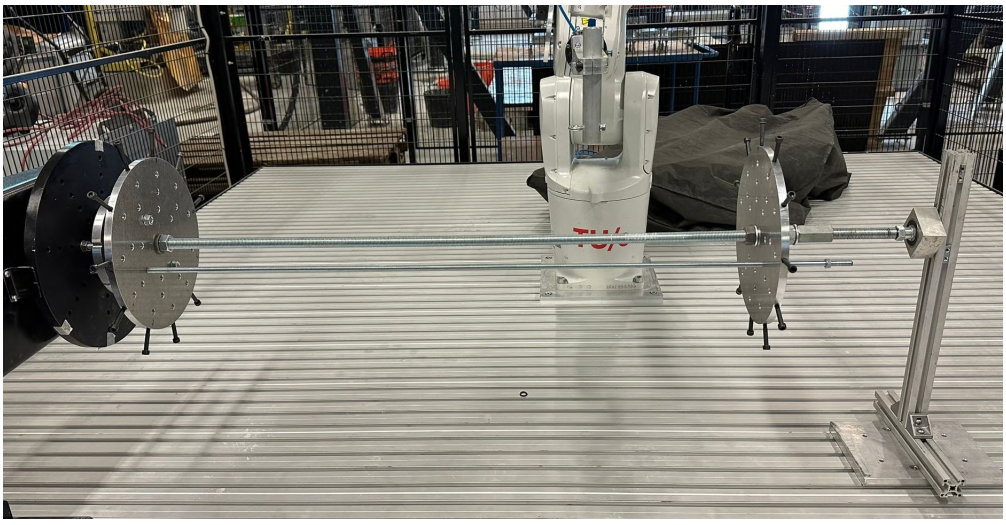

Figure 33: Aluminium end plates on threaded rod

5.1.2 Winding pin configuration

The winding pins are designed similar to those used in projects in Stuttgart [5] [13]. The pins consist of a bolt, a sleeve and washers. The sleeve helps minimise friction during winding, while the washers prevents the fibre from sliding off the pin. Figure 34 shows the actual look of the winding pin. The height of the winding pin is set at four centimetres, corresponding to the width of the fibers, which measures about one centimetre. With option 1, five times should be winded around this pin, so extending the length to four centimetres.

Figure 34: winding pin configuration

The calibration process in Robot Studio included the addition of end plates and the robot end effector. To ensure smooth running of the winding process, a trial run is conducted using sisal rope. Since the rope was not impregnated with epoxy resin in this trial run, there was no mess or material waste. Figure 35 displays the sisal test rounds of option (1), (2) and (3), during which several observations were made:

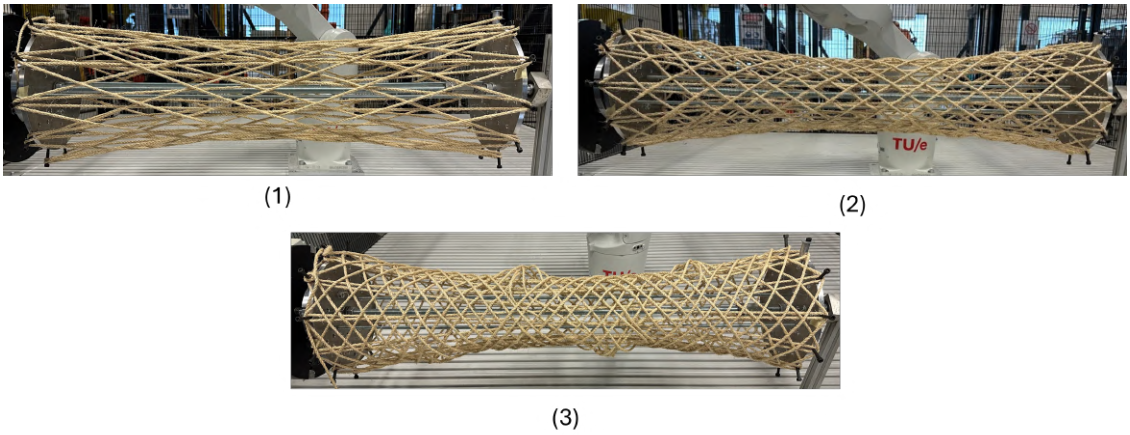

Figure 35: Sisal test rounds of option (1), (2) and (3)

- Robot end-effector: The current end-effector design does not fulfill the requirements for the robot's manufacturing process. Although the ring intended to reduce friction between the fibers functions as planned, its attachment to the end-effector causes issues. Specifically, the plate used to mount the ring will collide with the fibers that have already been winded. Therefore, a new end-effector design is required to overcome this issue, as detailed in section 5.2.
- Deformation of ropes: During winding, the ropes start to deform, leading to the structure's anticlastic shape. In each testing round, one layer of sisal rope was used as the lattice layer. In option 1, this did not cause any issues since only five points were shifted, resulting in minimal rope deformation. However, options 2 and 3 encountered issues. The reinforcement layers in these options deformed the lattice layer significantly, causing the first layers of the reinforcement to become loose around the structure. Reasons for this loosening could be inconsistent tension in the rope during winding or an insufficiently strong lattice layer for the reinforcement layer. To address these issues when winding with flax fibers, it is necessary to maintain constant tension.

- Test rounds for verification of path planning and manufacturing set up: Test rounds were performed only to verify the path created by the Rhino Grasshopper script with the new end plates and end-effector setup. Because dry winding with flax fibers is not ideal, sisal rope was used instead. Sisal rope will no longer be used in ongoing research.

5.2 New Robot end effector

As described in section 3.2.2 this project introduces a redesigned end-effector for the robot, aimed at improving its performance in (natural) fiber winding tasks. The previous end-effector proved unsuitable due to its large contact area, which increased the risk of damaging the rovings. The new design utilizes the existing end-effector by incorporating an aluminium tube profile into a gap in the existing structure. This tube can be adjusted in height as needed. Figure 36 shows the new robot end-effector. After the round of testing described in section 5.5, the ceramic ring was glued to the aluminium tube since it came loose several times during the round of testing.

Figure 36: New robot end-effector

5.3 Drying of non-impregnated rovings

The preparation of flax fibers for use in composite materials involves several steps to ensure the structural integrity and performance of the final product. One of these steps is drying the flax fibers before they are impregnated by the resin matrix.

Because flax fibers are naturally hydrophilic, they absorb moisture from their surroundings. This absorbed moisture can create challenges during composite fabrication. For example, moisture on the fiber surface can impede adhesion between the fibers and the resin matrix. Effective adhesion is paramount to the mechanical strength of the composite material. According to Herrera Franco P. [19], insufficient drying can result in poor fiber-matrix adhesion, leading to sub-optimal mechanical properties of the composite. In addition, residual moisture in the flax fibers can lead to cavity formation during the curing process. When the composite is exposed to elevated temperatures, any residual moisture can evaporate, creating cavities or bubbles in the material. These cavities act as stress concentrators, which reduce the mechanical performance of the composite.

Figure 37: Drying of flax bobbins

To avoid these problems, the flax bobbins are dried at an average temperature of 40 degrees Celsius. This temperature is high enough to effectively remove moisture without causing thermal degradation of the fibers. Research by Ghazanfari et al [12] proposes different temperatures to dry flax fibers. The temperatures used in this research serve as a reference to establish optimal drying conditions. Ghazanfari et al.'s study indicates that drying flax fibers at approximately 40 degrees Celsius effectively reduces moisture content to

levels suitable for composite fabrication, thus preventing adhesion issues and void formation. The flax bobbins are dried in the drying oven as shown in figure 37, which is available in the SED Lab. The weight of the bobbin is measured before drying and after drying. The datasheet of Depestele flax roving states that the bobbins have a moisture content of 8%, which is the initial moisture content. Preferably, the moisture content should be below 5 %, ideally around 2-3 %. To calculate the final moisture content after drying the following equations are used:

$$\text{Removed Moisture (\%)} = \left(\frac{\text{Initial Weight (kg) - Weight after drying (kg)}}{\text{Initial Weight (kg)}} \right) \times 100 \tag{8}$$

$$\text{Final moisture content (\%)} = \text{Initial Moisture Content (\%)} - \text{Removed moisture (\%)} \tag{9}$$

5.3.1 Results drying process

The weight of one of the 6 bobbins is determined at different times. To see if indeed some of the moisture could be removed from the bobbins in this way. In this study, this bobbin, is named Bobbin 1 (B1). The result of the drying process of B1 is graphically shown in figure 38 which indeed shows that the weight of the bobbin is decreasing after drying the bobbins in the oven. This proves that this is the moisture removed from the bobbins. The bobbins remain in the oven throughout the fabrication phase to prevent them from absorbing moisture due to their hydrophilic nature. They are only removed from the oven when needed, with the assumption that they absorb negligible moisture during the short time they are out. Before each use, the bobbins are weighed. They are weighed again before being placed back in the oven after the manufacturing process, ensuring a reference weight is established for the next use.

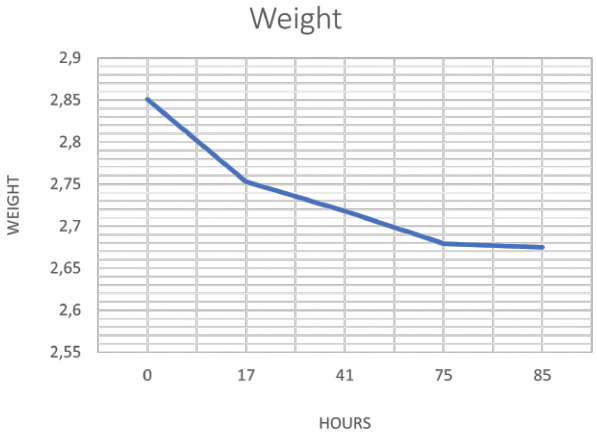

Figure 38: Graphic of drying process

5.4 Constructing resin bath and testing

As described in section 3.3, a revised design of the resin bath is proposed, using parts available in the lab. Figure 39 illustrates the new arrangement. The new resin bath configuration consists of five steel corner profiles attached to steel profiles (from the lab) on either side of the bath. These corner profiles provide support for the rollers used in fiber impregnation. The rollers with M10 threaded ends in M11 tubular profiles separated by washers allow three fibers to be impregnated simultaneously. These rollers have to be disposed because they are damaged by the epoxy resin, but replacement is cost-effective. A silicone container forms the resin bath, chosen for its non-adhesive properties with epoxy resin. After impregnation, the fibers are consolidated and guided to the robot.

Using bolts to fasten the corner profiles, allow easy adjustment of the resin bath. This facilitates optimizing the configuration of the resin bath by impregnation tests. These tests consist of impregnating flax fibers with SR infugreen 810 epoxy resin and Harder SD8824 and testing different configurations.

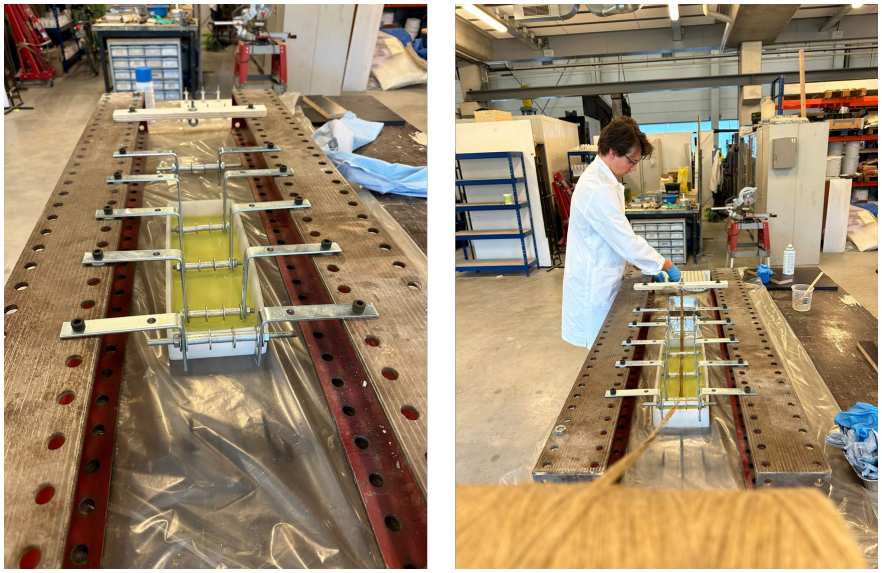

Figure 39: New resin bath configuration

5.4.1 Material properties

As discussed in section 4, the materials selected for use are a 2400tex Depestele flat flax fibers and Sicomin SR Infugreen810 Epoxy Resin combined with SD 8824 hardener. While individual mechanical properties of these materials can be found in data sheets, their combined properties are not known.

Referring to the the paper about the Livmats pavillion [13]: The mechanical properties and failure modes of the resulting composite are significantly influenced by the fabrication technique, the geometry achieved, the fiber volume ratio (FVR) and the compaction obtained. CFW structures rely on the tension applied by the robot during winding and the resulting geometry to ensure proper fiber interaction and adhesion. More pronounced curves in the structure can improve adhesion between fiber bundles better than flat layups, as the fiber bundle presses on the previously placed fibers. At the lattice level, insufficient compaction between bundles can cause weak resin bonding, which can lead to delamination of the system. Moreover, at beam level, voids can form between the resin and the fiber.

The impregnation of fibers can impact the Fiber Volume Ratio (FVR) of a composite. Enhanced impregnation results in a reduced FVR because more matrix material can bond with the fibers. According to the Livmats Pavilion paper [13], an FVR within the range of 30-40% is desired. As outlined in section 4.4, the FVR will be assessed through small specimen testing, which will be conducted in the following manner: To determine the Fiber Volume Ratio (FVR) of the composite, a small-scale experiment was conducted to study the interaction between the two materials. The main objectives of this experiment were to identify the most effective resin bath configuration for achieving the target FVR and to verify if the impregnation process is proceeding as expected. During this experiment, fiber sections are impregnated using a resin bath setup, with each section using a different resin bath configuration. The impregnation speed is timed with a stopwatch to replicate the speed achieved by the robot pulling the fibers. Measuring the weight is done of the dry samples before the test and the cured samples afterwards. The dry fiber weight is used to verify the data provided by Depestele's datasheet, referring to Appendix B. The resin and hardener are mixed in an aluminium container using a wooden spatula. Once thoroughly mixed, the fiber is impregnated with resin. Finally, the fibers are winded around a small test arrangement designed to simulate the manufacturing process. This arrangement with uncured bundle of rovings is shown in figure 40.

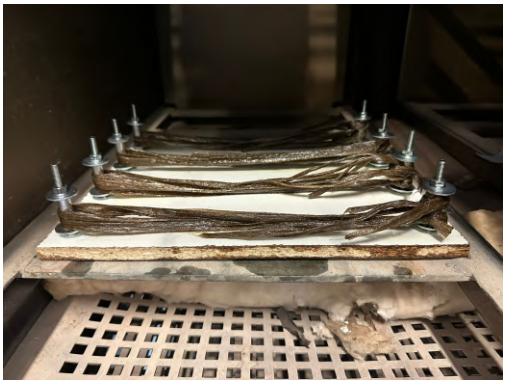

Figure 40: Uncured bundle of fibers of first impregnation test

After impregnation, the bundle was cured at room temperature, followed by an additional 8-hour curing process at 40 degrees Celsius in the oven in the SED lab. This curing process is based on the guidelines in the Sicomin Infugreen810 data sheet. Once the bundles were cured, the impregnation quality can be assessed. Visual inspection has shown that the new resin bath impregnates the bundles effectively, with sufficient resin content for composite fabrication.

This preliminary test serves as an important step to identify and prevent potential problems later in the study. The following observations were made during the inspection:

- Because the bundles were manually wound around the pins, there was limited control over fiber tension, causing some fibers to sag down and stick to the setup. When winding the structure with the robot, the tension will be induced by the bobbin holders.
- It is critical to ensure that the bundles are winded tightly together with no gaps between them. By using a ceramic ring which is smaller than three bundles. The bundles are merged before winding.
- Protection of the bolts from resin drops is necessary. In this test, resin damage to the bolts caused these to get stuck and not come off, so the fiber volume ratio (FVR) of the bundles could not be determined because they could not be removed from the mold and be weighed. Before winding the final structures. The supporting structure and winding pins will be protected using release agent spray wax.

5.5 Robotic coreless filament winding

With all phases of the manufacturing process complete, the winding of the final structure may begin. The first round of winding served to test every aspect of the fabrication process, since no previous testing was done. The total manufacturing process utilized in the first round of winding is shown in figure 41. following a series of specific steps. First, the flax rovings were removed from the oven and weighed to determine their dry weight. Next, these rovings were taken from the bobbin holders into the resin bath to be impregnated with epoxy resin. After impregnation, the three rovings were assembled into a single bundle. This bundle was guided around the winding pins of the supporting structure by the robot. The final RAPID program module and system module scripts are loaded into Robot Studio to drive the robot and rotation table. A network cable was used to connect the computer to the robot. The script is visible on the robot teach pendant during manufacturing, to control all movements. As can be seen in 41, the full setup was packed in foil, to prevent material from the SED lab from being damaged by the epoxy resin. Furthermore, the end plates and winding pins are sprayed with a release agent wax so that it can be re-used.

Figure 41: Final manufacturing process

5.5.1 1^{st} Version Option 1 (V1O1)

This round of testing used the script for design option 1, This process resulted in the creation of a first version of Option 1, as shown in Figure 42. The flax bobbins used for this structure are labeled bobbin 4, bobbin 5, and bobbin 6. The initial weights of the bobbins are 2.747 kg, 2.727 kg, and 2.669 kg, respectively. Assuming all three bobbins use the same amount of roving to form the bundle, this results in a total initial weight of 8.143 kg. Before drying, the weight of these bobbins was also measured. Being: 2.922kg, 2.902kg and 2.845kg respectively. So the moisture content can be adjusted by equation 8 and 9. The final moisture content of the bobbins is respectively 2.01%, 1,97%, 1,81%, which meets the requirements stated in section 5.3.

Figure 42: First version of option 1

After constructing the structure, the bobbins were weighed again, resulting weights of 2.455 kg, 2.440 kg, and 2.400 kg, respectively. With a total final weight of 7.295 kg. Therefore, the weight of the material used is 0.848 kg. The weight of the final element is 2.733 kg, which is the weight of the composite minus the weight of the 22 sleeves.

Using this data, the mechanical properties can be defined. The results of the mechanical properties that can be used in the calibration of the model are displayed in table 5.

Table 5: Material properties version 1 option 1

Specimen	**No. rovings x passes**	**Specimen weight(g)**	**Fiber weigth(g)**	**FMR**	**FVR**
V1O1	3x1 3x4*	2733	848	0.310	0.226

* Upper row represents the number of rovings x passes for the lattice layer where the lower row represents the number of rovings x passes for the reinforcement layer.

The preliminary findings indicate that the structure of Option 1 can be made using this method. However, a number of issues emerged from this testing phase:

- The connection of the ceramic ring to the tube of the end effector proofed to be not sufficient. During winding this ceramic ring fell out several times, which delayed winding and eventually caused the ring to become stuck in the structure. For the next winding round the ceramic ring is glued to the end effector preventing for fall out.
- The angle between the robot's end effector and the approaching roving bundle was too sharp, leading to the removal of an excessive amount of epoxy resin. The solution for this is to modify the angle of the robot end effector. In this winding process, the end effector is positioned perpendicularly to the rotating work object. By rotating the end effector towards the resin bath, the angle between the approaching flax bundle and the robot end effector is reduced, thereby minimizing scraping.
- As shown in Figure 41, the bobbin holders are placed side by side and directed toward the resin bath by conductors. However, by positioning the spool holders side by side, the angle between the outer bobbin holders and the conductors becomes too sharp. This sharp angle results in the roving sliding off the outer bobbin holders and becoming entangled on the holder. To reduce this problem, it is suggested to place the bobbins vertically stacked. This vertical placement would reduce the angle and thus prevent the roving from sliding off the bobbin.

5.5.2 2^{nd} Version Option 1 (V2O1)

Since the first version of Option 1 was a test to validate the theoretical setup for fabricating the final elements, a second version of option 1 is manufactured. This new version addressed the issues raised during the first test and optimized the process.

This resulted in the creation of a second version of Option 1, as shown in Figure 43. In contrast to the first version of this variant, the creation process for this design proceeded smoothly. There were no interruptions in the winding process, unlike the multiple stops required to address issues in the first version. The winding time for this option is approximately 25 minutes, so no problems occur with the resin pot life.

Figure 43: Second version of option 1

The corresponding material properties associated with this design are listed in Table 6. There is a slight difference in fiber weight used between version 1 and version 2 of variant 1. This difference may be attributed to the residual material remaining at the end of the process. Some of the rovings are impregnated with resin but will not be used in the structure. This material cannot be reused because it already contains resin, making it waste after curing.

Table 6: Material properties version 2 option 1

Specimen	**No. rovings x passes**	**Specimen weight(g)**	**Fiber weigth(g)**	**FMR**	**FVR**
V2O1	3x1 3x4*	3064	836	0.273	0.196

* Upper row represents the number of rovings x passes for the lattice layer where the lower row represents the number of rovings x passes for the reinforcement layer.

5.5.3 1^{st} Version Option 2 (V1O2)

This round of winding used the script for design option 2, This process resulted in the creation of a first version of Option 2, as shown in Figure 44.

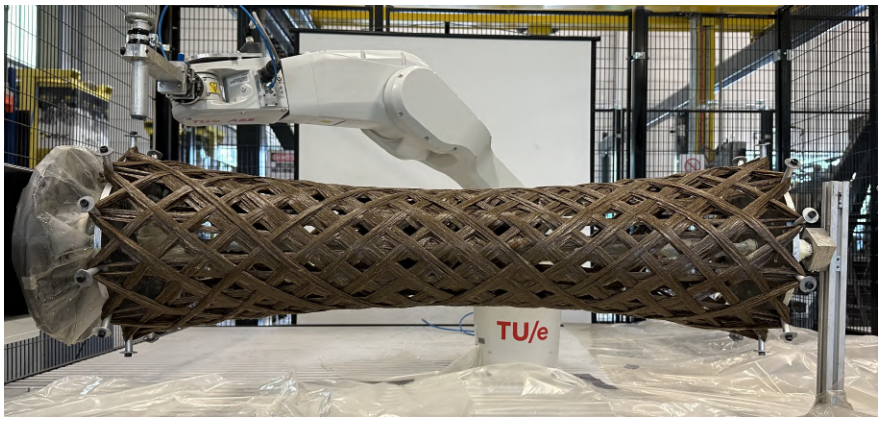

Figure 44: First version of option 2

During the winding process, the flax fibers deform, leading to tension in the first layer of the reinforcement. However, with each additional diagonal winding, the lattice layer deforms, causing the initially wound diagonals to become loose. This was evident during test rounds with the sisal rope.

The corresponding material properties associated with this design are listed in Table 7:

Table 7: Material properties version 1 option 2

Specimen	**No. rovings x passes**	**Specimen weight(g)**	**Fiber weigth(g)**	**FMR**	**FVR**
V1O2	3x1 3x4*	2752	783	0.285	0.205

* Upper row represents the number of rovings x passes for the lattice layer where the lower row represents the number of rovings x passes for the reinforcement layer.

5.5.4 1^{st} Version Option 3 (V1O3)

This round of winding used the script for design option 3, This process resulted in the creation of a first version of Option 3, as shown in Figure 45.

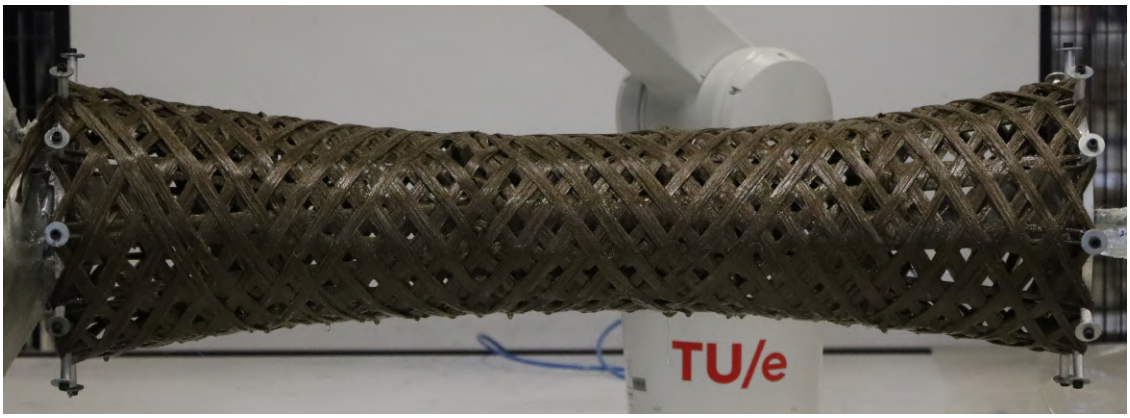

Figure 45: First version of option 3

There are also loose bundles with this design option. With this option, it is also worse and the loose bundles come out through the structure. These loose bundles will thus harden and testing should show how these loose bundles affect the structural aspect of the structures. It is also notable that with this option, the limits of robotic winding with the existing script are reached. This is because the robot passes very close to the winding pins and after curing it is difficult to remove the support structure from the structure since the structure is quite tight around these plates, because it has the most anticlastic shape of the three.

The corresponding material properties associated with this design are listed in Table 8:

Table 8: Material properties version 1 option 3

Specimen	**No. rovings x passes**	**Specimen weight(g)**	**Fiber weigth(g)**	**FMR**	**FVR**
V1O3	3x1 3x4*	2904	758	0.261	0.186

5.6 Curing cycle

After the filament winding process, the structures are taken off the robot set-up and transmitted to the climate-controlled room in the SED lab, where they are kept at ambient temperature. This procedure is followed to maintain a minimum temperature of 20 degrees Celsius, as detailed in section 3.4 on Curing. The next morning, the structures are moved to a different climate room set at 40 degrees Celsius for an eight-hour post-curing period. Table 9 provides a overview of the complete curing cycle for the structures.

Table 9: Curing cycle of manufactured elements

Specimen	**Temperature C**	**Time (hr)**
V1O1	20 (± 0.5)	20
	40(± 0.5)	8
V2O1	20 (±0.5)	19
	40(±0.5)	8
V1O2	20 (±0.5)	20.5
	40(±0.5)	8
V1O3	20 (±0.5)	20
	40(±0.5)	8

Figure 46: Disassembled composite

After the structures were fully cured, the end plates are removed. This is done by loosening the bolts which are connected to the endplates. The sleeves will stay in the structure. Figure 46 shows the cured structure after removing the disconnected end plates and threaded rod.

5.7 Final elements

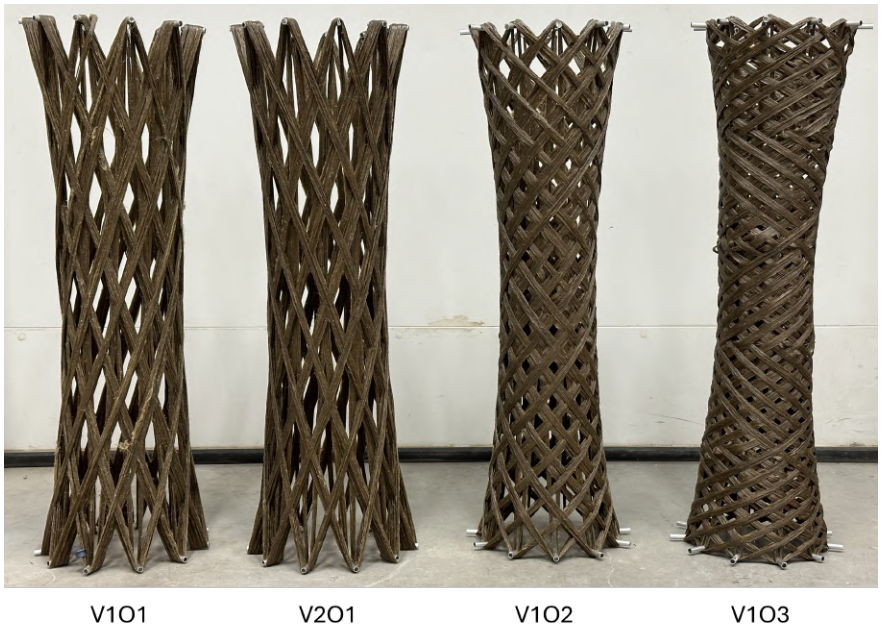

Figure 47: Final fabricated composite elements

Figure 47 shows the four manufactured structures after the internal formwork is removed. It can be seen that the structures feature some imperfections, V101 is the test version in which the ceramic ring got stuck. Where V2O1 is the best manufactured structure without imperfections. V1O2 and V1O3 have hardened loose ropes, which will affect the testing capacity. This is described in section 7.

The optimization took into account the multiplies in design variants. Where the assumption is made that the same mass will be used in the generation of design options. After manufacturing the elements were weighted. Hereby it can be assured that the assumption of equal lengths and mass in the design options can be validated. Table 14 describes the total weights of the composites and the weight of fibers used compared to the number of meters previously expected to be used. For the meters which are previously expected, the data from table 4 is used with the addition of 22,1 meters of the lattice layer. The amount of meters actual used is calculated by dividing the weight of fibers used by the weight 1 meters of bundle.

Table 10: Comparison of mass assumption

Specimen	**Weight of composite (g)**	**Weight of fibers used (g)**	**length of fibers used (m)**	**Length of fibers RG (m)**
V1O1	2733	848	120	116
V2O1	3064	836	119	116
V1O2	2752	783	112	113
V1O3	2904	758	108	115

The table demonstrates that generating the design by the number of meters is quite accurate. In winding design options 1 and 2, more meters were used in the real element compared to the model in Grasshopper. This deviation can be attributed to the extra meters that must be discarded due to impregnation but will not be wound, resulting in 2 to 4 meters of residual material. In option 3, the actual structure becomes

more anticlastic, requiring fewer meters of the bundle to wind the diagonals. This structural change is not accounted for in the model, potentially leading to fewer fibers being used than expected.

5.7.1 Point of interest during winding process

- During the winding process, much amount of resin drips onto various components, including the rotary table, robot end effector, the end plates on both sides, and the stand to which the rotary nut is attached. To protect these components from resin, cling film and plastic coverings have been used. However, certain elements, such as the end effector and winding pins, cannot be wrapped. Therefore, before each winding session, all exposed materials are sprayed with vaseline, which serves as a release agent, preventing the resin from adhering to these parts. After winding when the resin has not yet cured, acetone can be used to remove the excess resin from the elements that have been damaged by the resin.
- The initial two versions of the winding elements utilized M6 bolts with a length of 50mm. However, these bolts proved insufficient in providing the necessary strength, resulting in minor imperfections in the structure. Additionally, resin tended to seep through the holes in the end plates along the threads, which prevented the bolts from coming loose. To address this issue, it is recommended to use 60mm long M6 bolts coated with copper paste before installation. The copper paste prevents resin from infiltrating the threads, ensuring the bolts can be easily loosened when fully cured.
- Initially, the sleeves used for winding were cut to size with a handsaw. This method left the ends uneven, affecting the overall structure. In the final winding session, the sleeves were cut by machine, resulting in a more uniform and precise finish with fewer imperfections.

These observations can be taken into account for subsequent projects with these production methods to optimize the process.

6 Numerical model

As detailed in section 2, a computational geometrical model is created using Rhino software in cooperation with the Grasshopper plugin. The design created in Rhino Grasshopper is created for the manufacturing of the elements but is not suitable for direct numerical analysis. During manufacturing, the structure will undergo significant shape changes due to the absence of formwork and the use of the coreless filament winding technique.

6.1 Model configuration

Figure 48 shows the flowchart of the build up of the geometrical and numerical model. First, basic Grasshopper components (2) and Python programming (3) are used to generate the geometry, which can be influenced by the parameters discussed in section 2. After defining the basic geometry, a structural optimal form study is done through the Karamba3D plug-in (4). After the final form is defined, the structure is geometrically optimized using the octopus plugin (5). This plugin serves as the generator of the final design. When the final geometry is known, the winding path is determined. The Leafvein plug-in (6) is used to define an Eulerian path. The resulting point sequence can be used as input for the Robot Components plug-in (7). The RAPID-code created by this plug-in can finally be loaded into Robot Studio (8), to simulate the robotic winding path and to manufacture the structure. For numerical analysis, the model must be recreated in Oasys General Structural Analysis (GSA), which allows for the pre-tensioning of winding lines and construction in multiple stages, mirroring the robotic winding process in the lab. The design of option 1 was converted into a GSA structure model using the GSA plugin for Rhino Grasshopper (9). After manufacturing, the model is regenerated and calibrated with the python module and numerically analysed by the Karamba3D plugin. (10)

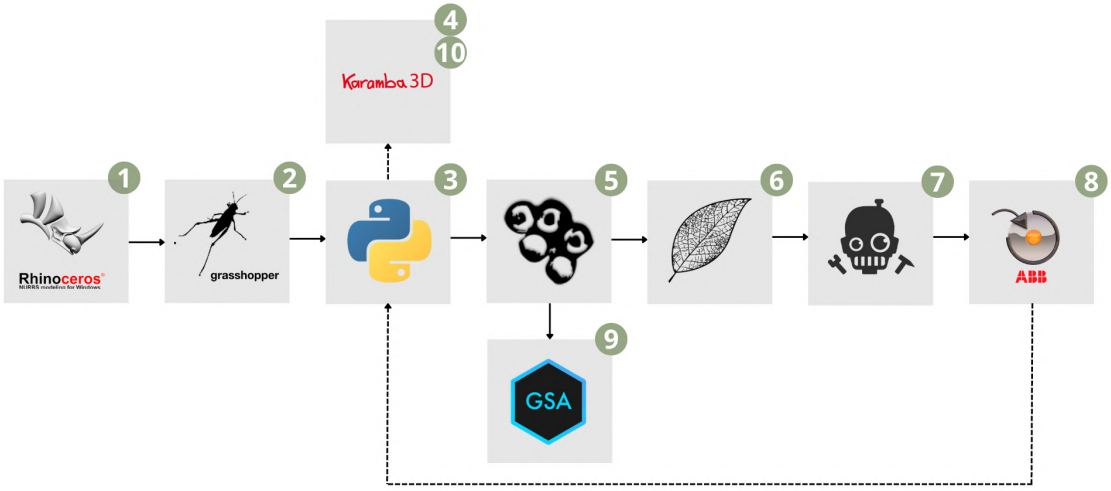

Figure 48: Flowchart design process

With the GSA plugin, winding lines can be divided into groups. The first group represents the entire lattice layer, while groups 2 to 23 each represent a single diagonal of the reinforcement layer. This allows for easy selection and assignment of information to individual diagonals. To simulate the production process in GSA, the staging analysis option in this modeling and analysis software was used: staging analysis is part of the structural analysis and design of complex structures, allowing engineers to simulate the fabrication sequence and assess the performance of the structure in different fabrication phases. In GSA, this process provides detailed insights into the behavior of structures under different loading and fabrication conditions. GSA facilitates staging analysis by allowing the user to define different fabrication phases. Each phase can include the activation of new structural elements, changes in boundary conditions and the application of different loads. Key features of incremental analysis in GSA include:

- Incremental load: Users can apply loads incrementally, reflecting actual load conditions during the construction process.
- Activation/deactivation of elements: Structural elements can be activated or deactivated at different stages, simulating phased construction processes.
- Time-dependent effects: The software can account for time-dependent effects such as creep and shrinkage, which are crucial for assessing the long-term performance of structures.
- Dynamic analysis: Phasing analysis can be integrated with dynamic analysis to evaluate the response of the structure to time-varying loads and seismic activity during different phases of construction. [27]

Using these features, it is possible to generate the manufactured design and simulate the winding of the structure as shown in figure 49. With this simulation the winding lines of the lattice layer have only a very small thermal load of -50 (which induces prestress), Whereas the reinforcement layer each has a thermal load of -1000. Thus, a model can be formed that simulates the manufacturing process. Section 6.3 describes the calibration of the numerical model with the manufactured structure.

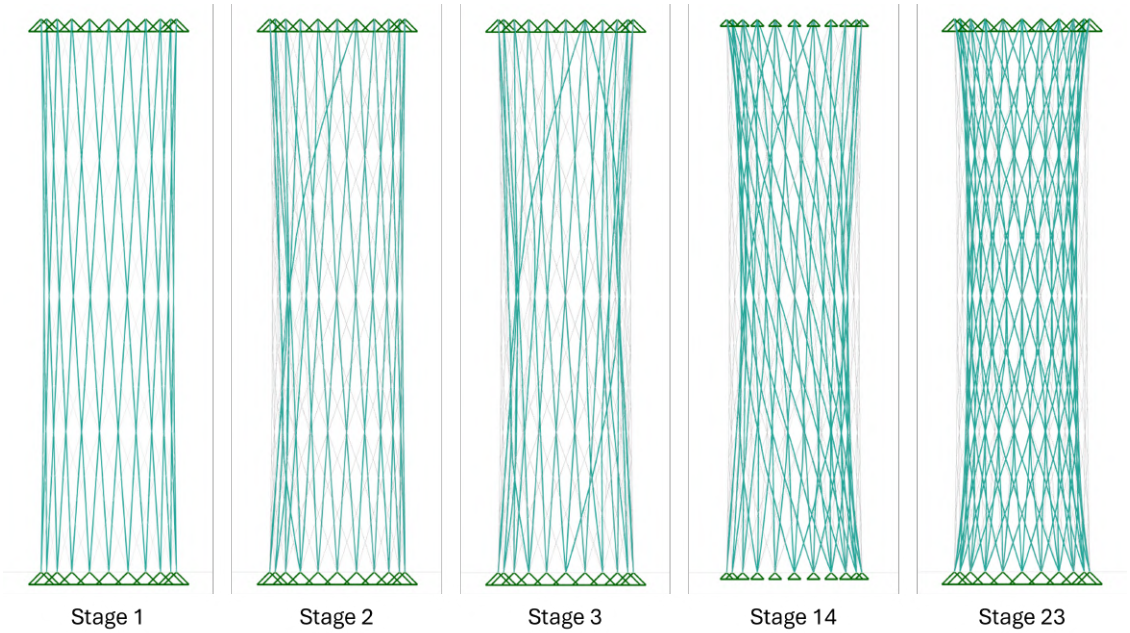

Figure 49: Several stages of staging analysis

6.2 Assumptions

Some assumptions are made for analyzing the structure, these are given here:

- In the Oasys GSA model created, the filament winding process is simulated with two layers of winding lines. The first assumption in this model is that each winding line undergoes the same amount of prestress. This simplification is necessary to facilitate the modeling process and keep the calculations manageable and, as yet, there is no way to control and monitor the prestress during winding. However, it is recognized that in reality the prestress applied to each filament during the winding process can vary due to various factors such as material inaccuracies, robot accuracy and robot speed. These variations can significantly affect the structural performance and behavior of the winded structure. Therefore, although the assumption of equal prestress provides a basis for the simulation, the results should be interpreted with caution.

- In the developed model, all 3D elements were interconnected to simulate a continuous and integrated structure. This modeling approach simplifies the complex interactions between individual elements, providing computational efficiency and facilitating the analysis process. However, it is recognized that in the actual prototype, the connections between 3D elements may not be as good as modelled. Factors such as manufacturing tolerances, material inconsistencies and imperfections in the fabrication process can lead to variations in the connections. These variations can affect load transfer mechanisms and the overall behavior of the structure. The idealized joints in the model assume perfect bonding and alignment, which may not fully reflect the actual structure conditions.

6.3 Calibration with numerical model

After winding and curing, the structure's diameter at the center ring is measured to determine the curvature of the composite. Since the exact prestress in the winding lines during the process cannot be measured, the model is adjusted based on the observed curvature of the structure. This allows the final designs to be replicated in Karamba3D. The material properties of the options are also implemented in the model in combination with equation 7 to calculate the E-modulus. The E-modulus value for the fibers was obtained from the paper by M. Gil Pérez et al. [13], as the Depestele technical data sheet does not provide this information. This value corresponds to a structure with an FVR of 40%. Therefore, it is used here solely for theoretical comparison. The data for calibration is listed in table 11. The results from this numerical analysis are used to compare the model with the test of the element, which is performed in the SED laboratory.

Table 11: Calibration of numerical model

Specimen	**V1O1**	**V2O1**	**V1O2**	**V1O3**
Lattice layer (mm) (width x depth)	10 x 5	10 x 5	10 x 5	10 x 5
Reinforcement layer (mm) (width x depth)	30 x 5	30 x 5	20 x 5	12 x 5
Inward deformation (mm)	30	30	40	50
Elastic modulus fibers (GPa)	55.1	55.1	55.1	55.1
Elastic modulus matrix (GPa)	3	3	3	3
Elastic modulus composite (GPa)	13.21	14.77	13.68	11.06

6.4 Results of staging analysis

The process of coreless winding, where structural deformation occurs due to the lack of a core, creates a challenge when modeling the structure to ensure structural integrity. Therefore during the winding process the structure is monitored to analyze the behavior of the winding lines throughout the process. This is done by taking pictures of the structure with a camera from the SED labaratory after each winding line, as can be seen in figure 41. By taking pictures after each winding line, deformation can be analyzed after the winding process. Figure 50 shows this process in which the difference in deformation was visualized using the photos.

Various stages of the Oasys GSA model were compared to the final winding process, showing that the current model accurately simulates the deformations of the structure. This comparison relates to design option 1, where the model functions as intended. Unfortunately, the models for options 2 and 3 could not be included in this analysis. As described, the initial winding lines become loose as the number of windings increases (multiple turns around the structure), as seen in Options 2 and 3. If this phenomenon can be simulated in the GSA model, the design can be optimized in advance to prevent the rovings from hanging loose.

This model serves as a valid initial setup to pre-simulate the behavior of a coreless filament wound structure. Currently, it is used primarily for visualization because the pretension in the rovings during the winding process is not known. Further details and refinements can be added as needed to improve accuracy.

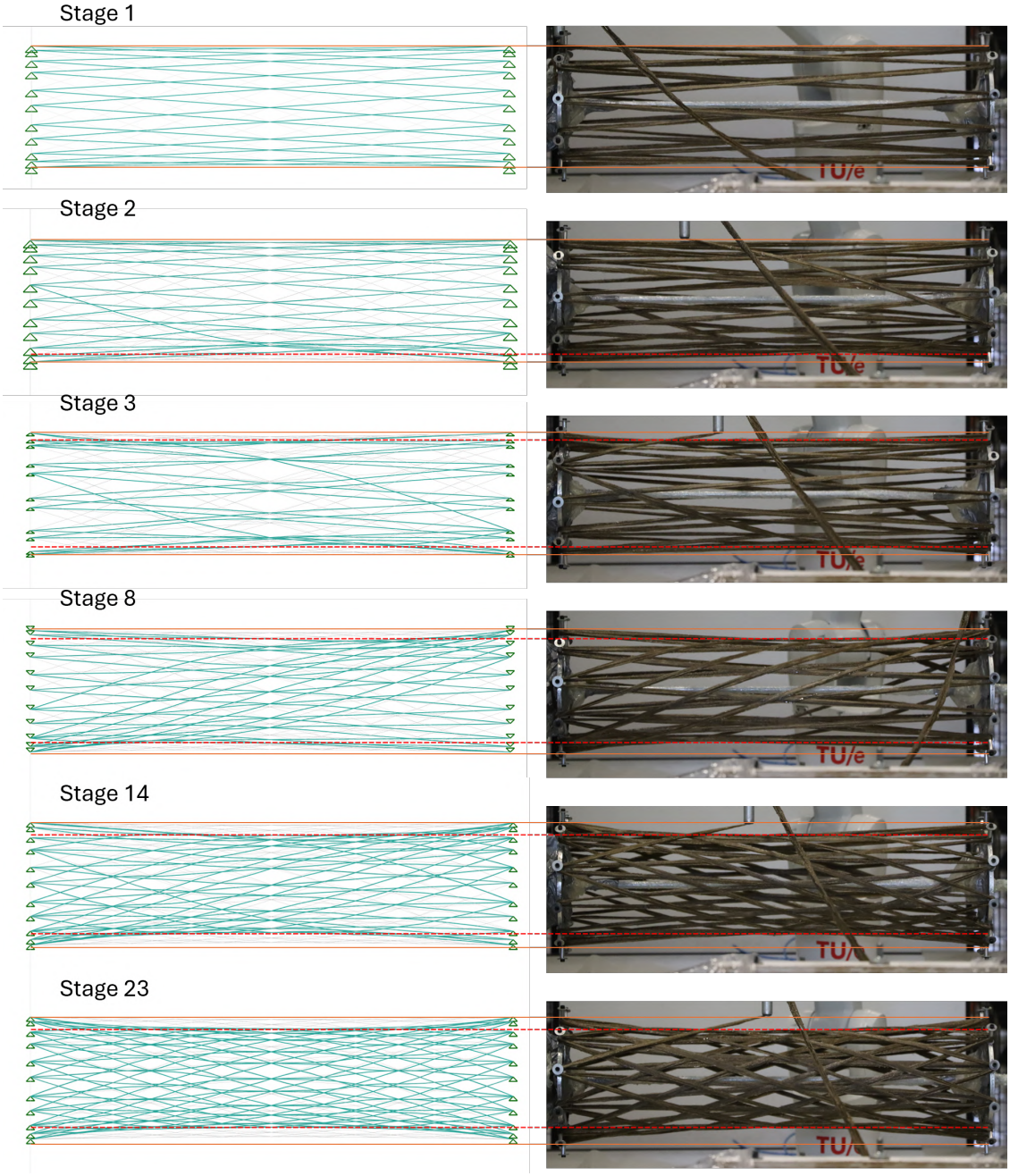

Figure 50: Comparison GSA model and reality

The behavior of the structure is described by the axial force in the winding lines. Since the values of the prestress are not known, No actual values were used. In the GSA model, each node relates to a cut element, resulting in a diagonal and a lattice consisting of multiple elements. It is important to understand the distribution of forces within these different elements. Therefore, for a diagonal and a lattice element, all relevant

information is extracted from the GSA model. Figure 51 shows the composition of the first diagonal and an element of the lattice layer in the GSA model. This information of the model is represented in a 2D bar graph, where each element is projected with the corresponding force in each stage. This is shown in figure 52.

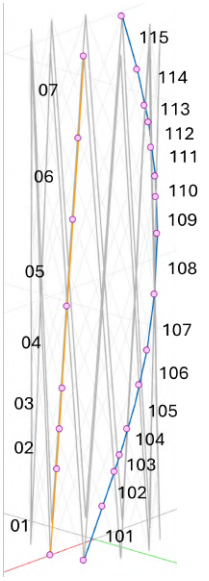

Figure 51: Element labels

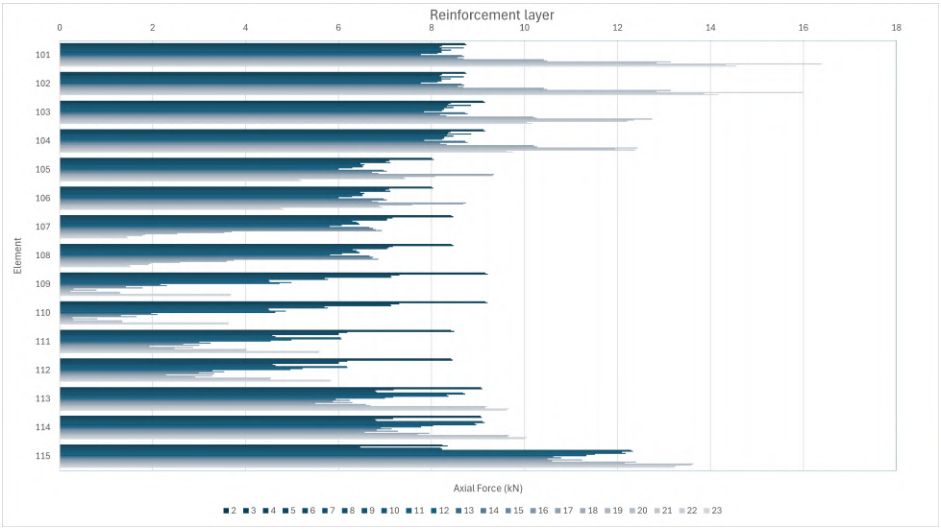

Figure 52: Graph of staging analysis

The hypothesis states that the lattice layer will experience an increasing axial force as it is pushed inward by the reinforcement layer, increasing the tension in this winding line. Conversely, the behavior is different for the first diagonal. As the diagonals deform the structure with each additional layer, the tension in the first winded diagonal decreases. This hypothesis is supported by the model for the lattice layer, as illustrated in Table 12, where the average force in the lattice and the diagonal is taken into account. Every stage represents the addition of a new diagonal. Table 12 shows the average value of one element of the lattice layer and one diagonal. However, for the diagonal, it can be seen that the average force increases in later stages. This is caused by the bottom and top elements (101/102 and 114/115), which get a very high axial force. where in the middle element, this force is constantly decreasing. This can also be seen in the graph of figure 52. the data from this analysis along with the graphs can be found in Appendix F

Table 12: Average axial force in elements

Stage	**2**	**3**	**4**	**5**	**6**	**7**	**8**	**9**	**10**	**11**	**12**
Element 1 (kN) (Lattice layer)*	2.43	2.452	2.69	2.68	5.15	5.16	6.62	6.59	7.82	7.69	7.66
Element 2 (kN) (Diagonal)*	8.64	8.69	7.25	7.36	7.50	7.59	7.69	7.59	7.61	7.23	6.94
Stage	**13**	**14**	**15**	**16**	**17**	**18**	**19**	**20**	**21**	**22**	**23**
Element 1 (kN) (Lattice layer)*	7.48	7.43	8.86	8.87	8.77	8.80	8.81	8.87	9.009	8.98	9.89
Element 2 (kN) (Diagonal)*	6.66	6.79	6.41	6.72	6.56	7.12	7.31	7.84	8.27	7.88	7.92

Since option 1 involves no loose rovings during the winding process, there is no compression in the winding layers. This model can be used to simulate the behavior of the rovings, specifically to determine if they will remain under tension and avoid "buckling" due to potential compression. By running a simulation on the design, it can be assessed whether the rovings will stay in tension without becoming loose.

6.5 Results of numerical analysis

Since the staging model is unfortunately not working with the an external force, a numerical model was created Karmaba3D plugin in Rhino Grasshopper. Karamba3D is a plug-in that uses the Finite Element Method (FEM) to perform calculations of parameterized geometric models in Grasshopper's environment. [20]. The initial geometric model consists of lines and points, which must be converted to beam elements with nodes containing physical properties for analysis. During conversion to the Karamba3D model, several assumptions are made in the assembly component. For instance, all points where lines intersect are considered fixed nodes. The material properties and the simplified cross-sections of the elements from table 11 are incorporated. Rigid elements are added to the top and bottom of the structure, representing the end nodes of the structure. These elements consist of a 'spider web' of lines. The properties of the rigid elements are manually entered to ensure the lines behave as rigid elements. Boundary conditions are then defined. The 'Beam-Joint' component defines the connection between the rigid elements and the filaments of the winded structure, allowing rotation and limiting translation. Supports are added to the center of the rigid elements: the bottom support prevents translation in the X, Y, and Z directions while allowing rotation, and the upper support restricts translation in the X and Y directions but allows translation in the Z direction. Additionally, rotation in the Z direction is restricted at the upper support to prevent torsional movement. The structure is axially loaded with a point load of 1 kiloNewton, which is transferred to the cross sections of the filament winded structure by the rigid elements.

Figure 53 illustrates the structure, showing the supports, cross-sections, rigid elements, and the applied point load. All defined elements, supports, connections, and loads are input for the 'Assemble' component, creating a structural model from the collected data. The 'Analyze' component is then used for the second-order buckling analysis of the structure, considering the deformation due to the applied point load. The output of the structural calculation includes the maximum displacement and the buckling load factor, as displayed in Table 13.

Table 13: Results of numerical model

	Option 1	**Option 2**	**Option 3**
Buckling load factor (-)	68.69	114.21	216.32
Reaction force (kN)	1	1	1
Displacement (mm)	0.03	0.08	0.06

After testing of the elements in the SED laboratory these results will be compared with the results of the test in the SED laboratory. After which a conclusion can be drawn as to whether this model is representable to simulate the behavior of the structure under compression.

Figure 53: Karamba model

7 Testing the element

Four fiber composite structures are tested in axial compression using the Instrom compression testing machine in the SED lab at TU/e. The structures were simply supported, allowing them to rotate freely at the structure supports while being fixed to prevent movement. Figure 54 illustrates the test setup for the axial compression test of the structure (V2O1). To distribute the load across all bundles and to equalize any unevenness between the bundles aluminum plates were used to fill the open spaces. Thus, each bundle is loaded simultaneously. A spherical hinge is positioned at both the top and bottom, with a steel plate attached to this hinge to cover the end of the structure and distribute the axial pressure point load uniformly across the structure.

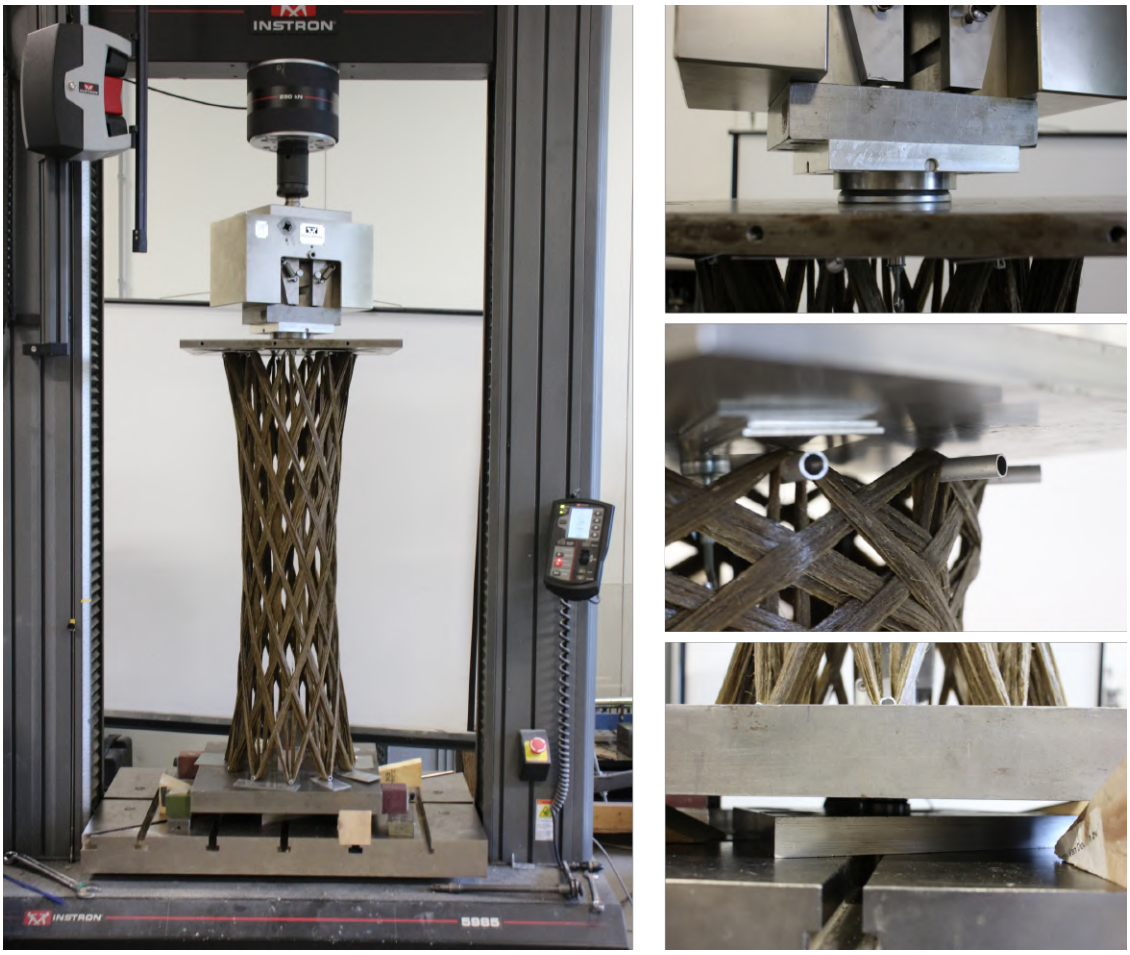

Figure 54: Test set-up

The compression tests aimed to analyze the structural behavior of the composite. For each test, a tensile wire sensor is installed to measure the vertical displacement of the structure, this is done with a magnet attached to the steel endplate of the compression test bench. The axial compression tests produced a force-displacement diagram that recorded the vertical displacement measured by the tensile sensor and the displacement of the bench.

7.1 Results

Finally four structures were fabricated and then tested in the test bench, the results of this test will be described in this section.

7.1.1 Compression test V1O1

This structure served as the test structure during the winding process. The structure suffered damage in several areas due to the ceramic ring detaching and damaging the fibers. Despite this, the structure was tested and achieved a maximum force of 23.64 kN. Figure 55 presents the test results in a force-displacement diagram.

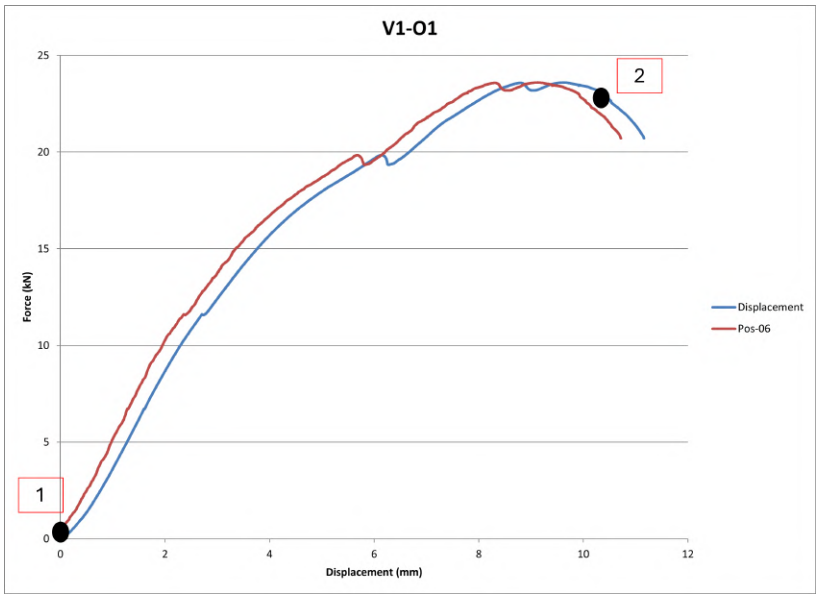

Figure 55: Force-displacement graph of V1O1

During this test, failure can be detected at the winding pins, as here the construction is, as it were, flattened and the sleeves are pushed out of the structure. It can also be clearly seen that the structure is buckling outwards at the top of the structure, as showed in figure 56.

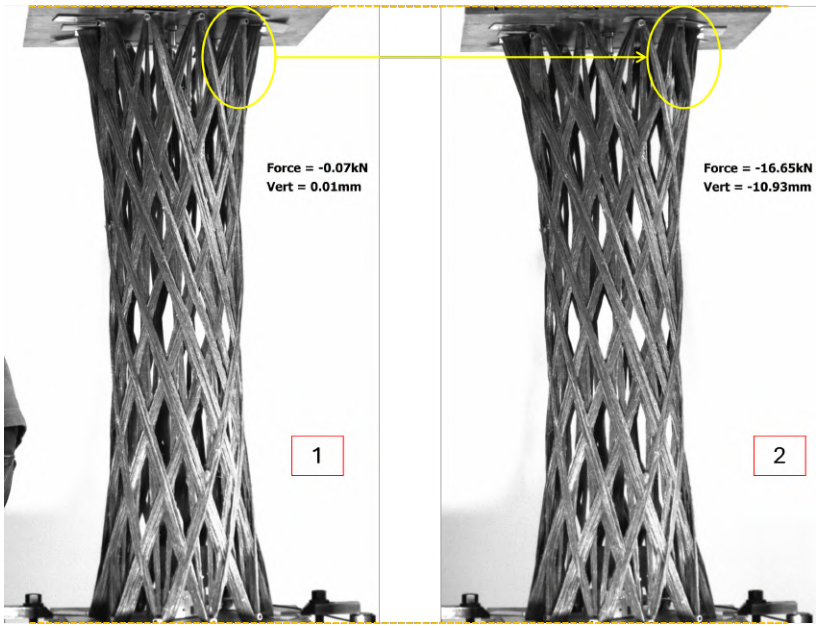

Figure 56: Buckling of bundle

7.1.2 Compression test V2O1

The second structure was visually rated as the most efficiently manufactured structure. The result of the test can be seen in figure 57, where the force-displacement graph of this test is displayed.

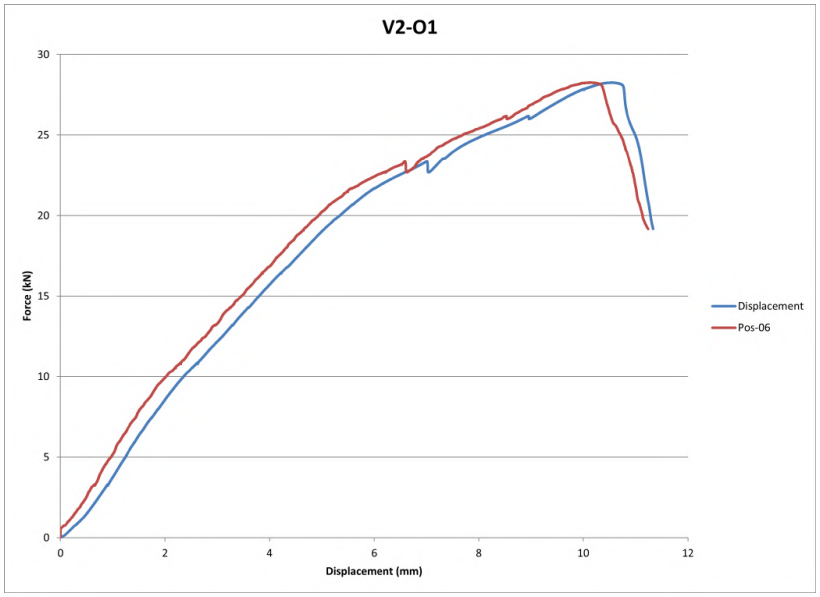

Figure 57: Force-displacement graph of V2O1

The structure failed as the unconnected bundles begin to buckle individually, leading to local failure of single bundles. This is visualised in figure 58, where it can be seen that the lattice layer buckled, due to delamination from the reinforcement layer. Afterwards the reinforcement layer starts also to delaminate. The delamination issue could have been mitigated by better analyzing the end conditions of the structure. Implementing an additional winding layer or using tyraps during testing might have prevented the delamination of these layers. This approach would likely result in test outcomes that are more consistent with the final model in Karamba3D. Additionally, the test setup could be improved by preventing lateral translation of the element, which is currently not accounted for.

Figure 58: Delamination of bundles

7.1.3 Compression test V1O2 and V1O3

All test results are listed in Appendix G: Test results physical tests, mainly for the test of options 2 and 3. These options already had many imperfections during winding so it was expected that these options would not perform as well as Option 1. Since it was assumed that the bundles would have a major role in the failure mechanisms. For Option 2, the failure mechanism is similar to that of Option 1. Where near the winding pins, the lattice layer delaminates from the reinforcement layer and then buckles as single bundles between two nodes. For option 3, no clear point can be found where this structure fails. It is assumed that on the inside of the structure (where the bundles have already buckled during the winding process) the bundles buckle further and thus the force can no longer be distributed. In the videos taken during testing, it can be seen how the structures react to the force and how it behaves. These videos are added in Appendix H.

7.2 Comparison with numerical model

For a comparison between the laboratory test result and the numerical model results, Table 14 summarizes the axial compression test results, showing the maximum compression force achieved and the maximum force according to the numerical model.

Table 14: Comparison of results

Specimen	Max compressive force reached [kN]	Max force in numerical model [kN]	Factor difference
V1O1	23.64	68.69	2.91
V2O1	28.49	68.69	2.41
V1O2	15.34	114.21	7.45
V1O3	16.69	216.32	12.96

7.2.1 Discussion of comparison

The comparison between the test results and the numerical model predictions for the axial compression tests reveals significant differences. The maximum compressive forces observed in the physical tests are considerably lower than those predicted by the numerical models. Possible reasons for these differences may be:

- Material properties and assumptions: The numerical model uses idealized material properties and assumes perfect material behavior, which may not accurately reflect the actual properties of the composite materials used. Variations in material quality, inconsistencies in the manufacturing process and inaccuracies in the assumed material properties can all contribute to differences in performance. Also, the modulus of elasticity for fibers used in the model may not match actual materials, leading to overestimation of structural capacity. The numerical model also uses several simplifications to make the analysis computationally feasible. These include assumptions about material cross-sectional area and perfect bonding between elements.

- Fabrication errors and imperfections: Manufacturing defects such as voids, incomplete impregnation of fibers, and inconsistencies in the winding process can reduce the strength of composite structures. For example, the loose bundles in design option 2 and 3. The numerical model does not account for these imperfections.

- Test Setup and Boundary Conditions: The boundary conditions and load setups in the tests may differ slightly from those assumed in the numerical model. For example, aluminum plates were used to distribute the load evenly. In the numerical model, this is assumed to be perfectly straight and thus the load will be absorbed equally by each bar. The model also assumes the boundary conditions as a fixed hinge, where no lateral movement is possible. However, with the structure placed on the steel plates of the compression testing machine, lateral displacement can be possible, leading to differences between the numerical model and physical testing.

The results highlight the importance of calibrating and validating numerical models with experimental data. To improve the accuracy of predictions, extensive material characterization should be performed to obtain accurate input data for the numerical models. This includes detailed testing of the mechanical properties of composite materials and consideration of variability in natural fibers. In addition, a numerical model capable of addressing manufacturing and material inconsistencies must be developed. It is also essential that the tests closely match the model calculations.

In this project, option 1 appears to be the best. The structural depth and bonding between the layers have a greater impact on the structural capacity of the element than the number of nodes. If the bonding between the layers is poor, the elements will buckle separately, increasing the probability of structural failure. It is important to note that the manufacturing process was not optimal. As a result, multiple design iterations of option 2 and option 3 are not made to optimize them without loose bundles in the design. Unfortunately, this project cannot conclude whether a structure with fewer nodes but more structural depth is stronger than one with more nodes but less structural depth.

For reference, photos were taken of each test and combined into a video, For these videos, reference is made to Appendix H: Videos of physical testing.

8 Discussion

The use of bio-based materials, such as flax fibers, represents a significant advancement in sustainable construction practices. Compared to traditional building materials, bio-based materials reduce CO2 emissions and overall environmental impact. This study confirms that incorporating flax fibers in construction can help achieve sustainability goals, aligning with global efforts to mitigate climate change. However, making a composite with flax fibers requires the use of a resin. For this study, resin which is already available at TUe is used due to the known safety risks and established working processes. Introducing a new resin would introduce new safety risks and potentially require several new procedures.

Given that composite structures are intended to enhance sustainability in the construction industry, the choice of resin is important. In this project, the resin consists of 38 percent bio-based materials [33], with the remaining 62 percent not yet bio-based. Since the composite is approximately 80 percent resin, it cannot be fully claimed that the structure contributes to sustainability in the construction sector. To achieve this, a fully bio-based resin needs to be identified that, in conjunction with flax fibers, can form a durable composite structure.

The amount of waste material is also an issue. In the manufacturing process as currently set up. Every part that should not be damaged by the resin should be packed with plastic foil as well as the ground and table the robot is standing on, Aluminum trays have been used to catch the dripping resin, The bolts which are damaged by resin. These materials can all be disposed after a round of winding. Also, the process as designed leaves quite a lot of resin. This is because there must be a certain amount of resin in the bath to keep impregnating the rovings. With each version of the winding process, about 1 kilogram of the 3.5 kilograms of resin remains in the silicone container. After hardening this has to be disposed.

The innovation of CRFW technology offers several benefits over traditional production methods. This method eliminates the need for auxiliary structures, reducing material waste and simplifying the fabrication process. CRFW technology also allows for the production of complex geometries that would be challenging to achieve with conventional methods. However, the implementation of CRFW presented several challenges, including ensuring consistent fiber tension and achieving uniform resin impregnation. This resulted in the manufacturing issues adressing with design option 2 and 3. More manufacturing iterations are needed to adress loose rovings in the design phase.

The new resin bath configuration improved control over the impregnation process, resulting in a consistent fiber volume ratio (FVR). However, this FVR is too low for manufacturing high-quality composites. According to the LivMatS Pavilion paper [13], an ideal FVR should be around 40 percent to achieve better material properties.

A practical application of this technique in the construction sector involves the use of resin and robots. The resin currently in use has a pot life of 50 minutes, making it suitable for creating composites, as demonstrated in this project. However, when producing larger elements, this pot life becomes a significant limitation. Additionally, the restricted space and reach of the robot present further challenges. During the project, the robot encountered difficulties in reaching certain points. To better align the impregnation process with the robot arm, a script was developed to tilt the end-effector. Unfortunately, this adjustment led to issues in reaching the target points, and thus, this approach was not implemented in the project.

To enable the production of larger elements with the existing equipment, one potential solution is to connect smaller elements to form a larger structure. It is crucial to consider that the connections between these elements will be critical to the overall structural performance of the structure.

9 Conclusion

This research project aims for the design and manufacturing of a three-dimensional structure using bio-based materials and Coreless Robotic Filament Winding (CRFW) technology. By focusing on flax fibers impregnated with partially bio-based epoxy resin, the study aimed to address significant challenges in the construction industry, namely environmental impact and labor shortages. A structure of one meter height should be simply supported.

The research started by conducting a literature study into robotic filament winding, lightweight structures, and axially loaded simply supported structures. It is found that buckling is the governing failure mechanism for slender structures loaded in axial compression. From this an optimization goal is found. The digital design process, executed using Rhinoceros and Grasshopper software with optimization through Karamba3D and Octopus plugins, resulted in three optimized design options. These optimized designs all have an anticlastic shape, since a shape study demonstrated that this shape is optimal for use in filament-wound structures and is optimal for their fabrication, since the fibers used will deform during the winding process resulting in an anticlastic shape. These design options are optimized using the length of the fiber needed to manufacture the design. Therefore the mass is consistent in the three variants.

After finding the design options, a winding path is determined which allowed the structure to be manufactured in one continuous winding session. Robot Components is used to combine all actions with the moveable work object and specified robot. This resulted in a RAPID-code, which is loaded into Robot Studio to simulate the complete winding path and manufacture the structure. Furthermore, the design of the robot end-effector and existing resin bath is adapted several times to improve the winding process for optimal impregnation of natural flat fibers instead of sisal ropes, which were first used in filament winding on TUe. The final structure is manufactured using Depestele FR 2400 flat flax rovings, impregnated with InfuGreen 810 epoxy resin and SD 8824 hardener. This material is chosen to continue on previously conducted studies at TU/e. The flax rovings are unwound from the bobbin and guided through a resin bath, after which the impregnated rovings are bundled and directed to the end-effector. The full filament winding process is tested with sisal rope before final manufacturing. The manufacturing process involved the ABB IRB 1200-5/0.9 robot, which successfully produced the structures without auxiliary supports, only using two end plates with winding pins. Post-manufacturing, the structures underwent curing, and their performance is calibrated and analyzed using numerical models in Oasys GSA and Karamba3D.

A total of four structures were manufactured. Numerical modeling and monitoring during the winding process indicated that the staging analysis results were reasonably consistent with actual conditions. However, testing showed that the filament-wound structures, composed of multiple elements, exhibited local buckling before global buckling. These results highlighted significant differences between numerical predictions and actual test outcomes, primarily due to idealized material properties, fabrication errors, and test setup conditions.

The study confirmed the feasibility of manufacturing an optimized design using bio-based flax fibers through robotic filament winding. A new resin bath and end effector were developed, to continue on winding with bio-based natural fibers. The resin bath and end-effector are both reusable as research has been done to protect all parts in the process with release agents. While the structural performance is promising, imperfections in the process indicated a need for further research to enhance accuracy and reduce variability. Future investigations should focus on detailed material characterization, improved numerical models accounting for manufacturing inconsistencies, and the scalability of this technology for large-scale applications. Additions such as a robotic end effector that can measure pretension in roving bundles or an impregnation end effector could significantly improve research on filament wound structures at Eindhoven University of Technology. These tools would provide more accurate control and quality assurance in the production process, improving the overall efficiency and reliability of filament wound structures.

10 Recommendations

Reflecting on the entire process from design process to final testing, several elements deserve further research. One consideration is the environmental impact of the materials used. This research aimed to reduce the environmental pollution associated with the traditional design and manufacturing processes in the construction sector. As a result, the structure was constructed using bio-based flax fibers. However, the SR InfuGreen 810 epoxy resin used to impregnate the rovings contains only 38% bio-based content. To achieve a fully bio-based structure, further study on epoxy resins with higher green content is recommended, ensuring they maintain favorable curing cycles and viscosity during manufacturing. In future projects involving resin, it is recommended to consider the use of Oribond by the Orineo company, for example. Oribond is fully biobased, which underscores its environmental friendliness and aligns with the commitment to using sustainable materials. It has versatile curing conditions and non-toxic ingredients.

Further investigation is needed to increase the material properties and the filament winding process. This includes improving the flax fibers impregnation with bio-based epoxy resin and optimizing the winding techniques to ensure consistent structural properties. This can be done by more design iterations with the resin bath configuration, ensuring an optimal fiber volume ratio. Also conducting comprehensive testing to understand the long-term performance and durability of structures made using CRFW technology with bio-based materials. This includes studying the effects of environmental exposure, load-bearing capacity over time, and potential failure modes.

Improving the accuracy of numerical models used to simulate the manufacturing process and predict structural behavior involves calibrating these models with experimental data. Enhancing simulation tools to better replicate the complexities of the winding process and material behavior is essential. Currently, the project utilizes a numerical staging model for option 1, as other models do not accurately represent reality. This approach can be expanded to simulate various generated structure models, enabling better predictions of structural behavior during the winding process. This improvement is likely to lead to a more efficient manufacturing method, reducing material waste and producing more reliable structures without inequalities or defects, such as loose ropes. Additionally, this may decrease the differences between numerical simulations and physical testing results.

It is recommended that future testing of the elements should better align with the boundary conditions used in the numerical model. Currently, there are differences between the testing setup and the model assumptions. To achieve more accurate and reliable comparisons ensure that the boundary conditions in the physical tests closely match those assumed in the numerical models. For example, modify the test setup to prevent lateral displacement and to ensure even load distribution. For example, the use of spherical hinges and aluminum plates should be re-evaluated to match the fixed hinge conditions assumed in the model. Or develop a numerical model capable of addressing manufacturing and material inconsistencies. Include imperfections observed during the manufacturing process in the model to better predict the structural behavior.

Lastly, Adding advanced tools such as a robotic end effector capable of measuring pretension in rovings or an impregnation end effector, as shown by the university of Stuttgart [26], could substantially enhance research on filament winded structures at Eindhoven University of Technology. An innovative end effector design featuring two separate chambers for resin and hardener allows for impregnation directly within the end effector while keeping the two components isolated until the point of application. This design ensures precise control over the mixing process and prevents premature curing, thus enabling more accurate control and quality assurance during the production process. These improvements would lead to enhanced efficiency and reliability of the resulting filament wound structures and reducing waste by only use limited amount of resin. By integrating these tools, the university could achieve higher standards in their research and production capabilities, ultimately contributing to advancements in the field of filament winding technology.

References

[1] Stand van de Bouw . . . de bouwsector in economisch perspectief. Technical report.

[2] RESOURCE EFFICIENT STRUCTURAL ENGINEERING and DESIGN Arjan Habraken. Technical report, 2021.

[3] Ahmad Faiz Abd Rashid, Sumiani Yusoff, and Noorsaidi Mahat. A review of the application of LCA for sustainable buildings in Asia. In *Advanced Materials Research*, volume 724-725, pages 1597–1601, 2013.

[4] Bharat Bhaga and Craig Steeves. Compressive Instabilities In Metal-Coated Polymer Microtrusses. York University Libraries, 5 2018.

[5] SERBAN BODEA, NICCOLO DAMBROSIO, CHRISTOPH ZECHMEISTER, ACHIM MENGES, MARTA GIL PEREZ, VALENTIN KOSLOWSKI, BAS RONGEN, JAN KNIPPERS, MORITZ DÖRSTELMANN, and ONDREJ KYJANEK. BUGA FIBRE PAVILION:. In *Fabricate 2020*, pages 234–243. UCL Press, 7 2020.

[6] H. L. Bos. *The potential of flax fibres as reinforcement for composite materials.*

[7] Jorge Christie, Serban Bodea, Eth Zurich, James Solly, Achim Menges, J Christie, S Bodea, J Solly, A Menges, J Knippers, and Jan Knippers. Filigree Shell Slabs Material and Fabrication-aware Shape Optimisation for CFRP Coreless-wound Slab Components Maison Fibre View project Self-shaping wood View project The user has requested enhancement of the downloaded file. Filigree Shell Slabs Material and Fabrication-aware Shape Optimisation for CFRP Coreless-wound Slab Components.

[8] B ; Dean, J ; Dulac, K ; Petrichenko, and P Graham. Towards zero. Technical report, 2016.

[9] Moritz Doerstelmann, Jan Knippers, Achim Menges, Stefana Parascho, Marshall Prado, and Tobias Schwinn. ICD/ITKE Research Pavilion 2013-14: Modular Coreless Filament Winding Based on Beetle Elytra. *Architectural Design*, 85(5):54–59, 9 2015.

[10] Rebeca Duque Estrada, Fabian Kannenberg, Hans Jakob Wagner, Maria Yablonina, and Achim Menges. Spatial winding: cooperative heterogeneous multi-robot system for fibrous structures. *Construction Robotics*, 4(3-4):205–215, 12 2020.

[11] Muhammad Fahad, Sikandar Ali, Mukhtaj Khan, Mujtaba Husnain, Zeeshan Shafi, and Ali Samad. Asymptotically Effective Method to Explore Euler Path in a Graph, 2021.

[12] A. Ghazanfari, S. Emami, L. G. Tabil, and S. Panigrahi. Thin-layer drying of flax fiber: I. Analysis of modeling using Fick's second law of diffusion. *Drying Technology*, 24(12):1631–1635, 2006.

[13] Marta Gil Pérez, Yanan Guo, and Jan Knippers. Integrative material and structural design methods for natural fibres filament-wound composite structures: The LivMatS pavilion. *Materials and Design*, 217, 5 2022.

[14] Marta Gil Pérez, Bas Rongen, Valentin Koslowski, and Jan Knippers. Structural design assisted by testing for modular coreless filament-wound composites: The BUGA Fibre Pavilion. *Construction and Building Materials*, 301, 9 2021.

[15] Andreas Göbert, Arjen Deetman, Andrea Rossi, Ole Weyhe, and Philipp Eversmann. 3DWoodWind: robotic winding processes for material-efficient lightweight veneer components. *Construction Robotics*, 6(1):39–55, 3 2022.

[16] Groupe Depestele. Production of Flax, 2024.

[17] Yanan Guo, Gokhan Serhat, Marta Gil Pérez, and Jan Knippers. Maximizing buckling load of elliptical composite cylinders using lamination parameters. *Engineering Structures*, 262, 7 2022.

[18] Bryan Harris. ENGINEERING COMPOSITE MATERIALS. Technical report, The Institute of Materials, Londen, 1999.

[19] Pedro J. Herrera Franco and Alex Valadez-González. Fiber-matrix adhesion in natural fiber composites. *Natural Fibers, Biopolymers, and Biocomposites*, pages 177–230, 1 2005.

[20] Karamba. Karamba3D, 2024.

[21] Azizatul Karimah, Muhammad Rasyidur Ridho, Sasa Sofyan Munawar, Danang Sudarwoko Adi, Ismadi, Ratih Damayanti, Bambang Subiyanto, Widya Fatriasari, and Ahmad Fudholi. A review on natural fibers for development of eco-friendly bio-composite: characteristics, and utilizations, 7 2021.

[22] Krijnen L P J. Final thesis version 1.0 — Graduation Project Numerical optimization and manufacturing of a bio-based 3D structure through robotic filament winding. Technical report, 2023.

[23] L. Louer. Optimization and Production of a Bio-based Bridge Railing through Robotic Filament Winding. Technical report, Eindhoven University of Technology, Eindhoven, 1 2022.

[24] Feray Maden. Geometric and Kinematic Analysis of Deployable Doubly Ruled Hyperboloids. *MEGARON / Yıldız Technical University, Faculty of Architecture E-Journal*, 2017.

[25] Achim Menges, Moritz Dörstelmann, Jan Knippers, and Thomas Auer. Elytra Filament Pavilion, 2016. In *Robotic Building*, pages 34–36. DETAIL, 12 2019.

[26] Pascal Mindermann, Serban Bodea, Achim Menges, and Götz T. Gresser. Development of an impregnation end-effector with fiber tension monitoring for robotic coreless filament winding. *Processes*, 9(5), 2021.

[27] Oasys. Oasys GSA Help Guide. Technical report, 1985.

[28] OPTI 222. Buckling-Other End Conditions. Technical report.

[29] Yujun Qi, Wei Xiong, Weiqing Liu, Hai Fang, and Weidong Lu. Experimental study of the flexural and compression performance of an innovative pultruded glass-fiber-reinforced polymer-wood composite profile. *PLoS ONE*, 10(10), 10 2015.

[30] Robert Vier. Octopus plugin, 3 2020.

[31] Luc Roex and Daan Janssen. Final Report Research Project. 2021.

[32] Kevin Saslawsky, Christian Steixner, Michael Tucker, Vanessa Costalonga, and Hanaa Dahy. FlaxPack: Tailored Natural Fiber Reinforced (NFRP) Compliant Folding Corrugation for Reversibly Deployable Bending-Active Curved Structures. *Polymers*, 16(4), 2 2024.

[33] Sicomin. Infugreen 810, 2024.

[34] Nadine Stoiber and Benjamin Kromoser. Topology optimization in concrete construction: a systematic review on numerical and experimental investigations, 10 2021.

[35] T.S. Pannekeet. Optimization and Analysis of the Structural Performance of a Sisal Beam in Robotic Filament Winding. Technical report, Eindhoven University of Technology, 2023.

[36] Wikipedia. Mass Fraction. International Union of Pure and Applied Chemistry (IUPAC), 9 2024.

[37] Wiktionary. Pot life, 2024.

A Appendix: Sicomin technical datasheet

SR InfuGreen 810

Green Epoxy systems for Injection and Infusion

The ***InfuGreen* 810** is a two-component epoxy system. It has been specially formulated for resin transfer processes, such as injection or infusion.
This system has a very low viscosity at ambient temperature.
The different hardeners allow the production of small to very large parts.
The cured system gives a temperature resistance up to 100°C (Tg onset)
The hardeners SD 4770 and 4771 are designed for very thick laminates by infusions.

***SR InfuGreen* 810** Epoxy resin is produce with about 38 % of carbon from plant origin and has a lower environmental impact than standard Epoxy systems.
The bio-based Carbon content of our resin is certified by an independent laboratory using Carbon 14 measurements (ASTM D6866 or XP CEN/TS 16640).
This percentage is function of the carbon origin contained in the epoxy molecule.

***SR InfuGreen* 810** is DNV-GL *Maritime* approved DNV·GL.

GreenPoxy®

Sicomin, 31 avenue de la Lardière, 13220 Châteauneuf les Martigues, France
T: +33 (0)4 42 42 30 20 / F: +33 (0)4 42 81 29 29 / E: info@sicomin.com / www.sicomin.com

Epoxy resin *SR InfuGreen* 810

Aspect		Clear liquid
Color Gardner		1 maximum
Viscosity (± 20 % mPa.s)	@ 15 °C @ 20 °C @ 25 °C @ 30 °C @ 40 °C	2 200 1200 750 470 210
Carbon Green content (± 3 %)	GreenPoxy®	38 %
Density Pycnometer (±0.01) Helium (±0.005)	@ 20 °C	 1.16 1.152
Refractive index (± 0.0020)	@ 25 °C	1.5491
Storage stability		24 Months @ ambient temperature

Can crystallize at low temperature or after a long storage.
If SR InfuGreen 810 develops a haziness or crystallizes during storage, warming it @ 50 to 60 °C, with stirring, will restore it to its original state

Hardeners SD 882x SD 477x

Reference		SD 8825.2	SD 8824	SD 8822	SD 4772	SD 4771	SD 4770
Reactivity type		**Fast**	**Standard**	**Slow**		**Ultra-slow**	**Mega slow**
Aspect / colour		Light yellow liquid					
Color Gardner		3 maximum	4 maximum	5 maximum	3 maximum		
Viscosity	@ 15 °C	9	7	27	13		
(+ 20 % mPa.s)	@ 20 °C	7	6	20	11		
	@ 25 °C	6	5	16	9		
	@ 30 °C	5	4	13	7		
	@ 40 °C	4	3	9	5		
Carbon Green content	%	none					
Storage stability	AT	24 months Hardeners react with carbon dioxide and moisture. Keep tightly closed packaging, minimize maximum contact with the air.					
Density Pycnometer (±0.010)	@ 20 °C	0.915	0.944	0.935	0.927	0.944	0.944
Refractive index (± 0.002)	@ 25 °C	1.4785	1.4982	1.4712	1.4822	1.4594	1.4604

SR InfuGreen 810 / SD 8822 SD 477x Mixes

References		SD 8825.2	SD 8824	SD 8822	SD 4772	SD 4771	SD 4770
Mixing ratio by weight		100 / 22	**100 / 22**	**100 / 31**		**100 / 29**	
Mixing ratio by volume		100 / 28	**100 / 27**	**100 / 39**		**100 / 36**	
Initial mix viscosities	@ 20 °C	230	200	320	330	235	142
	@ 30 °C	130	100	120	90	115	100
Time to reach 300 cps " Optimal infusion time''	@ 20 °C	28'	44'	/	/	60'	3 h 20'
	@ 30 °C	40'	50'	67'	90'	130'	160'
Carbon Green content maximum Calculated (+/- 3 %)	GreenPoxy®	31	31	29	29	29	29

Viscosities increase on 1 mm film thickness

@ 20 °C

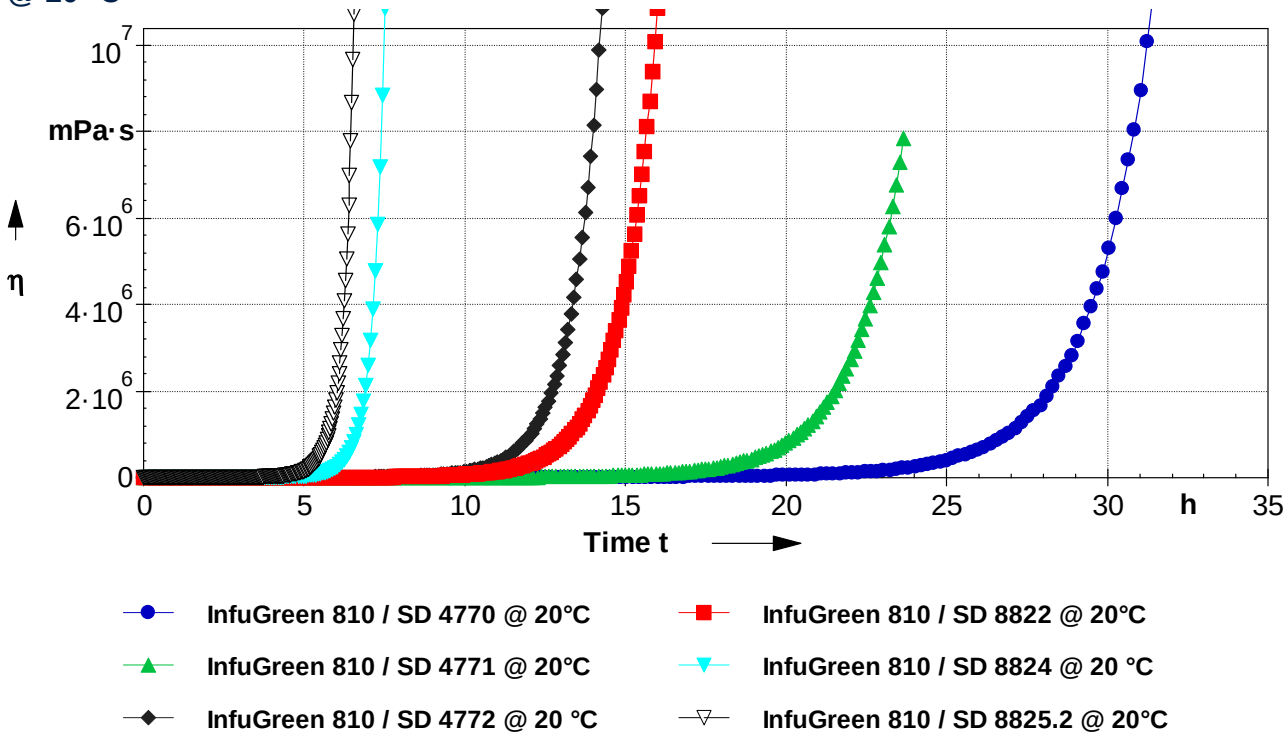

Zoom initial @ 20 °C

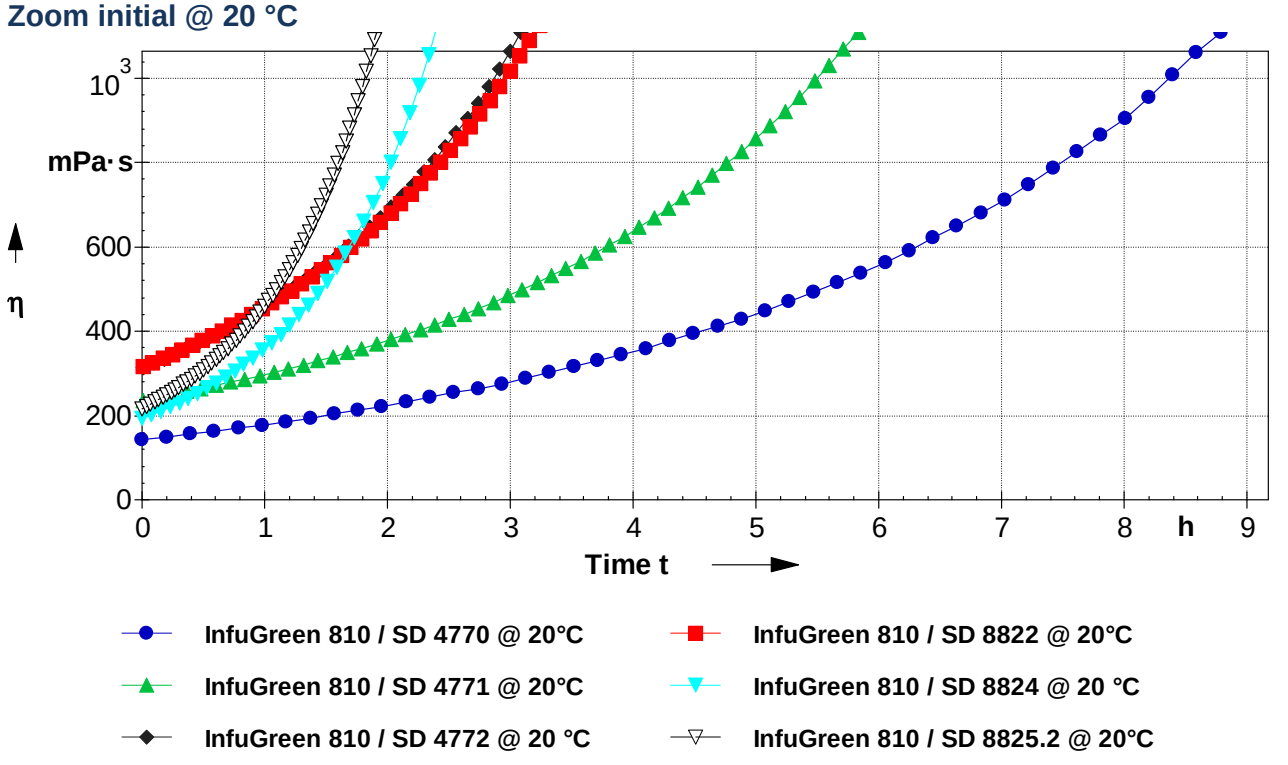

@ 30 °C

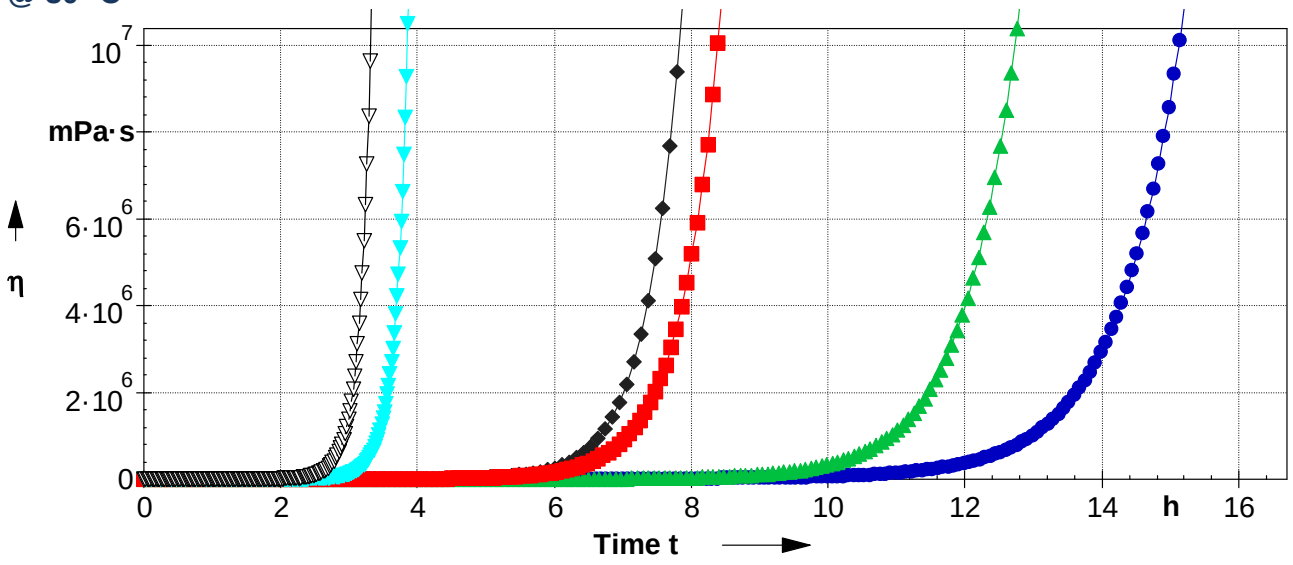

- InfuGreen 810 / SD 4770 @ 30 °C
- InfuGreen 810 / SD 8822 @ 30°C
- InfuGreen 810 / SD 4771 @ 30 °C
- InfuGreen 810 / SD 8824 @ 30 °C
- InfuGreen 810 / SD 4772 @ 30 °C
- InfuGreen 810 / SD 8825.2 @ 30 °C

Zoom initial @ 30°C

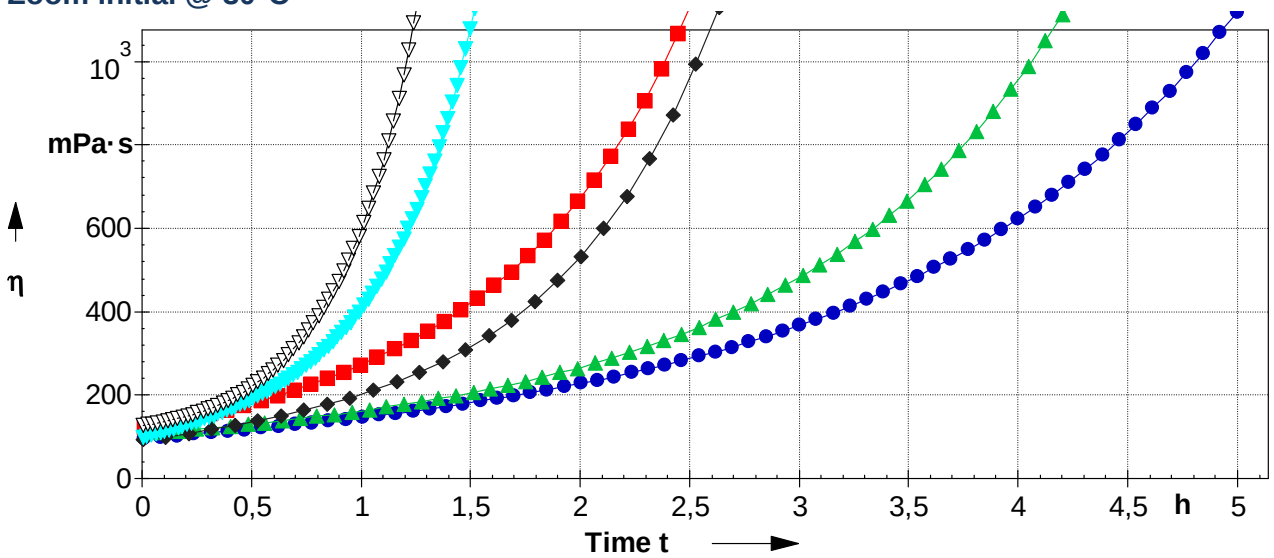

- InfuGreen 810 / SD 4770 @ 30 °C
- InfuGreen 810 / SD 8822 @ 30°C
- InfuGreen 810 / SD 4771 @ 30 °C
- InfuGreen 810 / SD 8824 @ 30 °C
- InfuGreen 810 / SD 4772 @ 30 °C
- InfuGreen 810 / SD 8825.2 @ 30 °C

Mechanical properties on cast resin

		***SR InfuGreen* 810 / SD 8825.2**			***SR InfuGreen* 810 / SD 8824**		
Curing cycle →		AT + 24 hrs 40 °C	AT + 16 hrs 60 °C	AT + 8 hrs 80 °C	AT + 8 hrs 40 °C	AT + 16 hrs 60 °C	AT + 8 hrs 80 °C
Tension							
Modulus of elasticity	N/mm^2	3000	2700	2600	3000	2800	2600
Maximum resistance	N/mm^2	69	68	67	68	65	60
Resistance at break	N/mm^2	55	53	64	57	57	52
Elongation at max.load	%	3.8	4.8	5.7	3.6	4.4	5.0
Elongation at break	%	5.9	9.1	8.0	5.3	5.9	9.5
Flexion							
Modulus of elasticity	N/mm^2	3000	2700	2600	3100	2800	2600
Maximum resistance	N/mm^2	113	112	108	109	107	101
Elongation at max.load	%	4.9	6.1	6.6	4.6	5.7	6.0
Elongation at break	%	12.6	11.6	11.9	12.6	9.3	13.4
Shear strenght							
Maximum resistance	N/mm^2	46	45	45	43	42	41
Compressive							
Compressive yield strength	N/mm^2	98	95	93	91	87	82
Offset compressive yield	%	11.7	15.1	15.7	12.3	13.0	14.9
Impact Choc Charpy							
Resilience	KJ/m^2	80	80	70	100	90	90
Glass Transition							
Tg1 onset	**°C**	72	91	96	69	83	82
Tg1 onset maximum	**°C**			94			82

		***SR InfuGreen* 810 / SD 8822**			***SR InfuGreen* 810 / SD 4770**		
Curing cycle →		AT + 24 hrs 40 °C	AT + 24 hrs 40 °C	AT + 16 hrs 60 °C	AT + 8 hrs 80 °C	AT + 16 hrs 60 °C	AT + 8 hrs 80 °C
Tension							
Modulus of elasticity	N/mm^2	3000	2900	2700	3160	3100	2700
Maximum resistance	N/mm^2	66	67	61	71	74	70
Resistance at break	N/mm^2	55	60	53	70	68	69
Elongation at max.load	%	3.5	4.4	4.9	3.1	4.2	5.0
Elongation at break	%	4.3	6.1	8.0	3.2	5.1	5.6
Flexion							
Modulus of elasticity	N/mm^2	2900	2800	2700	3250	3000	2770
Maximum resistance	N/mm^2	99	106	101	116	116	115
Elongation at max.load	%	4.4	5.6	6.0	4.6	5.4	6.4
Elongation at break	%	15.5	13.6	13.6	9.8	7.4	7.8
Shear strenght							
Maximum resistance	N/mm^2	43	43	41	47	47	45
Compressive							
Compressive yield strength	N/mm^2	91	91	84	104	100	95
Offset compressive yield	%	11	12	13	11.3	12.8	14.6
Impact Choc Charpy							
Resilience	KJ/m^2	85	88	75	85	83	80
Glass Transition							
Tg1 onset	**°C**	63	74	85	69	84	97
Tg1 onset maximum	**°C**			84			98

Measures undertaken according to the following norms:

Tests carried out on samples of pure cast resin, without prior degassing, between steel plates.

Tension:	*ISO 527 - 2*
Flexion:	*ISO 178*
Charpy impact strength:	*NF T 51-035*
Shear Strength:	*ASTM D 732 - 93*
Compression:	*ISO 604*
Water absorption:	*Internal. Polymerization according to cycle, machining, weighing, time spent in distilled water at 70 °C / 48 hours, weighing 1 hour after emerging,*

Glass transition DSC:	*ISO 11357-2: 1999 -5°C to 180 °C under nitrogen gas*	
	T_{G1} or Onset: 1st point at 20 °C/min	*T_{G1} maximum or Onset: second passage*
Glass transition DTMA:	*ISO 11357-1 - T_G onset G'*	*Temperature ramp 0 °C to 180 °C @ 2°C/min*
	ASTM D4065 - T_G peak G''	

Physical tests according standard:

Gardner color:	*NF EN ISO 4630*	*Visual method*
Refractive index:	*NF ISO 280*	
Viscosity:	*NF EN ISO 3219*	*Rheometer 50 mm, shear 10 s^{-1}*
Density:	*NF EN ISO 2811-1*	*Pycnometer*
Density solid	*NF EN ISO 845*	
Gel time:	*Cross G' G''*	*Rheometer CP50 - Shear rate 10 s^{-1}*
Green Carbone content:	*ASTM D6866 or XP CEN/TS 16640 Avril 2014*	

AT: *Ambiant temperature*

LEGAL NOTES:

The information given in writing or verbally, in the context of our technical assistance and our trials, do not engage our responsibility. They are given in good faith based on SICOMIN's current knowledge and experience of the products when properly stored, handled and applied under normal conditions in accordance with SICOMIN's recommendations. So, we advise the users of SICOMIN products, to check by some practical trials they are suitable for the envisaged processes and applications. The customer's storage, the use, the implementation and the transformation of the supplied products, are not under our control and your responsibility only will respond for it.

SICOMIN reserves the right to change the properties of its products. All technical data stated in this Product Data Sheet are based on laboratory tests. Actual measured data and tolerance may vary due to circumstances beyond our control.

If our responsibility should nevertheless be involved, it would be, for all the damages, limited to the value of the goods supplied by us and implement by the customer. We guaranty the non-reproachable quality of our products, in the general context of sales and delivery. Users must always refer to the most recent issue of the local Product Data Sheet for the product concerned, copies of which will be supplied on request.

B Appendix: FR 2400 technical datasheet

FR 2400

ROVING LIN 100% LIN LINCORE®

LINCORE® 100% FLAX ROVING

FICHE TECHNIQUE / *PRODUCT DATAS*

DEFINITION / DESCRIPTION

Fibre *Fiber*	100% lin (Label European Flax) *100% flax (European Flax Label)*
Type de ruban *Type of roving*	Plat et non retordu *Flat and untwisted*

CONDITIONNEMENT / *PACKAGING*

Longueur de ruban* *Roving length**	1041 m
Masse nette de la bobine (teneur en eau 8%)** *Bobbin net weight (8% water content)***	2,50 kg
Type de bobine *Type of bobbin*	Dévidage extérieur *External unwinding*
Diamètre interne du mandrain en carton*** *Inside diameter of cardboard core****	3 pouces - 76 mm *3 inches -76 mm*
Longueur du mandrin en carton*** *Length of cardboard core****	11 pouces - 28 cm *11 inches - 28 cm*
Diamètre extérieur de la bobine *Bobbin external diameter*	20 cm max
Conditions de stockage recommandées *Recommended storage conditions*	Température ambiante, humidité relative = 60 ± 15% Ambient temperature, relative humidity = 60 ± 15%

CARACTERISTIQUES DU RUBAN / *ROVING CHARACTERISTICS*

Titre du roving (teneur en eau 8%) *Roving linear density (8% water content)*	2400 tex ± 4%	0,41 Nm ± 4%
Epaisseur** *Thickness***	min : 0,3 mm	max : 0,5 mm
Largeur** *Width***	11 mm ± 2 mm	
Force à rupture (jaugé sur 1m)**** *Strength at break (1 meter gauge)* ****	> 30 N, Moy>50 N	> 1,5 RKM, Moy=2,5 RKM
Densité* *Density**	d_{lin}=1,45 g/cm^3 d_{flax} *=1,45 g/cm* ^{3}	

* mesure informative */ just for information,* ** non contractuel */subject to variation,* *** selon spécificités fournisseur/*according to supplier specifications*

**** hors épissure */ without splice*

TRANSFORMATIONS & APPLICATIONS

Mise en œuvre *Forming process*	Tissage, tricotage, tressage, NCF, pultrusion, enroulement filamentaire *Weaving, knitting, braiding, NCF, pultrusion, filament winding*
Applications usuelles *Product applications*	Transport, sports et loisirs, réservoirs et membranes... *Transportation, sports and leisure, tanks and vessels…*

IMPORTANT

Les renseignements contenus dans la présente fiche produit sont fondés sur notre savoir faire et sur les résultats d'essais Ils doivent être adaptés à chaque cas particulier. Les performances du produit après utilisation étant liées aux conditions particulières de mise en oeuvre, elles ne sauraient engager notre responsabilité.

All information is believed to be accurate. Users should make their own assessment of the suitability of any product for the purpose required. All sales are made subject to our standard terms of sales which include limitations on liability and other important terms.

Mise à jour le 28/03/2023, version FR 2400 V4

DEPESTELE
teillage Vandecandelaere - Rue de l'église - 14540 Bourguébus
Tél. : + 33 (0)2 31 23 11 08
E-mail : contact@depestele.com - Site internet : www.groupedepestele.com

C Appendix: Product specifications ABB IRB 1200-50.9

Product specifications ABB IRB 1200-5/0.9 (ABB, 2022)

Manipulator axes

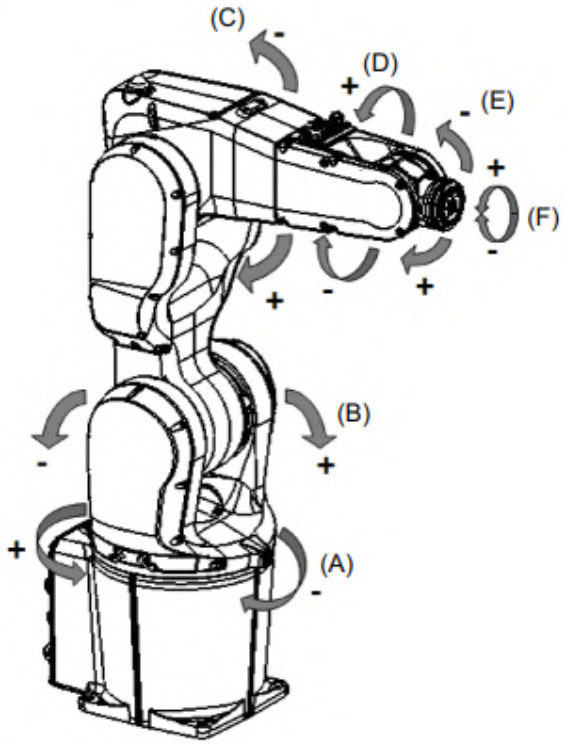

xx1300000365

Position	Description	Position	Description
A	Axis 1	B	Axis 2
C	Axis 3	D	Axis 4
E	Axis 5	F	Axis 6

General

The IRB 1200 is available in two versions and both can be mounted on floor, inverted or on wall in any angle (around X-axis or Y-axis).

Robot type	Handling capacity (kg)	Reach (m)
IRB 1200	5 kg	0.9 m

Weight, robot

The table shows the weight of the robot.

Robot model	Weight
IRB 1200	IRB 1200-5/0.9: 54 kg IRB 1200-7/0.7: 52 kg

Note

The weight does not include tools and other equipment fitted on the robot.

Dimensions IRB 1200-5/0.9

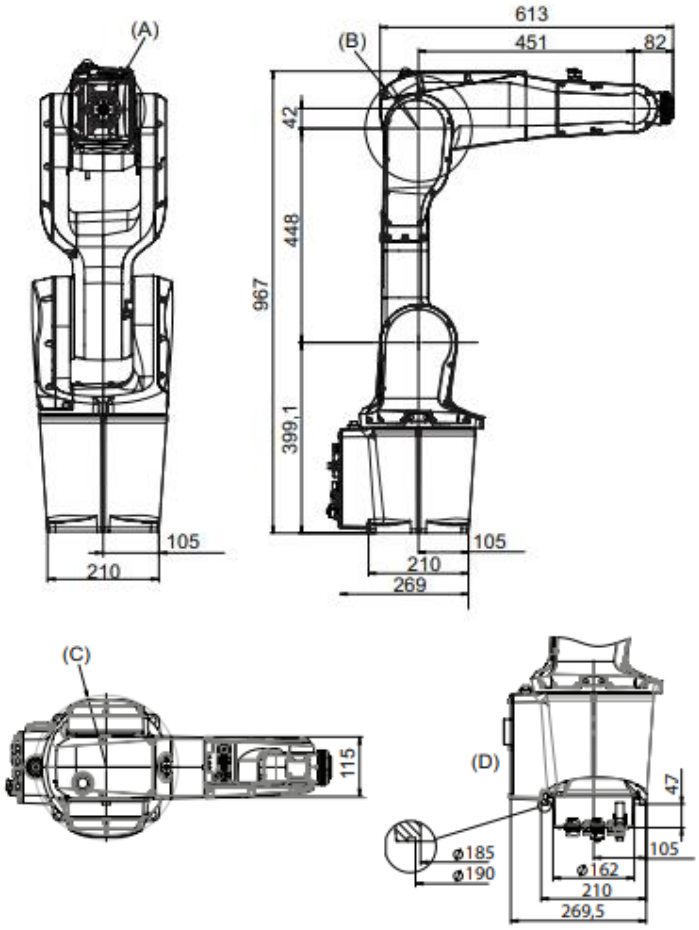

xx1400000339

Pos	Description
A	Minimum turning radius axis 4 R=79 mm
B	Minimum turning radius axis 3 R=111 mm
C	Minimum turning radius axis 1 R=138 mm
D	Valid for option Robot cabling routing, 966-1 From below

Robot tool flange

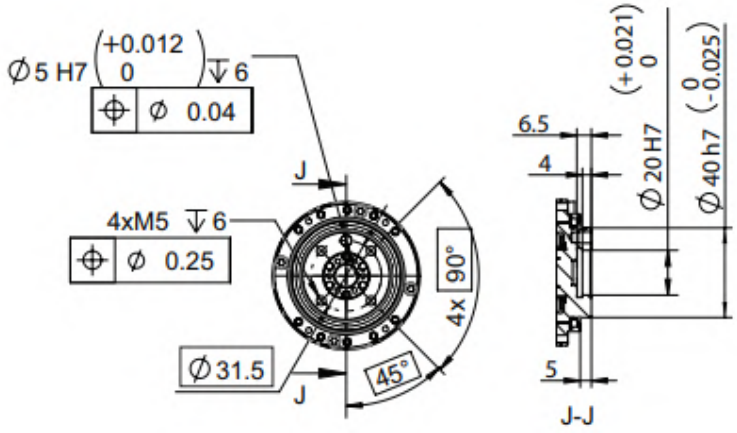

Robot motion

Location of motion	Type of motion	IRB 1200-7/0.7	IRB 1200-5/0.9
Axis 1	Rotation motion	+170° to -170°	+170° to -170°
Axis 2	Arm motion	+135° to -100°	+130° to -100°
Axis 3	Arm motion	+70° to -200°	+70° to -200°
Axis 4	Wrist motion	+270° to -270°	+270° to -270°
Axis 5	Bend motion	±130° (not Hygienic robots) ±128° (Hygienic robots)	±130° (not Hygienic robots) ±128° (Hygienic robots)
Axis 6	Turn motion	Default: +400° to -400° Maximum revolution: ±242[i]	Default: +400° to -400° Maximum revolution: ±242[i]

[i] The default working range for axis 6 can be extended by changing parameter values in the software. Option Independent axis can be used for resetting the revolution counter after the axis has been rotated (no need for "rewinding" the axis).

Working range

IRB 1200-5/0.9 Working range, positions at wrist center and angle of axes 2 and 3

The illustration shows the unrestricted working range of the robot.

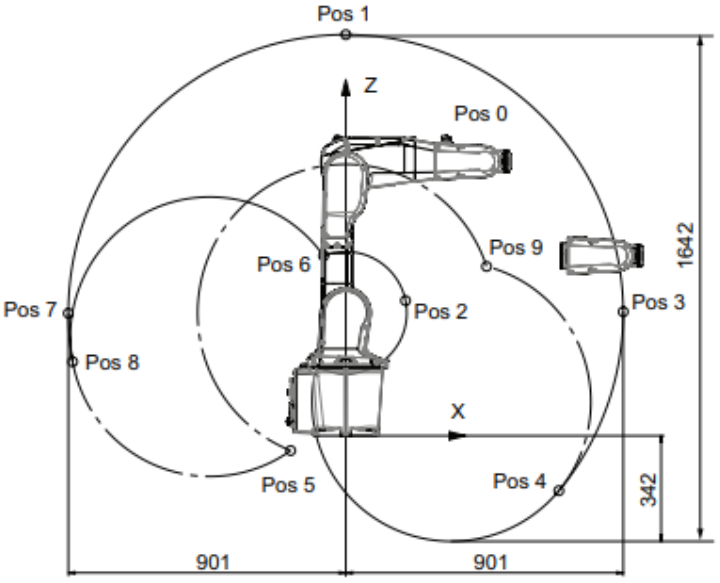

Position in the figure	Positions at wrist center (mm)		Angle (degrees)	
	X	Z	Axis 2	Axis 3
Pos0	451	889	0º	0º
Pos1	0	1300	0º	-85º
Pos2	194	438	0º	+70º
Pos3	901	402	+90º	-85º
Pos4	692	-178	+130º	-85º
Pos5	-179	-48	-100º	-200º
Pos6	-72	583	-100º	+70º
Pos7	-901	397	-90º	-85º
Pos8	-887	240	-100º	-85º
Pos9	458	549	+130°	-200°

D Appendix: Overview Grasshopper script

Geometrical part

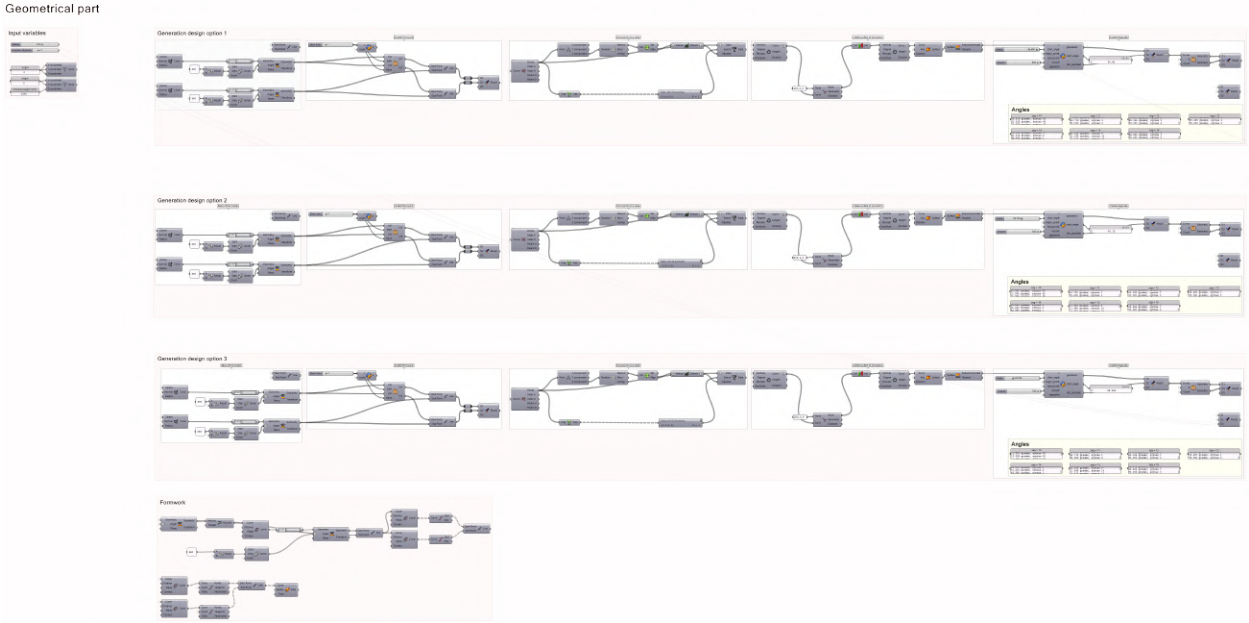

Manufacturing part

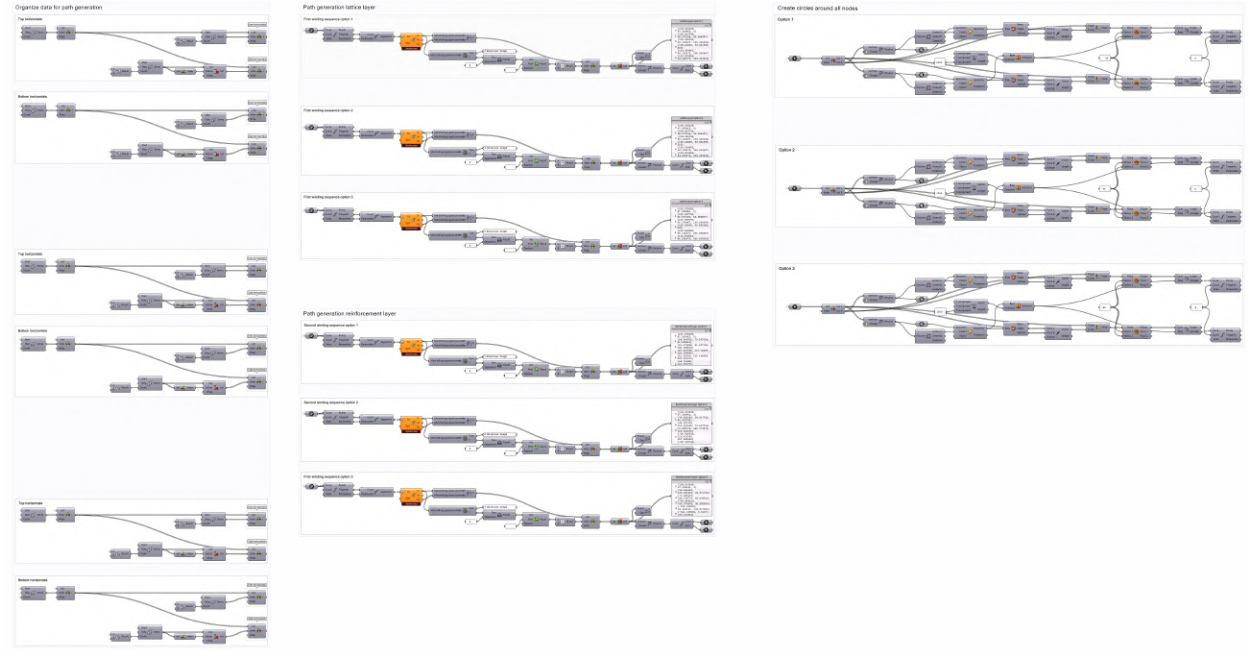

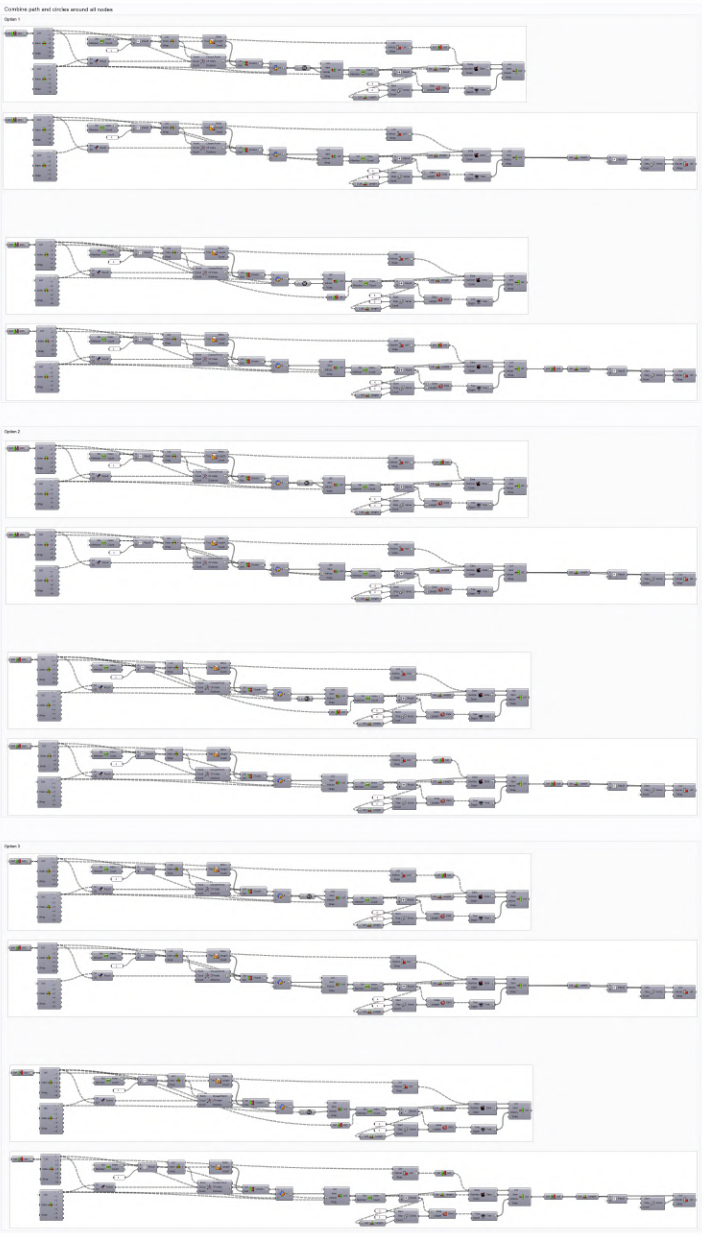
Combine path and circles around all nodes
Option 1
Option 2
Option 3

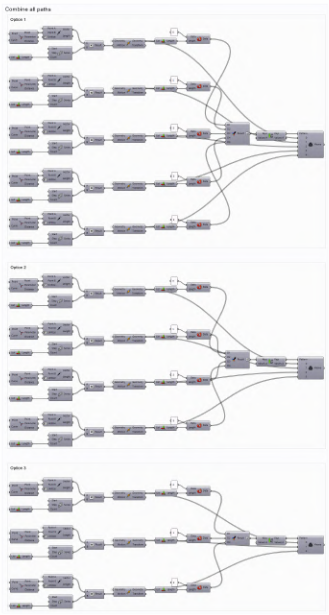
Combine all paths
Option 1
Option 2
Option 3

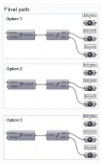
Final path
Option 1
Option 2
Option 3

Analysis part

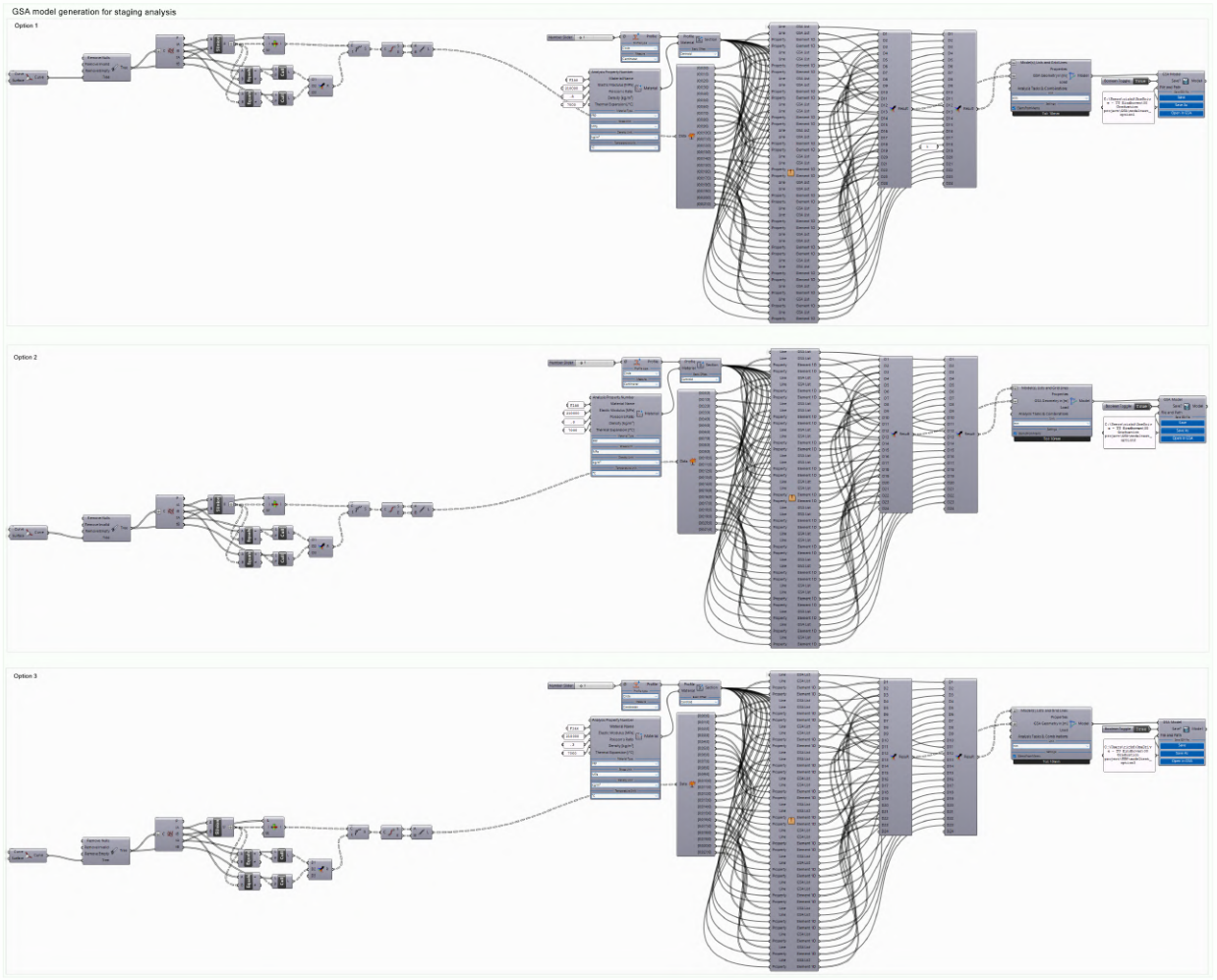

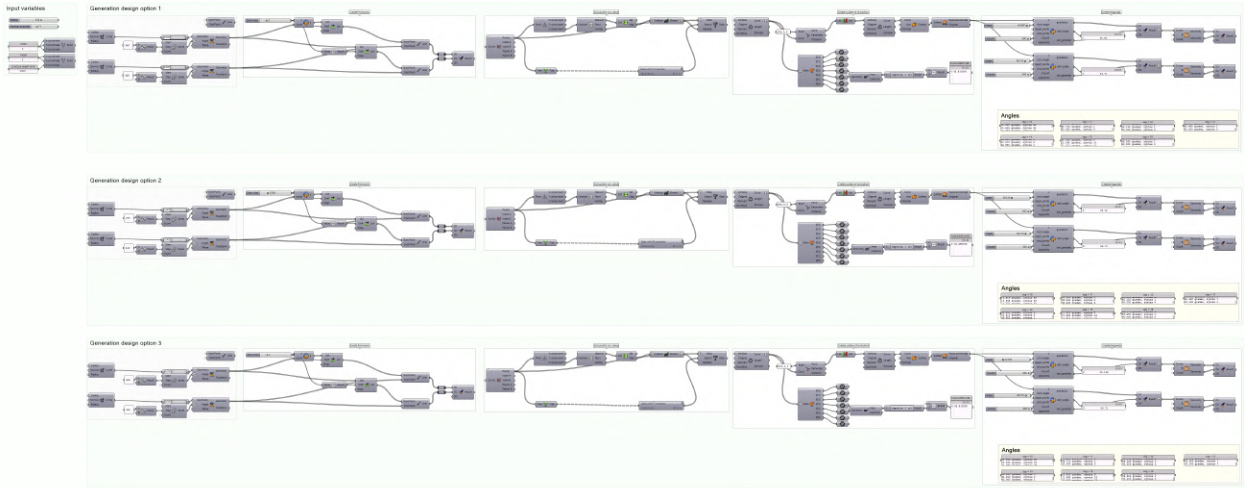

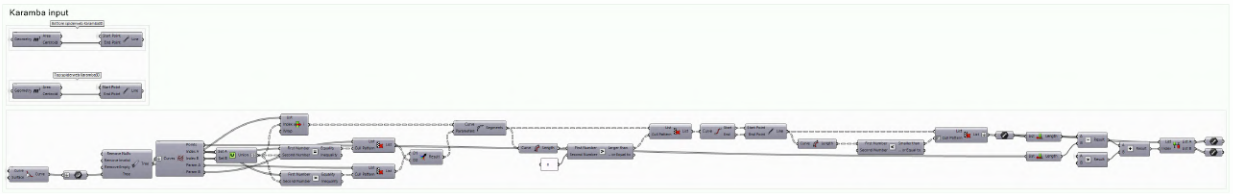
Karamba input

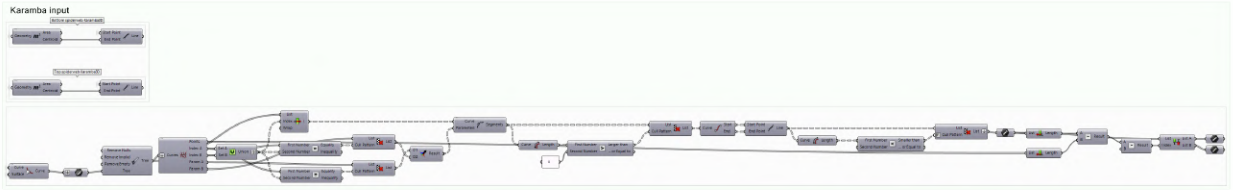
Karamba input

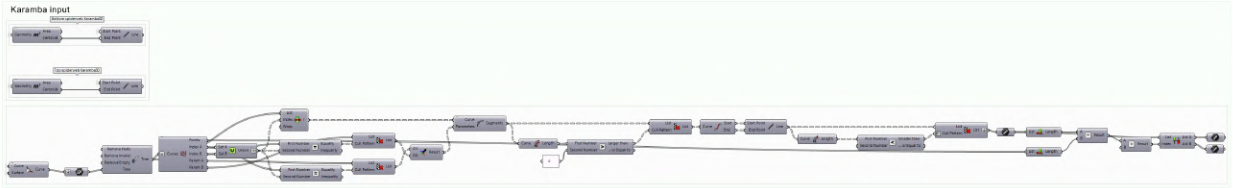
Karamba input

Karamba Structural analysis Option1

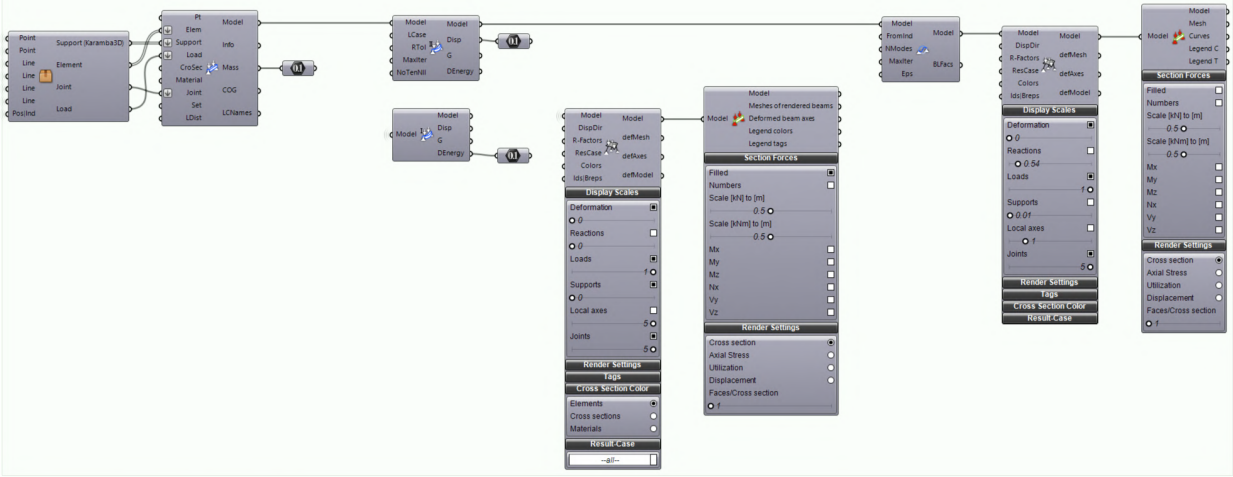

Karamba Structural analysis Option2

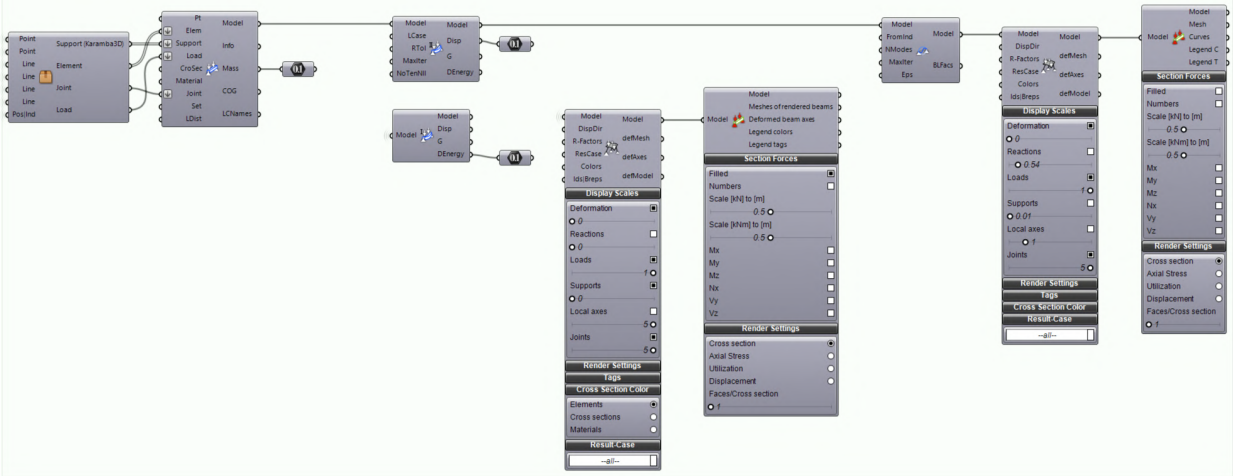

Karamba Structural analysis Option3

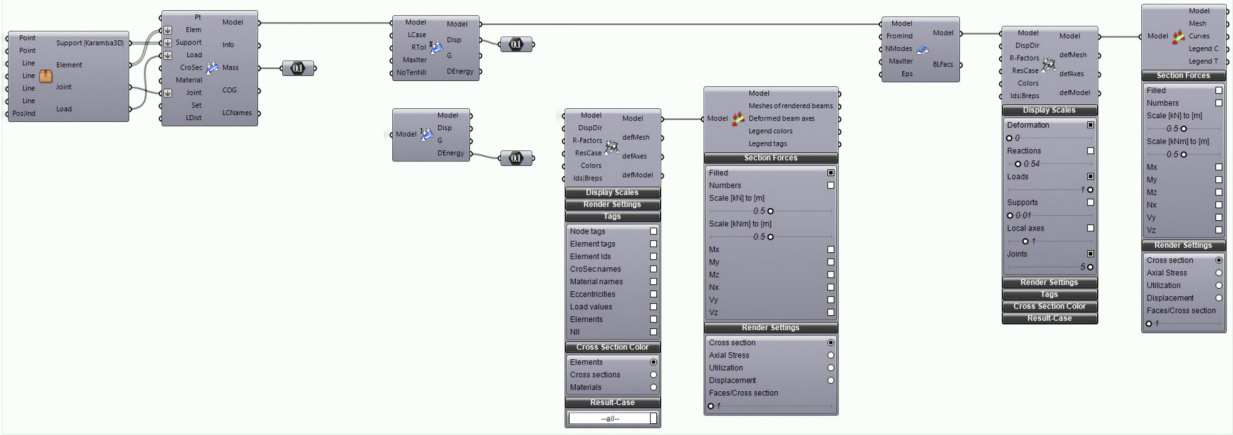

E Appendix: Overview Robot Components script

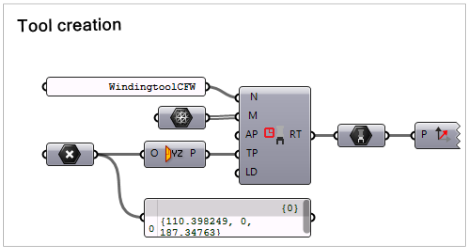

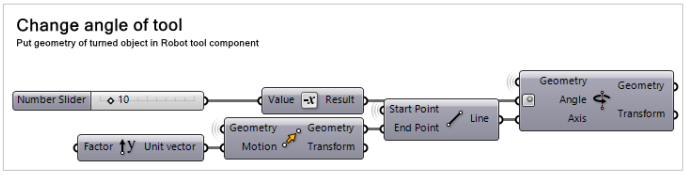

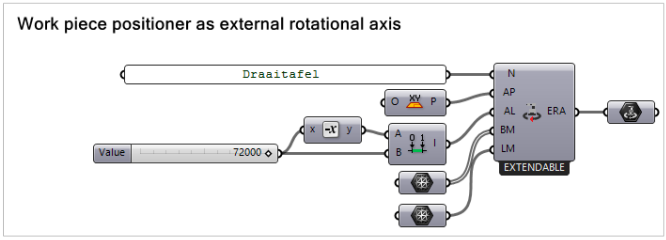

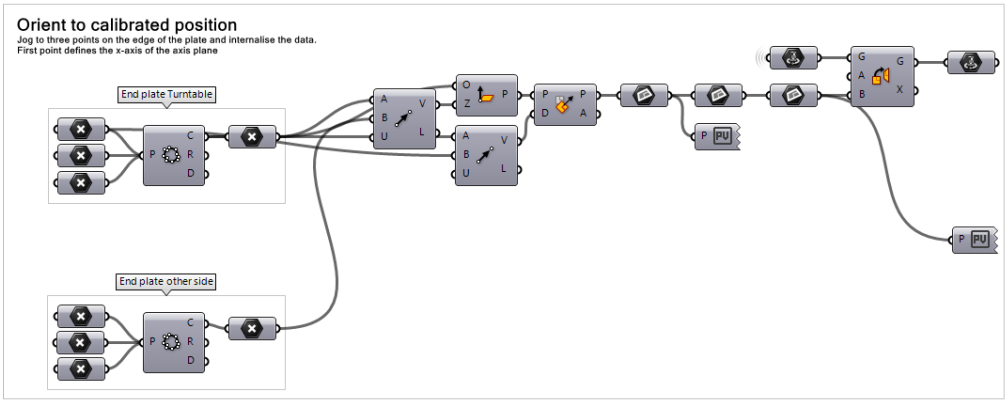

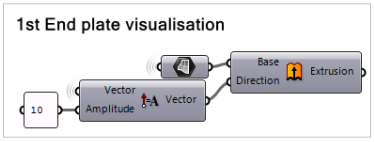

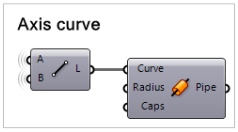

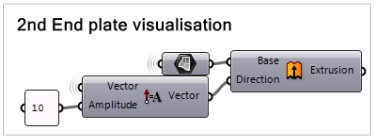

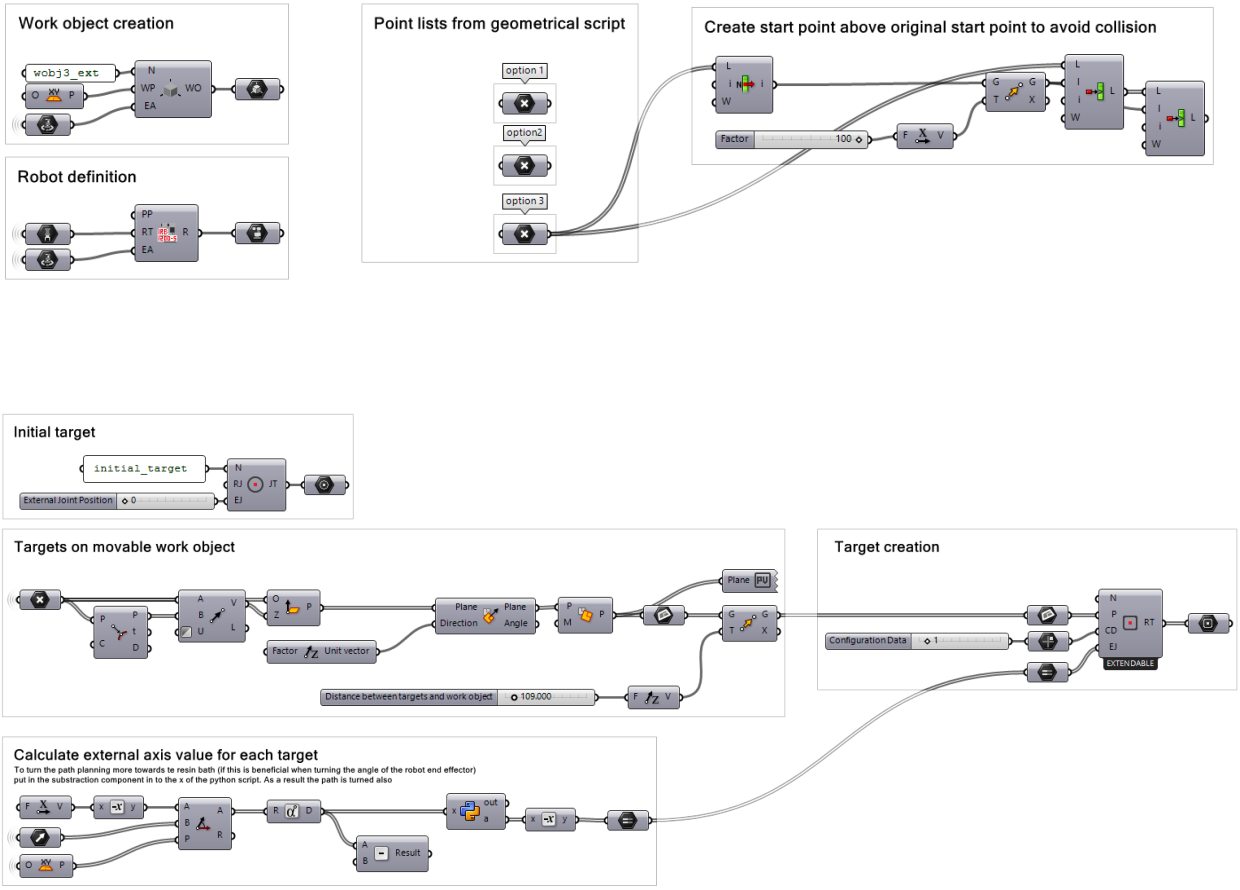
Work object creation
wobj3_ext
Robot definition
Point lists from geometrical script
option 1
option2
option 3
Create start point above original start point to avoid collision
Factor
100
Initial target
initial_target
External Joint Position
0
Targets on movable work object
Plane
Direction
Angle
Factor
Unit vector
Distance between targets and work object
109.000
Target creation
Configuration Data
1
EXTENDABLE
Calculate external axis value for each target
To turn the path planning more towards te resin bath (if this is beneficial when turning the angle of the robot end effector)
put in the substraction component in to the x of the python script. As a result the path is turned also
Result

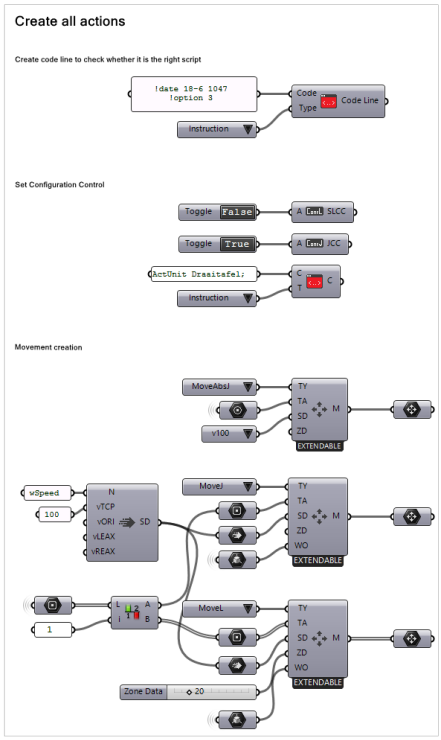
Create all actions
Create code line to check whether it is the right script
!date 18-6 1047
!option 3
Code
Type
Code Line
Instruction
Set Configuration Control
Toggle
False
A
SLCC
Toggle
True
JCC
ActUnit Drasitsfel;
C
T
Instruction
Movement creation
MoveAbsJ
TY
TA
SD
ZD
M
EXTENDABLE
v100
wSpeed
100
N
vTCP
vORI
vLEAX
vREAX
MoveJ
WO
1
L
I
A
B
MoveL
Zone Data
20

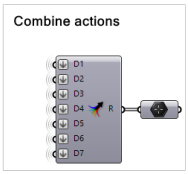
Combine actions
D1
D2
D3
D4
D5
D6
D7
R


Plane visualizer
P
PU

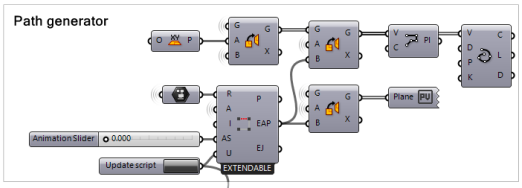
Path generator
XY
P
G
A
B
X
V
C
PI
D
L
K
Plane
PU
R
I
AS
U
EAP
EJ
EXTENDABLE
Animation Slider
0.000
Update script

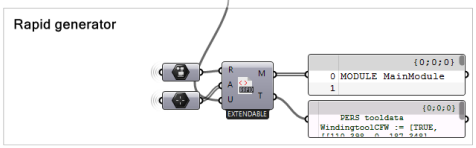
Rapid generator
R
A
U
M
T
EXTENDABLE
{0;0;0}
0 MODULE MainModule
1
{0;0;0}
PERS tooldata

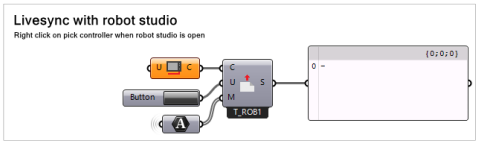
Livesync with robot studio
Right click on pick controller when robot studio is open
U
C
Button
A
C
U
M
S
T_ROB1
{0;0;0}
0 -

F Appendix: Results of staging Analysis

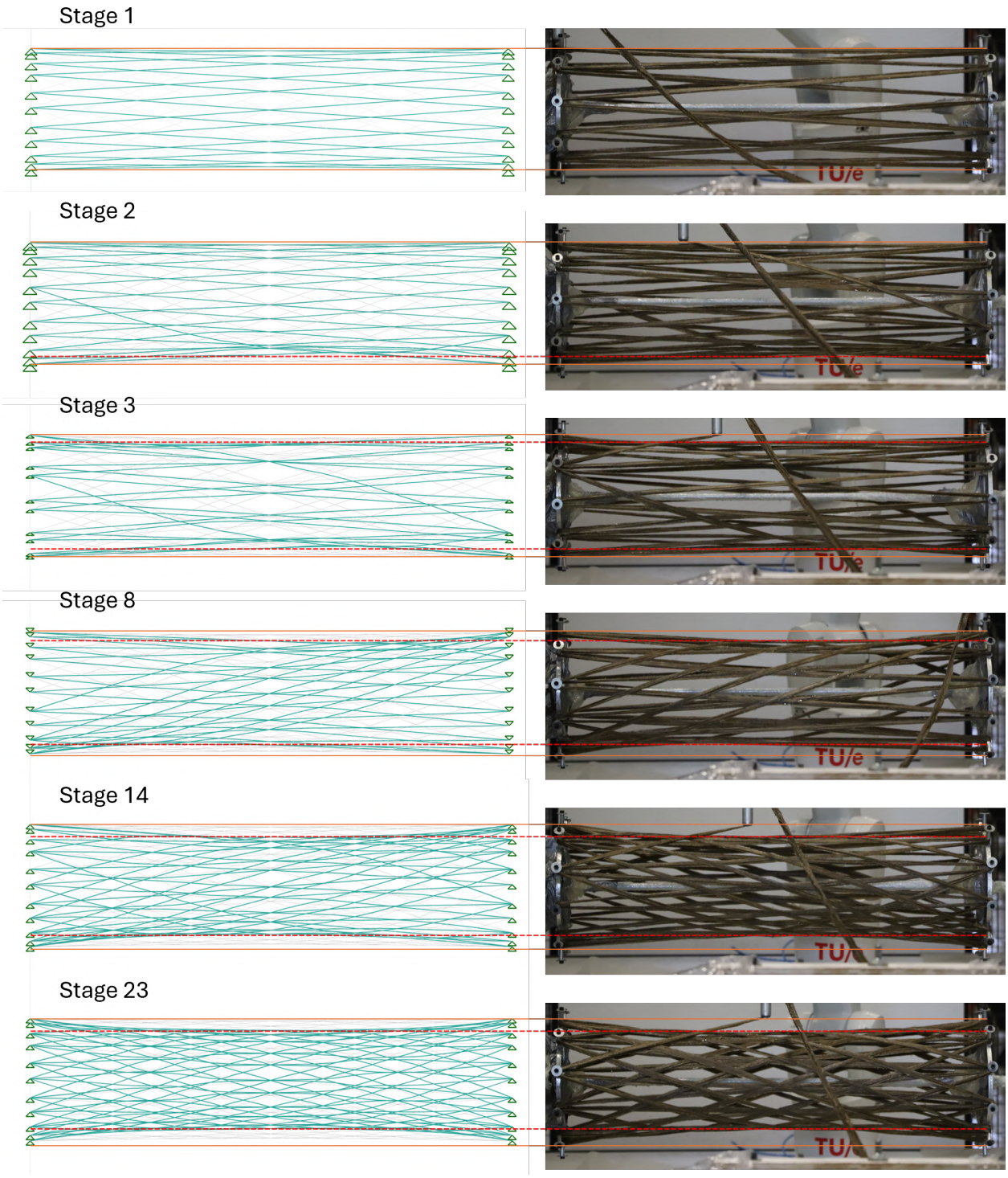

	2	3	4	5	6	7	8	9	10	11	12	13	14	15	16	17	18	19	20	21	22	23
1	2.4	2.452	2.258	2.238	3.648	3.658	6.004	5.981	7.074	6.818	7.082	6.549	6.476	6.955	6.944	7.88	7.904	7.411	7.469	5.761	5.794	3.094
2	2.4	2.452	2.258	2.238	3.648	3.658	6.004	5.981	7.074	6.817	7.081	6.548	6.475	6.955	6.944	7.884	7.904	7.411	7.469	5.76	5.789	7.229
3	2.4	2.452	2.258	2.238	4.848	4.855	7.737	7.741	9.278	9.068	9.206	8.654	8.577	9.23	9.214	10.12	10.18	9.314	9.364	6.932	6.995	11.82
4	2.4	2.452	2.258	2.238	4.849	4.855	7.733	7.742	9.279	9.064	9.207	8.655	8.578	9.229	9.215	10.12	10.18	9.315	9.635	12.29	12.37	15.31
5	2.48	2.452	3.289	3.28	6.368	6.369	6.288	6.244	7.676	7.715	7.444	7.76	7.757	11.84	11.86	10.78	10.79	11.55	11.56	13.31	13.28	13.22
6	2.48	2.452	3.289	3.28	6.368	6.369	6.288	6.245	7.676	7.714	7.44	7.759	7.755	11.84	11.86	9.028	9.043	10	9.992	11.39	11.27	11.2
7	2.48	2.452	3.289	3.28	6.368	6.369	6.288	6.245	6.693	6.662	6.194	6.446	6.402	6.039	6.072	5.599	5.633	6.725	6.661	7.563	7.408	7.368
average	2.434286	2.452	2.699857	2.684571	5.156714	5.161857	6.620286	6.597	7.821429	7.694	7.664857	7.481571	7.431429	8.869714	8.872714	8.773	8.804857	8.818	8.878571	9.000857	8.986571	9.891571

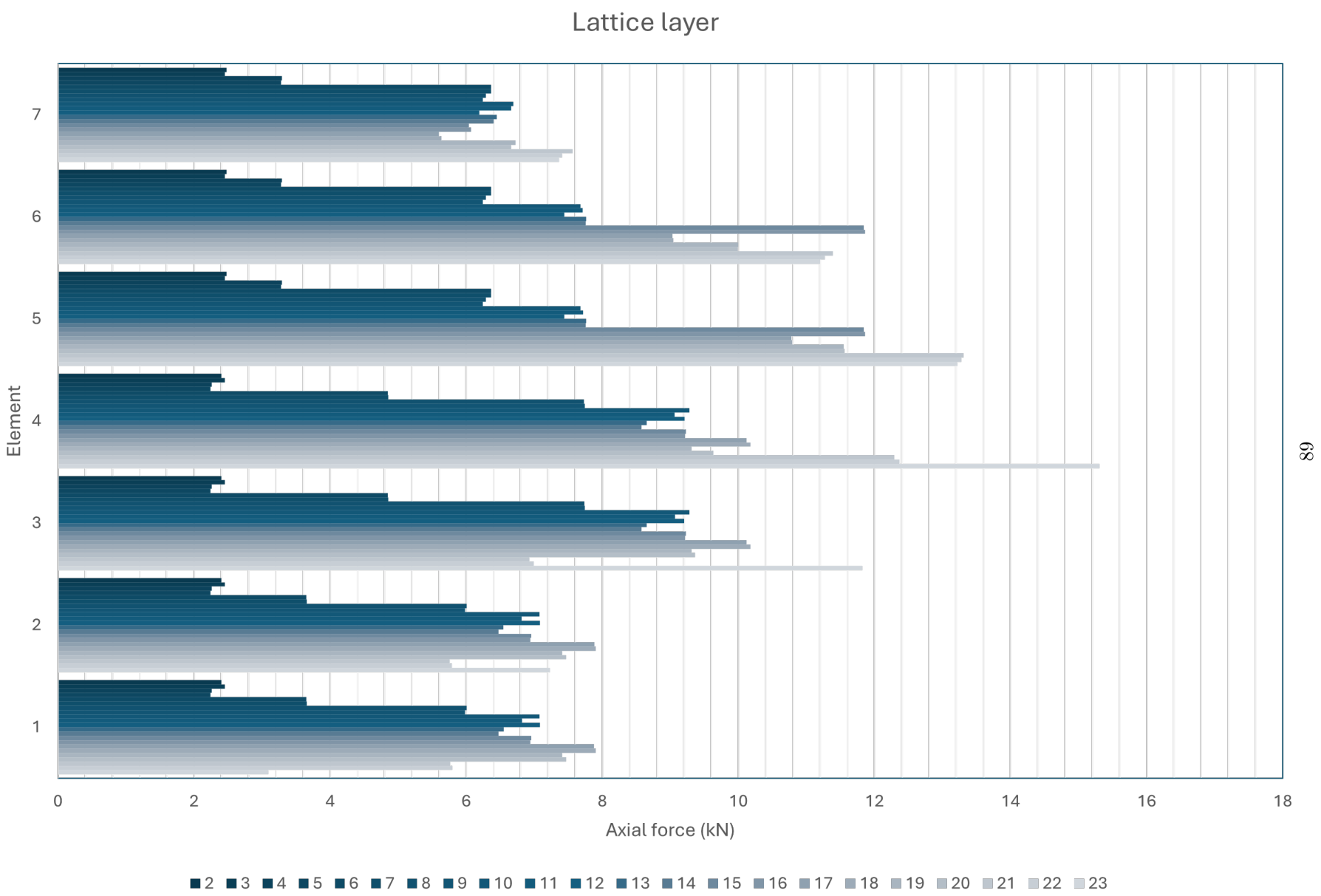
Lattice layer
Element
7
6
5
4
3
2
1
0
2
4
6
8
10
12
14
16
18
Axial force (kN)
2 3 4 5 6 7 8 9 10 11 12 13 14 15 16 17 18 19 20 21 22 23

	2	3	4	5	6	7	8	9	10	11	12	13	14	15	16	17	18	19	20	21	22	23
101	8.722	8.752	8.229	8.182	8.695	8.214	8.417	8.215	8.222	8.132	7.769	8.657	8.707	8.564	8.69	10.42	10.49	13.15	12.84	16.39	14.33	14.55
102	8.72	8.751	8.227	8.18	8.694	8.213	8.416	8.214	8.221	8.131	7.768	8.656	8.706	8.563	8.688	10.42	10.49	13.15	12.84	15.99	13.87	14.17
103	9.113	9.149	8.407	8.356	8.849	8.328	8.471	8.274	8.269	8.228	7.836	8.722	8.777	8.187	8.319	10.19	10.26	12.75	12.35	12.21	10.05	10.18
104	9.119	9.155	8.41	8.359	8.852	8.331	8.474	8.277	8.272	8.231	7.838	8.725	8.78	8.191	8.323	10.2	10.27	12.43	11.95	12.38	9.607	9.753
105	8.008	8.047	7.094	7.019	7.119	6.473	6.561	6.521	6.527	6.294	6.004	6.974	7.043	6.72	6.86	9.35	9.321	8.075	7.405	7.441	5.145	5.199
106	8.001	8.041	7.089	7.013	7.114	6.468	6.557	6.516	6.522	6.289	5.998	6.967	7.035	6.714	6.855	8.742	8.687	7.586	6.874	6.945	4.764	4.821
107	8.425	8.469	7.164	7.047	7.04	6.298	6.383	6.434	6.455	6.069	5.812	6.662	6.741	6.796	6.934	3.704	3.544	2.529	1.832	1.78	1.45	1.473
108	8.429	8.473	7.167	7.077	7.044	6.301	6.386	6.436	6.458	6.073	5.814	6.666	6.745	6.718	6.862	3.752	3.592	2.588	1.971	1.916	1.507	1.53
109	9.162	9.212	7.309	7.128	7.142	5.702	5.773	4.498	4.517	4.986	4.731	2.162	2.306	1.423	1.785	0.3021	0.7938	0.2274	1.304	1.297	3.688	3.69
110	9.158	9.208	7.304	7.122	7.136	5.696	5.768	4.493	4.512	4.869	4.636	1.97	2.105	1.319	1.655	0.2768	0.8075	0.2997	1.346	1.343	3.631	3.633
111	8.416	8.488	6.187	6.011	6.003	4.577	4.641	6.045	6.063	4.979	4.539	3.002	3.245	2.662	3.007	1.936	2.869	2.473	4.024	4.012	5.586	5.569
112	8.421	8.453	6.189	6.012	6.005	4.579	4.643	6.176	6.192	5.225	4.962	3.286	3.539	2.989	3.319	2.291	3.281	2.91	4.542	4.533	5.836	5.821
113	9.067	9.095	7.183	6.792	6.817	8.68	8.727	8.325	8.363	7.173	7.003	5.942	6.242	5.879	6.296	5.5	6.593	6.68	9.18	9.144	9.658	9.615
114	9.057	9.084	7.172	6.785	6.811	9.101	9.146	8.926	8.963	8.034	7.774	6.914	7.145	6.824	7.278	6.569	7.955	7.707	9.66	9.638	10.04	10.01
115	8.238	8.348	6.47	8.202	8.23	12.29	12.33	12.1	12.18	11.52	11.33	10.62	10.79	10.5	11.24	10.59	12.4	12.16	13.63	13.59	13.26	13.22
average	8.1285	8.170313	6.850063	6.830313	6.971938	6.828188	6.918313	6.840625	6.8585	6.514563	6.238375	5.995313	6.119125	5.753063	6.006938	5.890181	6.334581	6.544694	6.98425	7.413063	7.026375	7.077125

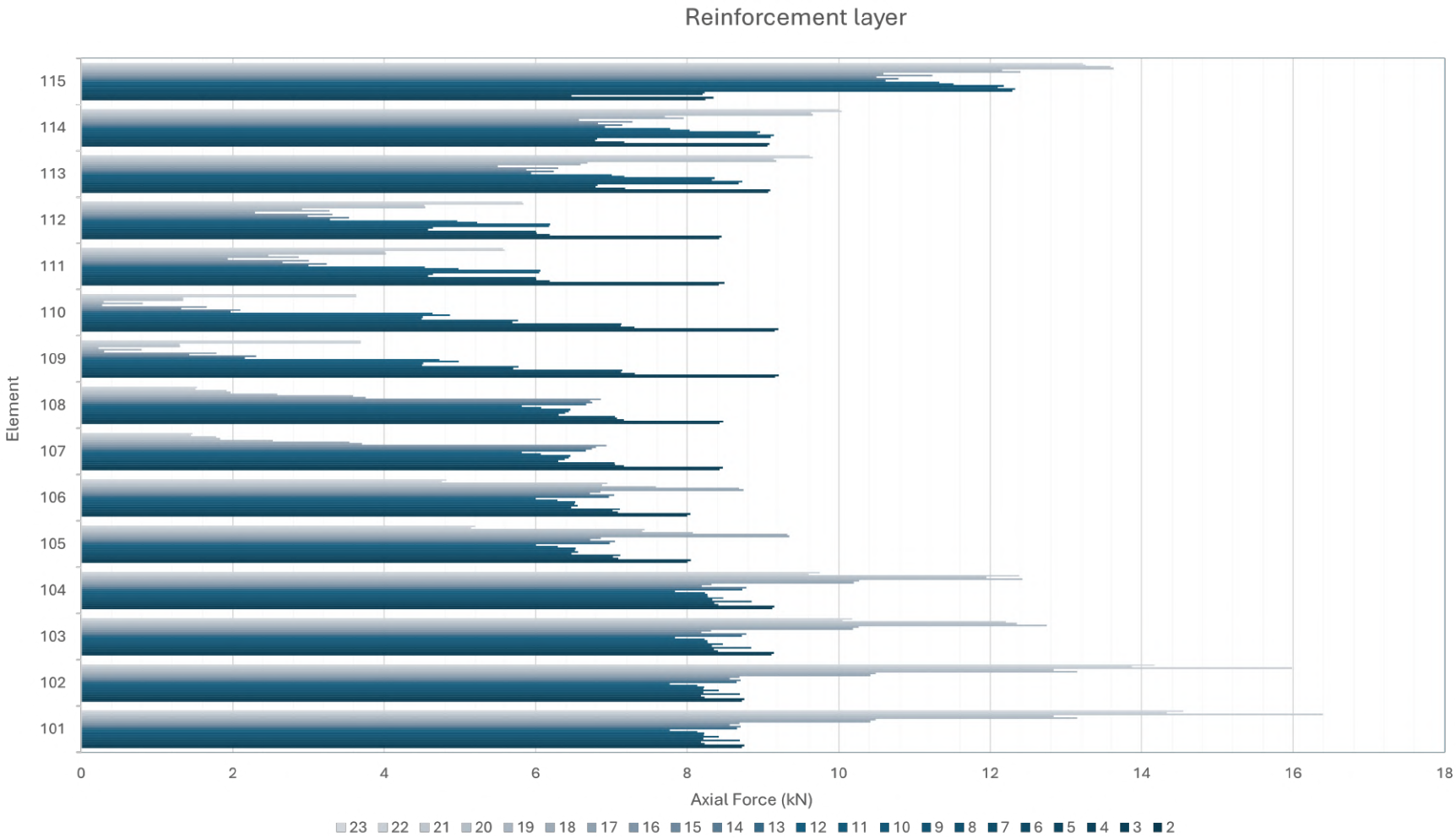
Reinforcement layer
Element
115
114
113
112
111
110
109
108
107
106
105
104
103
102
101
0
2
4
6
8
10
12
14
16
18
Axial Force (kN)
23 22 21 20 19 18 17 16 15 14 13 12 11 10 9 8 7 6 5 4 3 2

G Appendix: Results of physical tests

Force-displacement diagram V1O1

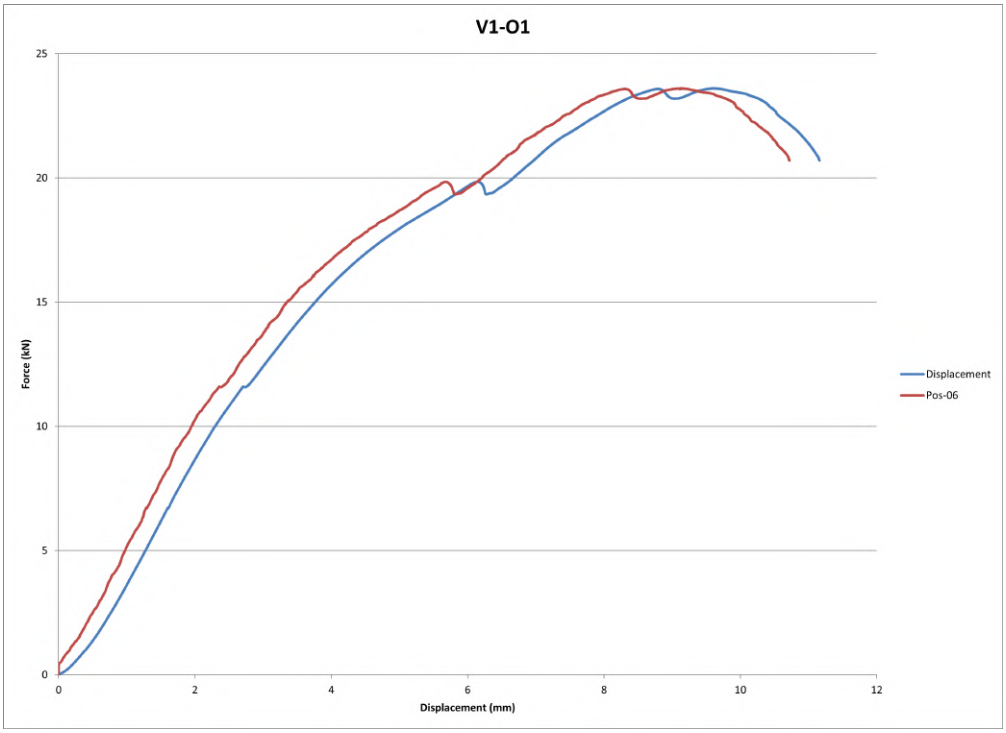

Force-displacement diagram V2O1

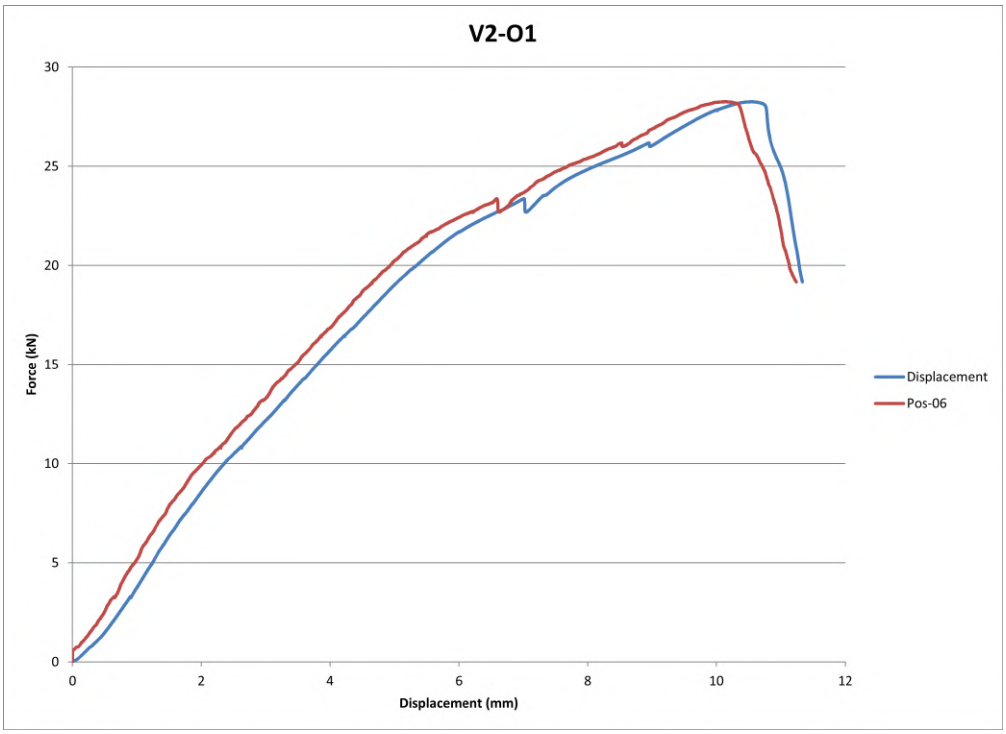

Force-displacement diagram V1O2

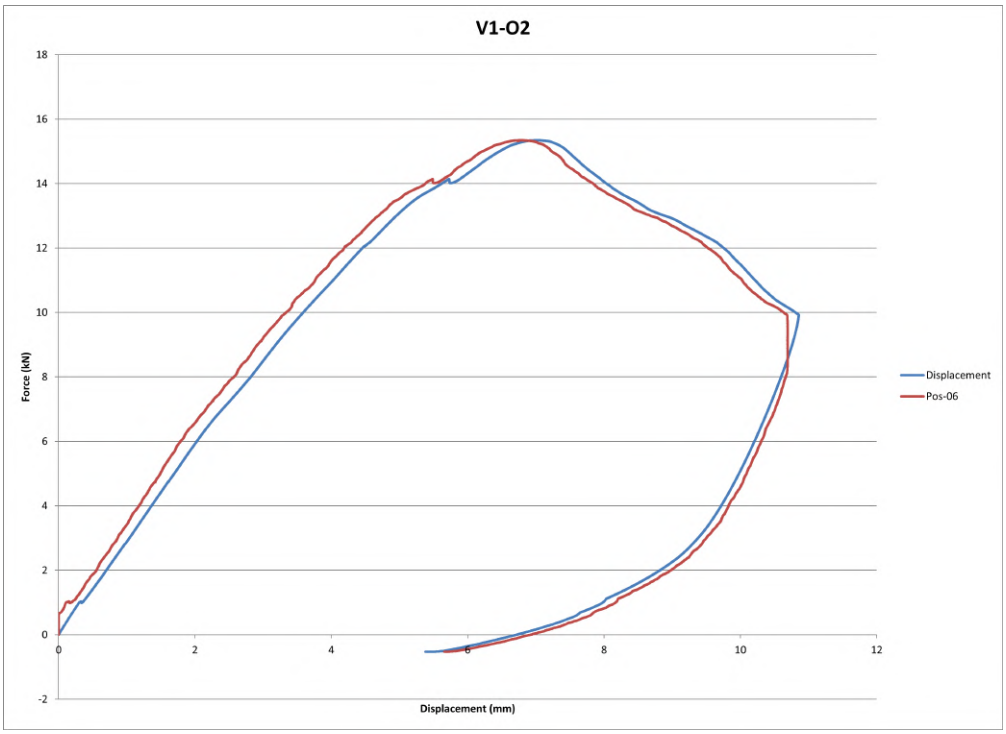

Force-displacement diagram V1O3

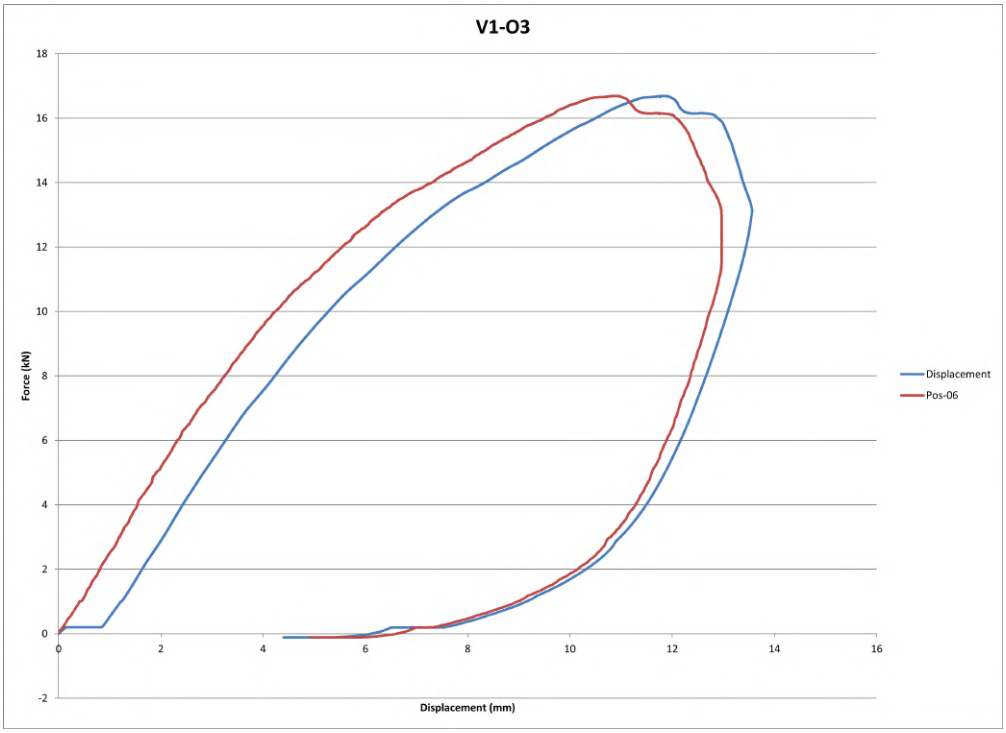

H Appendix: Videos of physical tests